uOttawa

L'Université canadienne
Canada's university

FACULTÉ DES ÉTUDES SUPÉRIEURES ET POSTOCTORALES

uOttawa

L'Université canadienne
Canada's university

FACULTY OF GRADUATE AND POSDOCTORAL STUDIES

John Sandness
AUTEUR DE LA THÈSE / AUTHOR OF THESIS

M.A.Sc. (Mechanical Engineering)
GRADE / DEGREE

Department of Mechanical Engineering
FACULTÉ, ÉCOLE, DÉPARTEMENT / FACULTY, SCHOOL, DEPARTMENT

The Optimization of the Curing of Carbon Fibre Composite Rebar using a Heat Transfer FEA Model

TITRE DE LA THÈSE / TITLE OF THESIS

A. Fahim
DIRECTEUR (DIRECTRICE) DE LA THÈSE / THESIS SUPERVISOR

Mike Munro
CO-DIRECTEUR (CO-DIRECTRICE) DE LA THÈSE / THESIS CO-SUPERVISOR

EXAMINATEURS (EXAMINATRICES) DE LA THÈSE / THESIS EXAMINERS

François Robitaille

Paul Straznicky

Gary W. Slater
Le Doyen de la Faculté des études supérieures et postdoctorales / Dean of the Faculty of Graduate and Postdoctoral Studies

u Ottawa
l'Université canadienne
Canada's university

UNIVERSITY of OTTAWA
DEPARTMENT of MECHANICAL ENGINEERING

The Optimization of the Curing of Carbon Fibre Composite Rebar using a Heat Transfer FEA Model

John Sandness

A thesis submitted to the Faculty of Graduate and Postdoctoral Studies
in partial fulfillment of the requirements for the degree of

MASTER OF APPLIED SCIENCE

in Mechanical Engineering

Ottawa-Carleton Institute for Mechanical and Aerospace Engineering
University of Ottawa
Ottawa, Canada

May 2008

Your file Votre référence
ISBN: 978-0-494-59875-7
Our file Notre référence
ISBN: 978-0-494-59875-7

Abstract

A new fiber composite rebar for concrete developed at the University of Ottawa exhibits pseudo-ductility by having an aramid composite overwrap slide at a designated yield stress level. One challenge is how to cure the fibre composite core with respect to the overwrap. In this thesis a Finite Element Analysis model was created to predict how the fibre composite rebar would cure as it passed through the induction heating stage and the furnace stage. Eight processing combinations were evaluated with the FEA model using different induction and furnace heating settings, along with various production speeds. It was discovered that through the combination of induction and furnace heating, the curing could be controlled so that is possible to continuously produce the rebar while controlling the progression of the cure.

Acknowledgements

There are many people I'd like to acknowledge for their contribution to completion of this thesis. First and foremost, I'd like to thank Professor Fahim and Professor Munro for acting as my supervisors on this project. Without them, I would not have had the ability to conduct research on a topic that covered such a broad scope of engineering. It was an honour to work with them.

I am also indebted to Professor Mohareb for his guidance and insight in working with ABAQUS. Additionally, I was very fortunate to have the assistance of Professor Martin-Perez with integrating the Fortran user subroutines into ABAQUS.

I would not have been able to have much success gathering experimental data without the help of the Mechanical Engineering Machine Shop. I would like to express my gratitude to the entire machine shop staff for their help. I would also like to thank fellow graduate student Etienne Poisson for his innovative suggestions during our troubleshooting sessions.

Finally, I would like to thank my parents for their support and guidance.

Table of Contents

Abstract i

Acknowledgements ii

Table of Contents iii

List of Figures v

List of Tables viii

List of Symbols ix

Chapter 1: Introduction 1
- 1.1 General Area of Interest 1
- 1.2 Previous Research 4
- 1.3 Thesis Objective 5

Chapter 2: Literature Review 6
- 2.1 Fibre-Reinforced Plastic Composites 6
  - 2.1.1 Mechanical Property Deliberation 6
  - 2.1.2 Fibre Composite as Rebar 9
- 2.2 Pultrusion Process 11
  - 2.2.1 Description of Process 12
  - 2.2.2 Process Modifications 13
  - 2.2.3 Modeling Pultrusion Process 15
- 2.3 Available Polymerization Models 16
  - 2.3.1 Nth Order & Autocatalytic Model 17
  - 2.3.2 Loos-Springer Equations 19
  - 2.3.3 Horie Mechanistic Model 19
  - 2.3.4 Miscellaneous 20
  - 2.3.5 Selected Model 21
- 2.4 Challenges of Fabricating the Fibre Composite Rebar 21
- 2.5 Microwave Heating 22
- 2.6 Induction Heating 24
  - 2.6.1 Background Theory 25
  - 2.6.2 Induction Process Considerations 27
  - 2.6.3 Induction Heating Applications 30
  - 2.6.4 Adaption of Induction Heating for Fibre Composite Rebar Production 32

Chapter 3: Experimental Setup 33
- 3.1 Composite Production Process 33
- 3.2 Location of Steel Wires 38

3.3 Measuring Induction Heat Output 39
3.4 Epoxy Exotherm Testing 41

Chapter 4: Analytical Kinetic Model 44
4.1 Curing of Epoxy 46
4.2 Heat Transfer of FRP rods 48
4.2.1 Modeling Natural Convection 50
4.2.2 Modeling Thermal Radiation 51
4.2.3 Semi-Infinite Approach 52
4.2.4 Lumped Capacitance Approach 54
4.2.5 Validation of Analytical Model 54
4.3 Induction Heating 56

Chapter 5: Finite Element Model of Heat Transfer and Cure 59
5.1 Model Requirements 59
5.2 Choice of Finite Element Package 59
5.3 Construction of the Model 60
5.4 Assumptions and Simplifications 65

Chapter 6: Results & Discussion 66
6.1 Convergence Study of the FEA Model 66
6.2 Validation of FEA Model 71
6.3 Comparison between Furnace and Induction Heating 73
6.3 Parametric Study using FEA Model 80
6.3.1 Processing at 50 centimetres per minute 81
6.3.2 Processing at 75 centimetres per minute 85
6.3.3 Processing at 100 centimetres per minute 87
6.4 Cross-Sectional Profiles 89
6.4.1 Processing at 50 centimetres per minute 90
6.4.2 Processing at 75 centimetres per minute 96
6.4.3 Processing at 100 centimetres per minute 99

Chapter 7: Conclusions 103
7.1 Final Results 103
7.2 Proposed Production Settings 104
7.3 Suggested Future Work 104

References 106

Appendix A Epoxy Exothermic Reaction Test 109

Appendix B Physical Properties 111

Appendix C Sample Heat Transfer Calculation 112

Appendix D Finite Element Code 114

List of Figures

Figure 1.1 – Loading of a Beam 1
Figure 1.2 – Exposed Rebar 2
Figure 1.3 – Elastic Behaviour of Composites 3
Figure 1.4 – Mechanical Behaviour of Structural Steel 4

Figure 2.1 – Fibre Length Effect on Stress Transfer 7
Figure 2.2 – Failure Mechanisms of Composites 9
Figure 2.3 – Sample of Composite Rebar 11
Figure 2.4 – Commercial Pultrusion Process 12
Figure 2.5 – Basic Pultrusion Process 12
Figure 2.6 – Robust Pultrusion Process 13
Figure 2.7 – Hollow Pultrusion Process 14
Figure 2.8 – Induction Heat of a Tube 26
Figure 2.9 – Induction Coil Designs 28
Figure 2.10 – Coil Efficiency based on Bar Diameter and Air Gap 29
Figure 2.11 – Induction Melting 30
Figure 2.12 – Implant Induction Heating 31

Figure 3.1 – Creel Station 34
Figure 3.2 – Close up of Creel Station 34
Figure 3.3 – Fibre Sorter 35
Figure 3.4 – Braider 36
Figure 3.5 – Induction Heating and Furnace Entry 37
Figure 3.6 – Furnace Exit and Puller 39
Figure 3.7 – Location of Steel Wires in Millimetres 39
Figure 3.8 – Experiment to quantify Induction Heating 40
Figure 3.9 – Cross-section of Experiment to quantify Induction Heating 40
Figure 3.10 – Epoxy Reaction during a Controlled Furnace Heating Test 42
Figure 3.11 – Epoxy Reaction during a Controlled Temperature Test 43

Figure 4.1 – Sample Epoxy Exotherm Test conducted at 180 °C 44
Figure 4.2 – Sample Temperature Difference from 180 °C test 45
Figure 4.3 – Temperature Difference Profile 46
Figure 4.4 – Heating Rate as a function of Amount Cured for Selected Tests 47
Figure 4.5 – Calculated Curing Rate of Epoxy as a function of Temperature 48
Figure 4.6 – Illustrations of Conduction, Convection, and Radiation 49
Figure 4.7 – Heat Transfer through a Semi-Infinite Cylinder 52
Figure 4.8 – Temperature Profile of a Semi-Infinite Cylinder 53

Figure 4.9 – Comparison of Analytical Model with Experimental Results 55
Figure 4.10 – Heat Released by Induction Heating as a function of Current 58

Figure 5.1 – HETVAL Process 63
Figure 5.2 – Region Modeled by ABAQUS 64
Figure 5.3 – Rod Broken Down into Elements 64

Figure 6.1 – Temperature Convergence Study 67
Figure 6.2 – Cure Fraction Convergence Study 69
Figure 6.3 – Comparison of Analytical Model, Experimental Data and FEA 71
Figure 6.4 – Temperature at Centre of Rebar Comparison 72
Figure 6.5 – Cure Fraction Comparison 73
Figure 6.6 – Location of Nodes used in the Cross-Section Profile 74
Figure 6.7 – Temperature Cross-Section of a 25 mm rod cured at 115.5 A 75
Figure 6.8 – Cure Fraction Cross-Section of a 25 mm rod cured at 115.5 A 75
Figure 6.9 – Temperature Cross-Section of a 25 mm rod cured at 231 A 76
Figure 6.10 – Cure Fraction Cross-Section of a 25 mm rod cured at 231 A 76
Figure 6.11 – Temperature Cross-Section of a 25 mm rod cured at 200 °C 77
Figure 6.12 – Cure Fraction Cross-Section of a 25 mm rod cured at 200 °C 77
Figure 6.13 – Temperature Cross-Section of a 25 mm rod cured at 240 °C 78
Figure 6.14 – Cure Fraction Cross-Section of a 25 mm rod cured at 240 °C 79
Figure 6.15 – Location of Selected Nodes 81
Figure 6.16 – Sim 1: Induction 115.5 Amps, Furnace Heating 200 °C 82
Figure 6.17 – Sim 2: Induction 115.5 Amps, Furnace Heating 240 °C 83
Figure 6.18 – Sim 3: Induction 231 Amps, Furnace Heating 200 °C 84
Figure 6.19 – Sim 4: Induction 231 Amps, Furnace Heating 240 °C 85
Figure 6.20 – Sim 5: Induction 231 Amps, Furnace Heating 200 °C 86
Figure 6.21 – Sim 6: Induction 231 Amps, Furnace Heating 240 °C 87
Figure 6.22 – Sim 7: Induction 231 Amps, Furnace Heating 200 °C 88
Figure 6.23 – Sim 8: Induction 231 Amps, Furnace Heating 240 °C 89
Figure 6.24 – Node Location for Cross-Section Analysis 90
Figure 6.25 – Temperature Cross-Section profile for Sim 1 91
Figure 6.26 – Cure Fraction Cross-Section profile for Sim 1 91
Figure 6.27 – Temperature Cross-Section profile for Sim 2 92
Figure 6.28 – Cure Fraction Cross-Section profile for Sim 2 93
Figure 6.29 – Temperature Cross-Section profile for Sim 3 94
Figure 6.30 – Cure Fraction Cross-Section profile for Sim 3 94
Figure 6.31 – Temperature Cross-Section profile for Sim 4 95
Figure 6.32 – Cure Fraction Cross-Section profile for Sim 4 96
Figure 6.33 – Temperature Cross-Section profile for Sim 5 97
Figure 6.34 – Cure Fraction Cross-Section profile for Sim 5 98

Figure 6.35 – Temperature Cross-Section profile for Sim 6 98
Figure 6.36 – Cure Fraction Cross-Section profile for Sim 6 99
Figure 6.37 – Temperature Cross-Section profile for Sim 7 100
Figure 6.38 – Cure Fraction Cross-Section profile for Sim 7 100
Figure 6.39 – Temperature Cross-Section profile for Sim 8 101
Figure 6.40 – Cure Fraction Cross-Section profile for Sim 8 102

List of Tables

Table 2.1 – Comparison between Steel and Carbon Fibre Composite 10
Table 2.2 – Percentage Cured for Thermal and Microwave Heating 23
Table 2.3 – Curing Time for Thermal and Microwave Heating 23

Table 4.1 – Experimentally Derived Parameters for Epoxy Exothermic Reaction 48
Table 4.2 – Sample of Data gathered from an Induction Heating Test 56
Table 4.3 – Sample of Power Released from an Induction Heating Test 57

Table 5.1 – Material Properties 62
Table 5.2 – Interface Properties 62

Table 6.1 – Parameters Modified in the Finite Element Model 80

Table 7.2 – Proposed Settings 104

List of Symbol

l_C = critical fibre length
σ = stress
σ^* = tensile strength of fibre
σ_C = tensile stress in composite at failure
σ_f = tensile stress in fibres at fibre failure
σ'_M = tensile stress in matrix at fibre failure

d_f = fibre diametre
τ_C = fibre-matrix shear stress
V_M = volume fraction of matrix
V_f = volume fraction of fibres
E_C = elastic modulus of composite
E_M = elastic modulus of matrix
E_f = elastic modulus of fibres

α = extent of cure
$g(\alpha)$= rate of cure
t = time
A = intercept of reaction
n = slope of reaction
X = extent of conversion
E_a = activation energy

a_X = anime
a_0 = anime initial concentration
q_x = mole fraction of animo
[PA]= primary amine concentration

e = epoxy
e_0 = epoxy initial concentration
[Ex]= epoxy concentration

et = ether
L = fraction of ether reactions
K_X = reaction constants
OH = epoxy reaction impurity
HX = catalysis

A' = reaction constant
B = reaction correction variable

f = frequency
f_c = critical frequency
ε" = dielectric loss factor
ε_0 = dielectric constant
E = electric field strength
d = penetration depth
ρ = resistivity
P = power
P_W = power delivered to workpiece
R = resistance
I = current
d = diameter of workpiece
h = length of workpiece in coil
μ_0 = magnetic constant
μ_R = relative magnetic property
$\mu_r = \mu_0 \cdot \mu_R$
p_r = workpiece resistivity
N = number of turn in the induction coil

k = thermal conductivity
h = heat transfer coefficient
q_X = heat transfer
c = specific heat
ε = emissivity
β = volume coefficient of expansion
v = kinematic viscosity

σ_B = Bozeman's constant
Nu = Nusselt number
Gr = Grashof number
Pr = Prandtl number
Bi = Biot number

g = gravitional constant
x = thickness
R = radius of cylinder
A = surface area
V = volume
R = universal gas constant
T = temperature
T_0 = initial temperature
T_S = surface temperature
T_{Sur} = surrounding fluid temperature
T_∞ = surrounding region temperature
ΔT = temperature difference
T_{Ref} = reference temperature
T_P = exothermic peak temperature

Chapter 1
Introduction

1.1 Background

The use of concrete started several millennia ago. Even in modern society with new materials being developed at a rapid pace, it will continue to be a vital building material in the future. Concrete is a primary building material due to its excellent material properties; namely, excellent formability, good compression strength, strong corrosion resistance, and common availability. It does, however, possess a weakness when subjected to a tensile stress. While concrete is very good under compressive stress, it exhibits only one tenth of that strength when it is subjected to a tensile load. When designing arch bridges and columns subjected to vertical compressive loads only, this is not a problem as all the pieces experience compressive stress. Yet, when using concrete for beams, there are both compressive and tensile stress regions within the beam; this phenomenon is illustrated in Figure 1.1. Since beams are an essential part of civil engineering, it is imperative that the properties of concrete be improved when loaded in tension [1].

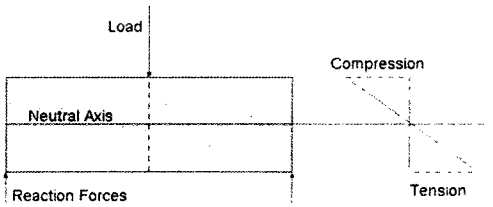

Figure 1.1 – Loading of a Beam

A solution to concrete's lack of strength in tension, whereby a material that is strong in tension is placed within the concrete to act as reinforcement, was discovered in the 19th Century. Thus, concrete can accommodate the compressive stresses while the reinforcement provides support in the tensile stress regions. Steel (rebar) was the initial choice for the tensile reinforcement called rebar. In addition to high tensile properties, steel is readily available, reasonably priced, and can be formed into the desired shapes. With the addition of the steel reinforcements, the regions subjected to a tensile load that would normally cause failure of the concrete beam instead have the steel support the majority of load [2].

The reinforcement of concrete with steel rods has proven to be an extremely useful and cost efficient method of improving the tensile load carrying capability. Yet this mechanical solution has created a problem of a chemical nature, the corrosion of the steel

rebar. While concrete is a very corrosion resistant material, cracks and voids within the concrete can allow water to reach the steel resulting in wet corrosion. As the steel rusts, its ability to support the tensile load is progressively diminished. More importantly, iron oxide's density is less than that of iron. This causes the rust to apply an outward stress on the concrete causing the concrete cover to fracture and fall away (spalling). This effect can be seen in Figure 1.2 where the rusted rods. Finally, some of the reinforcing effect of the steel rebar is lost.

Figure 1.2 – Exposed Rebar [2]

The rate of corrosion of the steel rebar varies greatly with the environmental conditions that are present during its service life. The corrosion rate is most prominent when reinforced concrete is used near seawater or in an environment where salt is used to melt snow and ice. Methods have been developed to slow the rusting of steel, such as by changing the chemistry of concrete or coating the steel with epoxy; however none of these processes eliminate the basic problem of corrosion. Instead, a possible solution to both the concrete's lack of tensile load carrying capability and steel's susceptibility to corrosion would be to select a non-corrosive material that possesses strong tensile properties.

One type of material that has been proposed to replace steel rebar is fibre-reinforced polymer (FRP) composite materials. These materials consist of two or more materials, with one material acting as the matrix in which the reinforcement is embedded. The reinforcement which is the stronger and stiffer material carries more of the tensile load. In many industries, including the construction industry, FRPs have been replacing traditional materials due to their superior properties. Even as far back as 1987, the Composite Institute of The Society of the Plastic Industry published that the construction industry used 224 million kilograms or 20.1% of all thermoplastic and thermoset composites [3].

For a FRP to be a direct replacement for steel, the type and quantity of both the matrix and fibre must be selected to ensure that it possesses the same mechanical properties;

namely tensile strength, tensile modulus and ductility. In addition, the material must be immune to corrosion and, ideally, weigh only a fraction of its metallic counterpart.

In spite of the many advantages mentioned above, there is a problem that must be solved; specifically FRP composite materials have significantly lower ductility than steel. While the type of steel used for rebar will undergo ductile deformation up to a strain of over 30% before failure, the fibres used for composite materials rarely exceed 4% before brittle failures. Figure 1.3 displays the stress-strain behaviour of several composites, including an epoxy/carbon composite identified as curve 4. In contrast, the stress-strain curve of steel is presented in Figure 1.4. The lack of ductility in high performance FRP composites is a critical concern to civil engineers. In steel reinforced concrete tensile cracks in concrete become visible as the ductile steel rebar elongates plastically. This provides visual cues that a component has been overloaded. Thus, while FRP composite materials possess many attractive properties that would make them excellent reinforcements for concrete, their lack of ductility must be addressed by redesigning how the reinforcement is used within the concrete, modifying the design codes, or building the composite in a fashion that provides additional ductility. The latter approach was selected for this work.

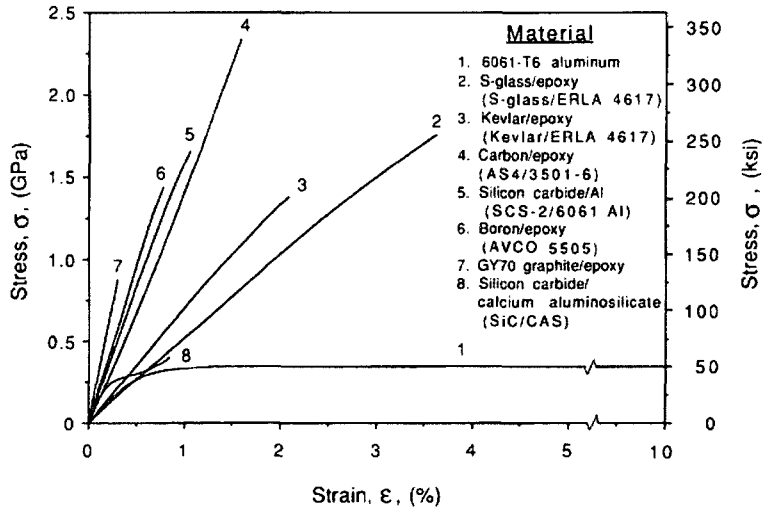

Figure1.3 - Elastic Behaviour of Composites [4]

Figure 1.4 - Mechanical Behaviour of Structural Steel [5]

1.2 Research Approach

Prior research conducted at the University of Ottawa [6] was directed towards creating a fibre composite rebar that would have the same tensile stress-strain response as steel, which is displayed in Figure 1.4. This means that the fibre composite rebar would possess comparable elastic modulus, yield strength, and ductility, and thereby be able to be used commercially without modifying current design codes. This type of composite would use traditional fibres, carbon and aramid, but would arrange them in such a way that complete failure would not occur suddenly with no warning. The rod developed consists of two fibre layers embedded in epoxy; the inner carbon fibre composite provides most of the stiffness and strength, while the outer layer is made of aramid fibres in epoxy. Even though these fibres are only able to elongate through an elastic manner and fracture after the strain reaches a few percent, the perceived ductile response (pseudo-ductility) is instead obtained by the sliding of the outer layer with respect to the inner carbon fibre composite. At a desired yield stress level, the outer layer will separate from the carbon fibre core and slide, where the friction from this motion prevents sudden failure from occurring. A more complete description of this composite and its design can be found in Section 2.1.2.

With this new composite design, an additional challenge arises on how to manufacture the rods so that the product is both functional and economical. The selected method was to modify a well known composite production process, pultrusion, so that the

outer layer breaks away from the inner core at a quantifiable level of stress and that the desired outer-layer sliding can occur. Therefore, the epoxy that serves as the matrix for this composite must be cured in a short time period (similar to pultrusion). It is for this reason that the use of a two stage heating cycle is critical to achieve proper curing. To have a strong control of the curing process, small diameter steel wires are embedded in the carbon composite core so that the first stage induction heating can be used to cure the core. After the induction heating phase, the rod passes through conventional furnaces that heat the outer layer, curing the remaining epoxy resin. Additional information about the production process and the unique heating requirements can be found in Section 3.1. As there are two forms of external heating, as well as epoxy's exothermic reaction, the production process' variables must be carefully calibrated to ensure the composite is sufficiently cured prior to exiting the production process.

1.3 Thesis Objective

The intent of this thesis was to develop a parametric heat transfer model for successfully producing the pseudo-ductile composite rods, so that they exhibit the desired mechanical properties while being produced as fast as possible. The selected parametric model variables were chosen based on how this composite's current production process could be modified; the parameters modified in this thesis include varying the location of the steel wires, the settings of the furnaces and induction coil, the fibre volume fraction, and the production rate.

Specifically, the interest is focused on how the epoxy is cured. To reach this goal, experiments were conducted to observe how heat was generated and transferred during curing, as well as how the induction coil interacted with the embedded steel wires. These results were compared with a Finite Element Analysis model that simulated the rod's curing as it progressed through production. This Finite Element model was then used to predict changes in parameters that would optimize the production of rods efficiently and effectively.

Chapter 2

Literature Review

2.1 Fibre-Reinforced Plastic Composites

Fibre composites are used in many different applications, such as in surfboards and other sporting equipment as well as structural components for aircraft. This diverse range of applications stems from the ability to customize the composite's properties from those of the constituent combination materials used and in what ratio they are combined. The use of high performance fibres, such as glass or carbon, and polymers produces a material that has exceptional mechanical strength, strong chemical resistance, relatively low density, and can be manufactured conveniently. The typical drawbacks for these materials are lower ductility and higher cost than the materials they replace.

2.1.1 Mechanical Property Discussion

Composite materials are composed of two or more distinct materials whose overall properties are more desirable than obtained by using a single material; these properties are strongly dictated by how the composites are assembled. In most cases, a composite consists of two constituents: a reinforcement that provides the strength and stiffness and a matrix that binds the reinforcement together. Reinforcement materials can be embedded into the matrix as either particles or fibres; however, in both situations, the reinforcement's task is to carry a sizable portion of the load. Of the two forms of reinforcement, fibre reinforcements provide a more significant improvement in strength and stiffness, provided the fibre length is sufficient.

In order to obtain the maximum reinforcement effect from the fibres, the external stress applied to the matrix must be properly transferred to the fibres. The ability to transfer this stress depends upon the strength of the interface between the two components of the composite, the surface area, and the tensile strength of the reinforcement. As the strength of the interface and diameter of the fibre are not easily changed, the length of fibres is instead modified to control the composite's performance. A relationship that relates the critical length (l_C) with the fibre's strength and diameter, along with the interfacial bond strength, follows [7]:

$$l_C = \frac{\sigma_f^* d_f}{2\tau_C} \tag{2.1}$$

When a fibre is used that has a length equal to the critical length, the maximum tensile strength of the fibres is achieved but only at the centre of the fibre. This effect can be seen in Figure 2.1.a. As the length of the fibre is increased beyond the critical length, more of the fibre length can carry the full tensile strength of the fibre, thus making the composite stronger. This is illustrated in Figure 2.1.b. In contrast, the loading conditions of a fibre that has a length below the critical length can be seen in Figure 2.1.c. By having shorter fibres, the performance of the fibres is less than optimal and is similar to that provided by particle reinforcements.

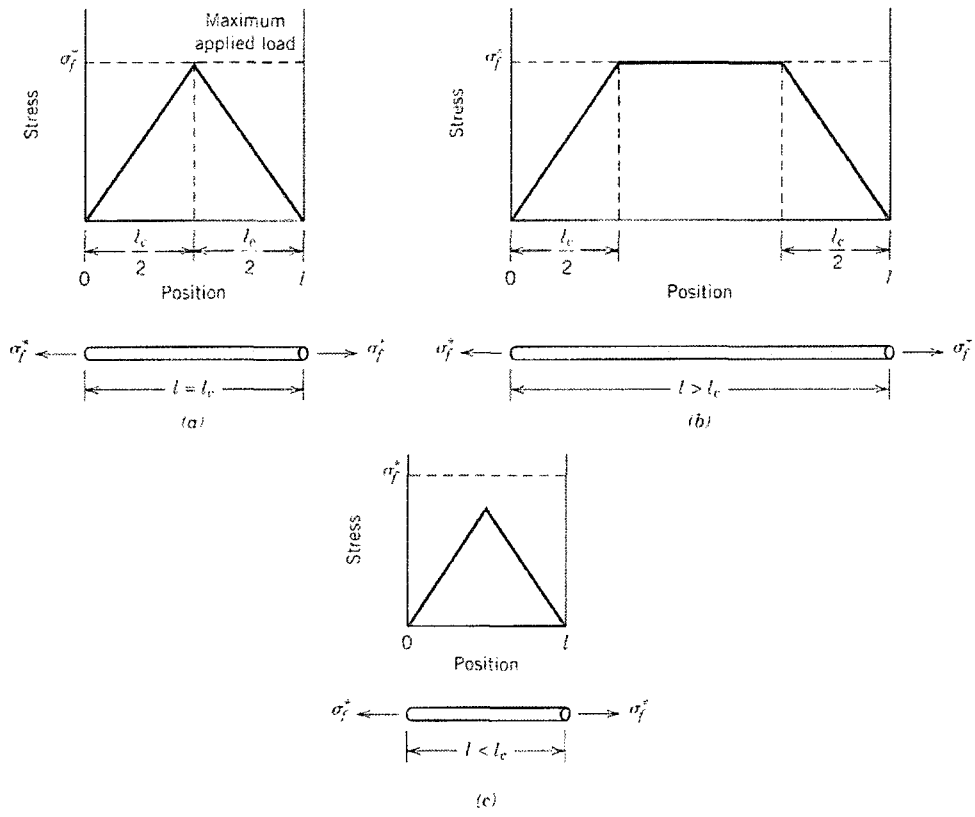

Figure 2.1 - Fibre Length Effect on Stress Transfer[8]
a) length of fibre is equal to critical length
b) length of fibre is above critical length
c) length of fibre is below critical length

In order to achieve the maximum performance of the fibres, the fibres should be as long as possible to have nearly the entire fibre length at the fibre's maximum tensile strength. Thus at a length of approximately fifteen times the critical length, the reinforcement is considered continuous; below this value, the reinforcement is considered discontinuous. When continuous fibres are used, the longitudinal tensile strength of the composite can be estimated by the following equation [7].

$$\sigma_C = \sigma`_M V_M + \sigma`_f V_f \tag{2.2}$$

The above equation uses the Rule of Mixtures which states that strength of the final composite is proportional to the volumetric weighted stress in the matrix and the strength of the fibre reinforcement. This principle can used for other mechanical properties of composites and thus can be applied to the tensile longitudinal elastic modulus of the composite, as can be seen with the following equation [7].

$$E_C = E_M V_M + E_f V_f \tag{2.3}$$

The Rule of Mixtures also works for the thermal properties of composites, with the exception of thermal conductivity. The Rule of Mixtures does not apply to conductivity because the rate at which the heat is conducted also depends on how the composite is constructed. For example, unidirectional carbon fibre, which has a very high conductivity, can conduct heat just as rapidly along its fibres whether it is enclosed in a thermoset or not. There have been several models created to predict a composite's conductivity based the properties of the constituents of the composite, as well as how the composite is fabricated. One study that reviewed various composite thermal conductivity model [8] found that the Lewis and Nielsen Semi-Theoretical model was the most successful at predicting the conductivity of a composite for a variety of matrix and reinforcement arrangements. The Lewis and Nielsen equation is displayed below along with its supporting equations [8].

$$k_e = k_c\left[\frac{1+AB\phi}{1-B\phi\psi}\right] \tag{2.4}$$

$$A = k_{en} - 1$$

$$B = \frac{\frac{k_d}{k_c} - 1}{\frac{k_d}{k_c} + A}$$

$$\psi = 1 + \left(\frac{1 - \phi_m}{\phi_m^2} \right) \cdot \phi$$

As mentioned previously, high-performance composites gain almost all of their stiffness and strength by having strong fibres that carry the load, while the purpose of the matrix is generally to align the fibres in the proper direction and to protect them. Since these fibres are brittle, a composite will fail suddenly when it reaches its ultimate strength. However, when subjected to this failure load in tension, there are three different ways a composite can fail. As seen in Figure 2.2, the composite can fail in a purely brittle fashion (part a). Yet, there is also the possibility that, when the composite fails, some of the fibres will separate from the matrix and pull out. The third method of failure is when the matrix breaks before the fibres do and debonds from the fibres. Which failure method that occurs depends strongly on the volume fraction. At lower volume fractions, a simple brittle fracture is the most likely failure, while at moderate fractions, pullout is most common. At even higher fibre volume fractions, matrix failure is the dominating mode of failure [9]. However, this trend does not apply for carbon composites, as they rarely fail by debonding or matrix failure; this phenomenon occurs because the fibres are more prone to fail than the matrix [10].

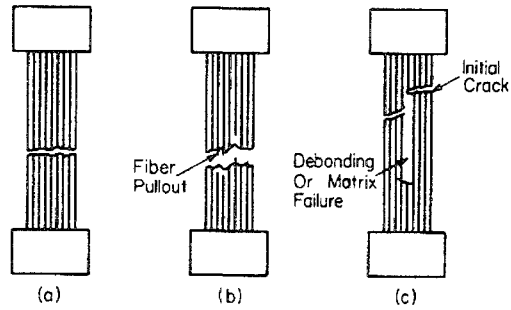

Figure 2.2 - Failure Mechanisms of Composites [7]:
a) brittle fracture b) fibre pullout c) debonding and/or matrix failure

2.1.2 Fibre Composite Rebar

For the advantages mentioned previously in this section, fibre composite materials offer attractive properties for a rebar replacement. In Table 2.1, a comparison of steel and carbon FRP (Fibre Reinforced Plastic) is presented. From this comparison, it can be seen that the range of strength and stiffness properties of carbon fibre composite includes those values for steel and thus a direct replacement is possible. While the composite's strength at

elevated temperature suggests some concern, the main obstacle for a composite rebar is minimal ductility. Since the repair cost of steel rebar in concrete for bridges and other large structures is expensive, a promising candidate to replace steel rebar would be one that has similar ductility as well as comparable yield strength and elastic modulus.

Property	***Steel***	**Carbon FRP**
Tensile Modulus (GPa)	206	13 - 520
Yield Strength (MPa)	250	N/A
Ultimate Tensile Strength (MPa)	400 - 550	64.19 -2100
Ductility	20 %	<3.5%
Temperature Resistance	Maintains strength up to 400 °C	poor
Corrosion Resistance	low	high

Table 2.1 - Comparison between Steel and Carbon Fibre Composite [11]

In the work by Ewen [6], a fibre composite rebar that exhibits displays a stress-strain curve that resembles ductile behaviour when a tensile load is applied was presented. This composite is in the shape of a rod and is comprised of a carbon FRP core covered with a thin braided aramid FRP overwrap. Despite both FRP's lack of ability to yield, the composite is able to behave in a ductile manner by having the overwrap detach from the core and slide along it. This behaviour is referred to as pseudo-ductile behaviour since it comes from the material's structure instead of an innate property.

The original design of the pseudo-ductile rod is comprised of a thirteen millimeter diameter carbon fibre composite rod with a one millimeter thick aramid fibre over-wrap, which results in a rod with a total outside diameter of fifteen millimeters. However, it is likely that this rebar would be produced under a range of diameters, with a maximum diameter of twenty-five millimetres. In this situation, the aramid layer would remain one millimeter thick, while the carbon core would enlarge to twenty-three millimetres. The aramid fibre over-wrap is braided at forty-five degrees and is comprised of Kevlar^{TM} 49 fibres. The matrix of this composite is an epoxy, the resin being Epon^{TM} Resin 826 with the hardener being LS-81K anhydride curing agent, manufactured by Itexian and Lindau Chemicals, Inc., respectively. Figure 2.4 contains an image of the composite after processing. This formulation of epoxy was selected due to its desirable properties – both mechanical and chemical – along with its short curing time at elevated temperatures. A

modified pultrusion process was selected to produce this composite. Pultrusion is used to produce high quality fibre composites continuously with minimal downtime. The pultrusion process is discussed in the next section, along with a discussion of common modifications.

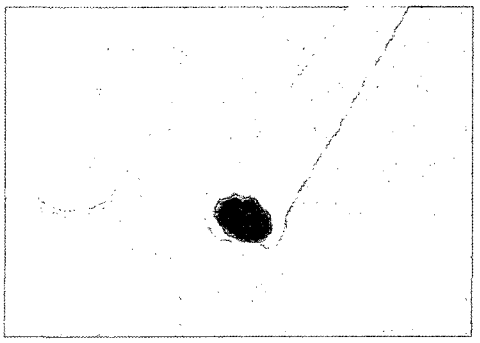

Figure 2.3 – Sample of Composite Rebar

2.2 Pultrusion Process

Pultrusion is a method of continuously manufacturing a fibre composite that has a constant cross-section; shapes such as rods, tubes, and bars are the typical products of the pultrusion process. However, complex shapes can also be made with pultrusion. At the turn of the century, pultrusion processes were producing 5.5 million tons of composite a year, valued at roughly 140 million USD, with strong projected growth [9]. This growth in pultrusion products is being fueled by innovations that expand the variety of products that can be made with this process. An example of a commercial pultrusion process is displayed in Figure 2.4. Fibre composites that are made from pultrusion generally have a thermoset resin matrix and can have a fibre volume fraction of up to 70% which is high compared to other continuous processes. While the pultrusion process has been successfully modified to adapt to different manufacturing needs, several limitations remain. Thermosets that do not produce a condensation by-product are applicable – notable examples are polyester and epoxy. There has been limited success with making pultruded parts with thermoplastics. As a consequence of their much higher viscosity, special impregnation equipment is required [12].

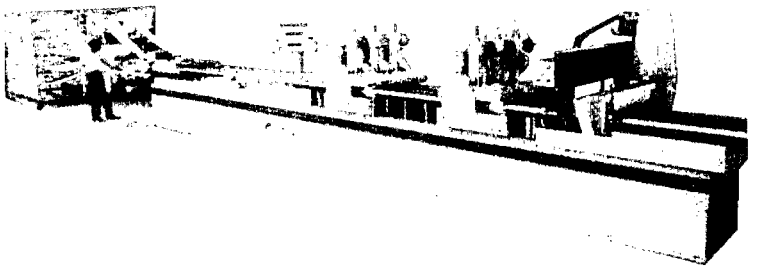

Figure 2.4 - Commercial Pultrusion Process [14]

2.2.1 Description of Process

A Pultrusion machine is typically composed of six elements: creel, resin wet-out tank, forming dies, heated matched metal die, puller, and cut-off saw; Figure 2.5 presents an illustration of how these pieces are arranged. The creel's purpose is to house the dry fibres and to allow them to be used at the proper time. As such, it is simply constructed, usually as metal shelves that the fibre spools are attached to. Once the fibres leave the creel they arrive at the resin wet-out tank. At this station, the fibres are exposed to the polymer that will become the composite's matrix. To ensure that the all fibres are wetted, this station typically involves a series of aluminum rolls that force the fibres into the polymer bath. An alternative method to removing excess resin is to use a specialized comb structure for the fibres to run through prior to being cured [13].

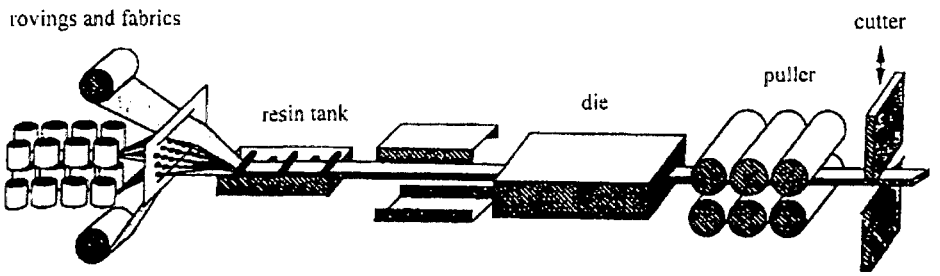

Figure 2.5 - Basic Pultrusion Process [16]

Once the fibres are wetted, they are carried to the molding station which cures the polymer into the desired shape through the use of a heated die. The heated die is typically made of highly polished steel and is held at a temperature of between 120 to 150 °C depending on the polymer. Heating can be provided by several different methods ranging from heated oil to induction heating. In many situations, the die is chrome plated to enhance

wear and corrosion resistance [14]. In addition to the temperature at which the polymerization reaction commences, the curing rate also depends strongly on the amount and type of catalyst that is used with polyester resins.

Before the cured composite is cut into desired lengths, it passes through the puller station, which provides the force required to drive the process. This puller usually consists of caterpillar belts that grip onto the composite and pull it forward. At the end of each pultrusion production line is a cut off saw that cuts the product into specific lengths. As cutting fibre composite parts wears tools very quickly, the saw is either made with an abrasive wheel or diamond blade. Water cooling the saw is advisable for both the saw's sake as well as the pultruded part, since both can be damaged with the heat created while sawing. Since this cut must be made during continuous production, the saw is attached to a set of wheels that move it at the same rate as the puller [13].

2.2.2 Process Modifications

Due to the pultrusion process' excellent initial success with producing fibre reinforced thermoset slab composites at an acceptable cost, there was a strong demand for this process to be modified to allow it to produce many other products. Figure 2.6 presents a pultrusion process that exhibits several modifications. These modifications can be implemented to allow for a different product to be manufactured or to improve productivity.

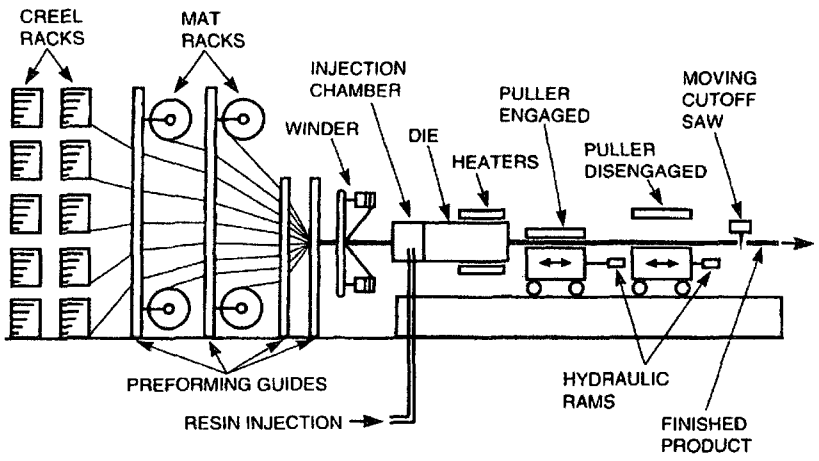

Figure 2.6 – Robust Pultrusion Process [15]

One of the first modifications that were made to a pultrusion line was to allow for the process to manufacture composites tubes and other hollow products. This is achieved by

having a mandrel inserted in the pultrusion line that extends into the heated die. As the fibres are laid down from the creel, they are positioned onto the mandrel before being wetted by the resin. As the uncured composite passes through the heated die, its inside surface cures in the shape of the mandrel. To ensure a proper finish on the inside surface, the mandrel must encompass the entire length of the heated die and an additional a half metre thereafter [13]. An example pultrusion process with mandrel is displayed in Figure 2.7.

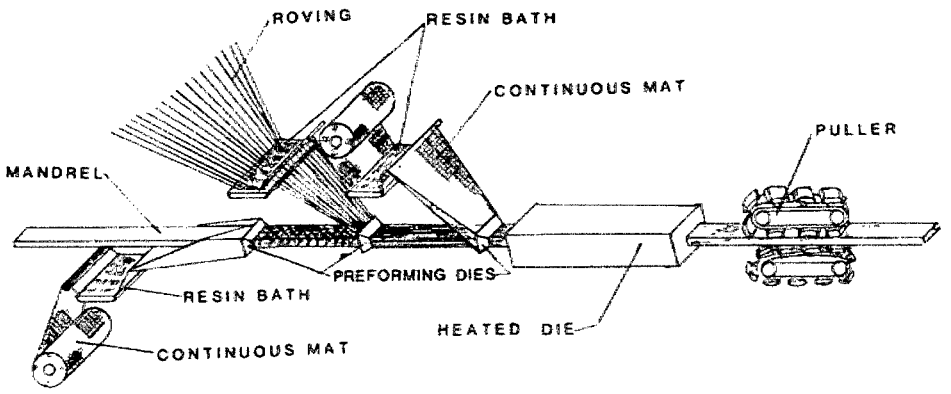

Figure 2.7 - Hollow Pultrusion Process [13]

The pultrusion process has also had modifications that have been made to heat the resin. One heating variant to complement the heated die is to pre-heat the fibres on their way towards the die. The benefit of pre-heating is that it reduces the amount of heating required by the die, as an excessive die temperature must be avoided to prevent overheating of the surface which will cause the resin to burn or otherwise be chemically compromised. This is of significant concern when manufacturing thick composite pieces where the surface temperature can be much higher than the internal temperature. An extension of the pre-heating application can be used as a total replacement of the heated die. For this heating method to be practical, the heating settings much be carefully arranged to ensure that the composite forms at a very specific location in the line. Even if it is possible, the primary caveat of this modification is that setting up a preheating apparatus is a much more expensive proposition than using a heated die, thus it is only applicable for those composites where a die is not an option [15]

A relatively new and more radical modification of heating the composite during the pultrusion process is the use of microwave heating. While typically more expensive to install than a heated die, microwave heating generally results in a completely cured product

at a faster rate. This benefit is obtained because the microwaves are able to penetrate the surface of the curing composite and provide volumetric heating. For additional information about microwave heating and its benefits in the pultrusion process, see Section 2.5.

2.2.3 Modeling Pultrusion Process

Due to the desire to optimize the pultrusion process, both for quality control and for minimizing production costs, computer models to simulate the pultrusion process have been developed by researchers [17-22]. The primary focus of this research is to better understand where and how the thermoset cures during the pultrusion process. The curing of the thermoset is important because, if the pultrusion process does not cure the composite sufficiently, the resulting product may exhibit diminished mechanical properties. This modeling of curing is achieved by simulating the heat transfer within the composite as it passes through the heated die. Since the resins that are cured in the pultrusion process are highly exothermic, there is a direct relationship between amount of heat released and the percentage of cure. By optimizing the curing of the thermoset, the pultrusion line ultimately can become more efficient by producing the product at the optimal rate, all the while using only the minimum required amount of energy.

Another area of interest in pultrusion research is the evaluation of the design and construction of the heated die. The heated die is the primary source of heat in pultrusion but it is not the only source, as the curing of thermosets releases a sizable amount of heat. Since thermoset resins have a low thermal conductivity, it is possible to overheat the composite during curing, thereby damaging it; some thermosets will burn at temperatures below 300 °C. Thus, it is imperative for die designers to understand how the composite is heated to prevent overheating. While designing the die, the primary parameters to study are the composition of the die, shape, thickness, and amount of input heat.

Finally, a third area of interest for the modeling of the pultrusion process is the formation of thermal residual stresses that develop during manufacture. These stresses are significant since any manufacturing stress that remains in the composite may affect its shape and behaviour. While residual stresses form in the processing of metals such as casting, welding, machining and cold working, such residual stress can be relieved during annealing. This heat treatment cannot be done with thermoset composites. Thus the proper evaluation

of the residual stress that forms during the process is important to predicting the composite's performance.

Thermal stresses develop in pultrusion due to the chemical reactions and heating that occur as the composite passes through the heated die. The type and cause of these thermal stresses depend on where the uncured composite is within the heating stage, each representing a different section. The first section is where the resin wetted fibres first come into contact with the die which causes the uncured composite to heat up. By heating the resin, it expands and causes the hydraulic pressures against the fibres and die to increase, acting as a thermal stress. The second form of thermal stress becomes a factor once the thermoset starts to cure which causes it to expand further and thus creates further pressure upon the die. The pressure on the die can induce significant friction between the die and the composite, requiring the puller to apply additional force to maintain the process. This pressure subsides only at the last section of the heating, where the composite begins to cool down, causing the thermoset to shrink and tighten its grip around the fibres [16].

2.3 Available Polymerization Models

One of the main advantages of using the pultrusion process is the ability to rapidly cure the composite in the heated die; typically the cure takes one to three minutes. The traditional matrix used in fibre reinforced plastics is thermoset polymers, although recently there has been much success in using thermoplastic polymers. The primary motivation for using thermoplastic matrices stems from their excellent formability which allows thermoplastic composites to be manufactured by only slightly modifying standard molding equipment. Even though manufacturing with thermosets requires specialized manufacturing procedures to allow proper polymerization with the fibres, the extra cost and effort is offset by their superior physical properties, both before and after curing. These properties range from higher mechanical strength and elastic modulus to lower viscosity during processing which allows for greater wetting of the fibres [23].

During manufacturing of thermoset composites, the thermoset polymerizes or crosslinks. When modeling the curing kinetics of a thermoset polymer, there are two groups of models that are employed: phenomenological and mechanistic [24]. Phenomenological models are developed by analyzing the experimental data and developing an equation that

fits the result accurately. While these models tend to give a mathematical model that follows the results well, the resulting equations have little to no physical relationship with the chemistry at hand and thus are somewhat incomplete. Conversely, mechanistic models focus entirely on which chemical reactions take place within the thermoset and develop equations based on them. While this approach does well to predict the various byproducts that are produced during curing, the actual curing rate predicted by mechanistic models generally does not fit well with experimental results. This lack of fit is caused by the complexity of the reactions that take place where the modeling of each individual reaction results in some errors that carry over to the final model.

Within each model group, there are various approaches these models select, depending on which specific aspects of the curing process are focused upon. In this thesis, the more commonly used models are presented, these being Nth Order & Autocatalytic [7,25-28], Loos-Springer [29-31], and Horie mechanistic model [32]. Additionally, the less popular curing models are grouped together and presented in the final section[27,33-35].

2.3.1 Nth Order & Autocatalytic Model

The Nth order & Autocatalytic are two separate models for predicting the curing of a thermoset resin. However, since they are commonly found together in the same papers [25,26], they are thus grouped together for the purpose of this literature review. The first component of this model, the Nth Order model, is strictly a phenomenological model. This model was developed on the basis that the curing rate is proportional to the concentration of the uncured epoxy. This concept combined with the Arrhenius equation yields the following equation [26]:

$$\ln\left[\frac{d\alpha}{dt}\right] = \ln(A) - \frac{E_a / R}{T_{ref}} + n\ln(1-\alpha) \tag{2.5}$$

The key problem with this equation is that the maximum rate of cure is calculated at the start of cure ($\alpha = 0$) and diminishes progressively as the curing continues. This is contrasted by experimental results that observe maximum curing to occur between 30 to 40 percent of total cure ($\alpha = 0.3$ or 0.4) [26].

As the Autocatalytic model looks at the chemistry part of the analysis, it is considered a mechanistic model. Thus, the emphasis of this model is to properly understand

the different reactions that occur during curing and assign a kinetic relationship accordingly. The Autocatalytic model for epoxy curing contains three reactions that occur during curing [26]:

$$a_1 + e\frac{K_1}{K_1'} \rightarrow a_1 + OH \tag{2.6}$$

$$a_2 + e\frac{K_2}{K_2'} \rightarrow a_3 + OH \tag{2.7}$$

$$OH + e\frac{K_3}{K_3'} \rightarrow et + OH \tag{2.8}$$

From these reactions, a set of equations can be derived to determine the rate of cure. The master expression that takes into account all the variables of the autocatalytic model can be seen below [27].

$$\frac{d\alpha}{dt} = \left[\frac{2(1-n)\varphi + n\varphi^{n/2}}{2-n} + LF(\varphi)\right](1-\alpha)\times[k_1 + k_2F(\varphi)] \tag{2.9}$$

$$\varphi = a_1/e_0;\ k_1 = e_0K'_1;\ k_2 = e_0{}^2K_1$$

$$F(\varphi) = 1 + \frac{[OH]_0}{e_0} - \frac{[(1-n)\varphi+\varphi^{n/2}]}{(2-n)} \tag{2.10}$$

Due to the complexity of the above equation, suitable simplifications are very desirable. The various simplifications that are made to the autocatalytic model depend strongly on the circumstances of the reaction, generally based on the chemistry of the reactants or the temperature of the reactants during curing. One such simplification, where the initial impurity concentration is negligible, is to assume that no ether is produced, and the two anime products are produced in the same ratio, reduces the previous cumbersome expression to the following [26].

$$\frac{d\alpha}{dt} = (1-\alpha)^2(k_1 + k_2\alpha) \tag{2.11}$$

Despite their differences, as each model develops from different approaches, these two models are often used together. When this is the case, the Nth order model is used to develop master thermal curves for the autocatalytic model. The autocatalytic model is then used to provide greater detail to the curing characteristics for a specific thermal curve.

2.3.2 Loos-Springer Equations

The Loos-Springer model is a phenomenological model that, like the Nth order model, is derived from the Arrhenius equation. The rate of cure is proportional to the amount already cured, though this model utilizes two equations in order to avoid having the curing rate slow down as the reaction progresses. By breaking the equation up into two parts, the formulae generate the maximum cure rate near 30% of cure. These equations work with rate constants (K_1, K_2, and K_3) that are derived from the Arrhenius equation. The two equations follow [36].

$$\begin{aligned} d\alpha/dt &= (K_1 + K_2\alpha)(1-\alpha)(B-\alpha) && \alpha \leq 0.3 \\ d\alpha/dt &= K_3(1-\alpha) && \alpha > 0.3 \end{aligned} \tag{2.12}$$

$$K_x = A_x exp\left(\frac{-\Delta E_a}{RT}\right) \tag{2.13}$$

In order to implement the Loos-Springer model, the Activation Energy (E_x) and Reaction Constant (A) must be known. The most accurate method for gathering this data for a particular reaction is having the epoxy cure within a Differential Scanning Calorimeter (DSC). This machine measures the change in temperature very accurately while the epoxy cures, thereby determining how much heat is released during cure over different intervals of time. This data allows one to determine the proper Activation Energy and Reaction Constant for the reaction.

2.3.3 Horie Mechanistic Model

This model focuses on the reactions with any hydrogen-bond donor molecule [HX] – generally a hydroxyl group – that acts as a catalyst for the ensuing epoxy reaction. There are four main reactions that this model employs to determine the reaction kinetics [37]:

$$a_1 + e + (HX)_A \xrightarrow{k_1} a_2 + (HX)_A \tag{2.14}$$

$$a_1 + e + (HX)_0 \xrightarrow{k_1'} a_2 + (HX)_0 \tag{2.15}$$

$$a_2 + e + (HX)_A \xrightarrow{k_2} a_3 + (HX)_A \tag{2.16}$$

$$a_2 + e + (HX)_0 \xrightarrow{k_2'} a_3 + (HX)_0 \tag{2.17}$$

From these reactions, a series of equations are developed, ending with a formula to determine the conversion of the epoxide group. From this relationship, the rate of cure can be determined with the following equation:

$$\frac{d\alpha}{dt} = k_1 a_1 e_X + k_1' e_0 + k_2 a_2 ex + k_2' e_0 \tag{2.18}$$

$$X = (a_0 / e_0)(q_1 + q_2) \tag{2.19}$$

Like the Loos-Springer model, DSC experiments are required to gather the necessary variables for the model. An extension of the Horie model has been developed by Cole [38] in which the ether reactions have been included. Ether reactions start to influence the epoxy curing above a curing temperature of 150 °C, though their effect on the curing process is typically minimal for most epoxy mixes.

2.3.4 Miscellaneous

In addition to the five models mentioned above, several other models have been developed. Typically, these models differ from the previously noted models since they have very good accuracy for only a specific situation or desired product. Thus, it is common for these models to only be used by the same group that developed the model since the model's criteria are only satisfied by that group. One such model is the St. John and George method [33], where the formulation is mainly focused on the consumption of the primary amine.

$$\frac{d[PA]}{dt} = k_1[EP][PA]^2 + k_{2a}[PA][E0][OH] + k_{2b}[PA][E1][OH] \tag{2.20}$$

Salla and Ranis [29] compare the analysis of the autocatalytic approach to two methods, Ozawa and Kissinger. During the comparison, the authors make the concession that there exist several different approaches because they all have strengths and weaknesses to how they model the polymerization. Thus, a wide variety of polymerization models are available since each model suits a particular reaction. For the Ozawa and Kissinger methods, the conclusion was that both approaches provide a similar value to the autocatalytic approach with less experimental analysis. Ozawa's rate equations are as follows:

$$g(\alpha) = \int_0^\alpha \frac{d\alpha}{f(\alpha)} = \frac{k_0}{\phi}\int_0^T e^{-(E_a/RT)}dT \tag{2.21}$$

$$\log\phi = A' - \frac{0.4567E_a}{RT} \tag{2.22}$$

The basis for the Kissinger's model is to connect the maximum reaction rate with the exothermic peak. This connection simplifies the experimental data required to determine the kinetic behaviour of the thermoset. However, because of this assumption, this model is limited to those reactions that develop a strong exothermic peak and displays characteristic

behavior afterwards. The following equation can be used in conjunction with other models to determine the total reaction time.

$$\ln\left[\frac{\phi}{T_P^2}\right] = \ln\left[\frac{k_0 R}{E_a}\right] - \left[\frac{E_a}{RT_P}\right] \tag{2.23}$$

2.3.5 Selected Model

For this work, the phenomenological approach was selected mainly because the rate constants for the mechanistic approach were much more difficult to obtain. The purpose of the finite element model is to simulate the curing rate of the matrix, which is best handled by phenomenological models. The model created by Loos-Springer, which is introduced in Section 2.3.2, was followed since this model was developed under a similar situation as in this thesis. However the required data from a Differential Scanning Calorimeter was unable to be obtained and therefore a simplified derivative of the Loos-Springer model was developed using the approach described in Chapter 4.

2.4 Challenges of Fabricating the Fibre Composite Rebar

The chosen rebar design differs from most commercially available fibre composite rebars in the method of transferring the shear stress between the concrete and the outer surface of the rebar. Most commercial designs use a sand coating as the surface of the rebar that is applied to the smooth surface of the pultruded rebar. In contrast, the chosen design utilizes a braided overwrap for this stress transfer. The resin in this braided overwrap is cured at the same time as the resin in the core. Thus, pultrusion in the classical sense – smooth heated dies – cannot be used. For this work, the initial approach was to use a series of tunnel furnaces to replace the heated die. The braiding head would apply the overwrap prior to carbon fibre core entering the furnace. At the maximum speed of the braiding head, the speed of the rebar through the oven would be approximately 0.7 metres per minute. Since the rate of heat transfer by natural convection in the furnace would be significantly less than the conduction rate for the heated die in conventional pultrusion, additional heat sources for curing were investigated as discussed in the following sections.

2.5 Microwave Heating

One alternative method of heating polymers and composites is microwave heating. This form of heating operates by projecting microwave radiation towards a polymer, whereby the waves interact with the polymer molecules, causing them to heat up. However, unlike conventional methods of heating objects through their surface, the microwaves penetrate the surface and create volumetric heat. This phenomenon is highly attractive in manufacturing composites because it gives a nearly uniform heating profile and thus reduces the possibility of residual stresses forming. This attractive heating profile is in addition to noticeably short curing durations that have been observed by several researchers [39].

Microwaves are electromagnetic waves that have a frequency between 0.3 to 300 GHz. This frequency range is useful for heating because it is high enough to have deeper penetration than shorter wavelength electromagnetic waves, yet does not cause bond cleavage. Once these waves penetrate the object, they are absorbed and quickly dissipated [40]. Microwave heating has been used in a wide range of applications: food tempering, pre-heating for rubber vulcanization, drying, cooking, pasteurization, sterilization, puffing, timber manufacturing, and processing of wastes. However, for the general public, the most familiar application, by far, deals with the heating of food products [41].

Microwave radiation has been used to cure thermoset polymers. In one such work that dealt with using microwaves to cure thermosets [27], the work sought to relate the curing rate obtained from microwave heating with a similar rate from thermal heating. This study involved curing samples of DiGlycidyl Ether of Bisphenol-A (DGEBA) epoxy resin by either thermal heating or microwave heating, with the temperature measurements made in a DSC: the curing agent of these samples was either 4,4' Diamino-Diphenyl-Methane (DDM) or meta-Phenylene-DiAmine (mPDA). Overall, the results presented in this document favoured microwave heating to conventional heating when comparing the amount cured over a finite amount of time. From this study, it was presented that even when both forms of heating brought the epoxy samples to the same internal temperature, the actual curing rate obtained in the one heated with microwave radiation was significantly faster. One example given in the paper suggested that despite the thermoset reaching only 130 °C for a brief interval, it had an effective curing rate as though the reaction was taking place at 170 °C.

A second study [42] also involved epoxy cured with microwaves. The purpose of this research was to compare the mechanical properties of several epoxy-anhydride resins, each having samples that were cured with either microwaves or standard thermal heating. Like the test mentioned above, this series of experiments involved DGEBA epoxy, though the seven different hardener and accelerant combinations were different. As can be seen in Table 2.2, the samples that were cured with microwave radiation were cured to a comparable degree as the thermal heated ones, despite being heated for only a fraction of the time, as illustrated in Table 2.3. Despite curing much faster, the article's evaluation of the mechanical properties test indicated that there generally is little lost in strength or stiffness by curing epoxy with microwave radiation. However, a few resin-hardener combinations did show noticeable weakening when cured with microwave heating. Therefore, before replacing conventional curing techniques with microwave heating, care must be taken that the epoxy used in the process cures properly.

Extent of Conversion of the Cured Samples				
	1% Accelerator		4% Accelerator	
Resin	Microwave (%)	Thermal (%)	Microwave (%)	Thermal (%)
II	97	90	97	97
III	~100	93	~100	97
IV	96	82	~100	~100
VI	95	95	98	97
VII	~100	~100	99	96
VIII	99	97	98	99

Table 2.2 - Percentage Cured for Thermal and Microwave Heating [42]

Effective Time for Curing				
	1% Accelerator		4% Accelerator	
Resin	Microwave (min)	Thermal (min)	Microwave (min)	Thermal (min)
II	6	20	6	14
III	4	20	4	14
IV	4	20	4	14
VI	6	20	6	14
VII	4	20	4	14
VIII	6	20	6	14

Table 2.3 – Curing Time for Thermal and Microwave Heating [42]

While still not a common modification, pultrusion processes have been fitted with microwave heating with good results [43]. The tests discussed in the article were focused on manufacturing glass fibre reinforced composites solely using microwave heating, though other experiments have been made using a combination of microwave radiation and a heated die. When solely using microwave radiation as the heat source, a microwave transparent die is used to obtain the desired shapes.

While microwave heating typically offers faster curing over conventional heating, its use depends on the thermal properties of the composite. The primary obstacle for implementing microwave heating in pultrusion is the high cost associated with integrating the equipment into the production line. Thus, cost-benefit calculations must be made. An equation that quantifies a thermoset's ability to be cured by microwave heating follows [43].

$$m = \frac{2\pi f \varepsilon_0 \varepsilon'' E^2 x^2}{k\Delta T} \tag{2.24}$$

For microwave heating to be a benefit, the microwave heating index (m) should be as high as possible. Therefore, microwave heating is the most effective when dealing with thick objects that have low thermal conductivity and a high dielectric loss factor. Since the majority of composites involve materials that have low conductivity and high dielectric constants, this formulation supports other researchers efforts to use microwave heating for processing thermoset composites. Even more so, as the thermoset resin cures, its dielectric loss factor reduces which causes less cured regions of the composite to absorb the radiation more than cured regions and thus to cure faster. This phenomenon helps to explains why microwave heating exhibits a near uniform heating profile. As the paper clearly states, this selectivity is nearly impossible to achieve with conventional thermal heating [43].

2.6 Induction Heating

An alternative form of heating through electromagnetic waves is induction heating which utilizes the Joule effect during the absorption of these waves to generate heat. This form of heating is used to greatly increase the temperature in the desired object by inducing an electrical current within it; this electrical current is caused by a primary electrical current that runs near the workpiece. As the induced current travels throughout the work piece, the material's inherent resistance transforms the flow of electrons into resistance heat. There are

several advantages of using this process in industry, such as its efficient ability to heat an object, the low start-up energy required for processing, high heating intensity, and fast production rates. As such, induction heating has found its way into many applications. However, it is not without disadvantages, as it almost always requires a ferromagnetic material to properly absorb the electromagnetic waves. Additionally, the initial costs to setup an induction heating in an industrial setting are quite high; however this is offset by lower operating costs from to the process' higher efficiency [44].

2.6.1 Background Theory

In the early 19th century, Hans Christian Oersted discovered that an electrical current could influence a magnetic field. This effect was observed when he placed a live wire near a compass. When the wire was placed sufficiently close to the compass, the needle would veer from its natural north position to a direction dictated by the direction of the current. At the time, Oersted concluded that as an electrical current travelled through a wire, it would broadcast a magnetic field [45]. Approximately a decade later, in 1821, Michael Faraday further investigated the magnetic effect of electricity with his own experiments; these experiments involved an iron rod that had two wires coiled around it. When an electric current passes through one of the wires, a voltage developed in the second wire, which was observed by an attached voltmeter. This phenomenon was caused by the electrical current in one wire inducing a current in the second one [46]. These two discoveries helped lay the foundation for induction heating.

When an electrical current passes through a wire, it emits a magnetic field. When the wire is coiled along a specific direction, as seen in Figure 2.8, the magnetic field orients itself in a direction based upon the direction of the current and the wind of the coil; the direction of the magnetic field can also be seen in the figure. If this magnetic field comes in contact with another object, an electrical current is induced. The majority of the current that is generated through inductance is in the form of eddy currents. Eddy currents are caused through the interaction of a conductor and magnetic field where one is moving. These currents do not travel in any specific direction and are desirable in this application because they are quickly converted into heat through the material's electrical resistance or by the

Joule effect. Since Eddy currents are a vital part of induction heating, an alternating current is used to power an induction coil [46].

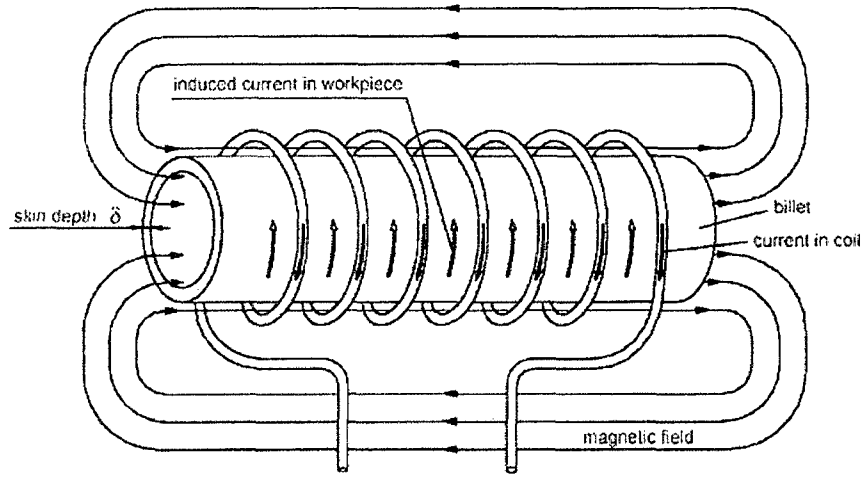

Figure 2.8 - Induction Heat of a Tube [47]

As electromagnetic waves pass through a material, some of the wave's energy is absorbed by the material. Objects that are readily heated by this form of heating will be able to convert strong induction waves into heat with only a few micrometers of penetration while the same intensity could travel through meters of an organic material. The depth at which the entire wave is absorbed depends on both the material properties – especially on whether it is ferromagnetic – and the frequency of the electromagnetic waves. The penetration depth for a ferromagnetic material is calculated from the following equation [48].

$$d = 5000\sqrt{\frac{\rho}{\mu f}} \tag{2.25}$$

As can be seen with the above relationship, waves with lower frequencies have greater penetration than those with higher frequencies. As previously mentioned, the equation is only valid for ferromagnetic materials; for the equation to be applicable for other materials, a much larger scalar (instead of the 5000 shown in Equation 2.25) would be applicable. Typically, most applications are not concerned with how far the waves travel, though in some cases deep penetration is required. Several applications are discussed in Section 2.6.3.

The amount of heat that is generated in the workpiece by the induction unit depends on two variables: resistance and current. Since induction heating is simply a non-contact method of running a current through a wire, Joule's law applies [45].

$$P = R \cdot I^2 \tag{2.26}$$

The resistance of the workpiece can be calculated from the material's resistivity and its shape. Since the resistivity is a function of temperature, the actual power output will vary as the workpiece heats up; typically the resistivity will increase with temperature, thus resulting in greater efficiency. Equation 2.26 describes a relationship to determine the rate at which a cylinder is heated. This equation assumes that a single workpiece is interacting with the electromagnetic waves [45].

$$P_w = 2\pi^2 \frac{d}{h} \sqrt{10^{-7} p_r \mu_r f} \cdot \left(N(I)^2\right) \tag{2.27}$$

As previously mentioned, lower frequency waves have better penetration. However, it can be seen in the above equation that increasing the frequency results in a greater power output. Thus a higher frequency will result in more heat being absorbed by a smaller area.

2.6.2 Induction Process Considerations

Since industrial induction heating units entered service late in the 19th century, much research and development work has been conducted to improve the efficiency and lower costs. When induction heating was in its infancy, the power supply was limited to spark-gap generators which would convert the input electrical energy into proper output frequency at approximately 50% efficiency. In contrast, it is not uncommon for today's variably tuned solid state converters to operate in excess of 95% efficiency [48].

In order to achieve the high level of efficiency now expected from induction heating, there are several design considerations that must be addressed. One such consideration is the coil design in relationship to the workpiece. The actual coil designs depends on the shape of the workpiece and the purpose for heating. Figure 2.9 presents six common designs that are used in induction heating. The first three designs (a – c) are the most common and are used to heat the surface of rod or bar; the Spherical-helical coil (e) is also used to heat a surface of a rod, but those of varying cross-section. When heating a plate or sheet, a Pancake coil (d) is used. As the name would suggest, the Internal coil (f) is designed to operate in an internal bore and is commonly used for heat treating purposes [49]. Tailoring the design of the coil is

critical because coil efficiency diminishes as the distance between the coil and the workpiece increases. This can be seen in Figure 2.10 with the various A – F lines. With a small part and a large air gap between the workpiece and the coil, the heating efficiency is very low.

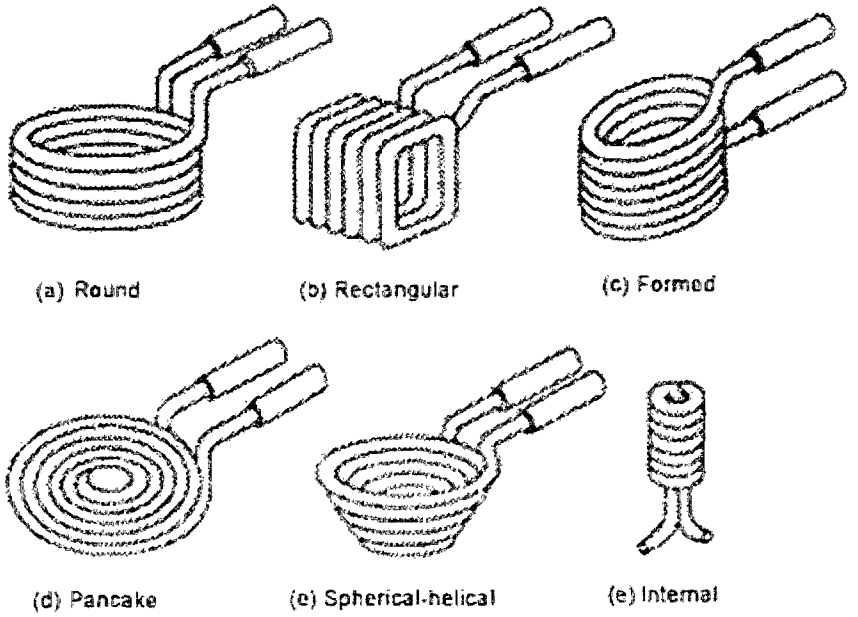

Figure 2.9 - Induction Coil Designs [49]

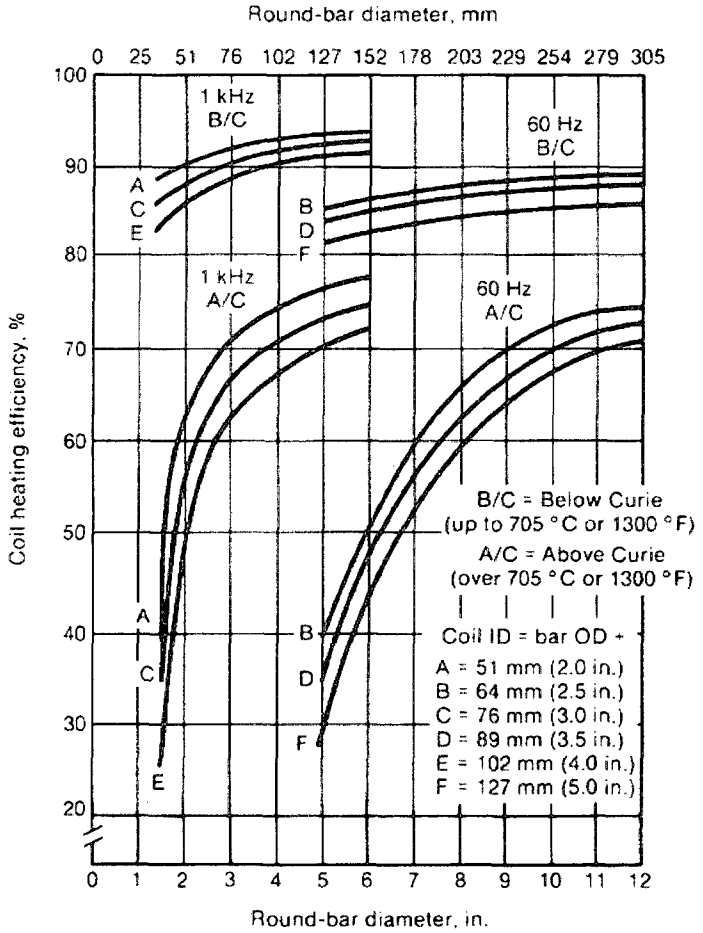

Figure 2.10 - Coil Efficiency based on Bar Diameter and Air Gap [48]

Another consideration of designing a proper induction process is the frequency generated from the induction coil. As displayed in Figure 2.10, coil heating efficiency was improved in all cases by increasing the frequency from 60 Hz to 1 KHz. However, this efficiency gain is not uniform, as there is a lesser improvement when dealing with thicker rods. This phenomenon is acknowledged by the theory of Critical Frequency. The critical frequency is the frequency above which there is very little efficiency gain, although below this frequency there are substantial gains achieved with a minor rise in frequency. When choosing the frequency to operate at, the desire for efficiency is balanced with penetration and processing time (power) mentioned in the previous section. The critical frequency can be calculated with the following equation [48].

$$f_c = 4\times10^8 \cdot \frac{\rho}{\mu \cdot a^2} \tag{2.28}$$

2.6.3 Induction Heating Applications

Due to its ability to heat objects very quickly, induction heating is extensively used to heat-treat parts made out of steel or another metal after they have been fashioned. Heat treating is a very important process at the final stages of producing a metal part, as it can alter the mechanical properties in very desirable ways, such as to enhance ductility through annealing or raise its yield strength through quenching; some heating processes include annealing, quenching, and tempering. However, in some cases, it is preferable to have different mechanical properties at different positions on the object. One such case would be a gear, where higher hardness is desirable on the surface and the gear's teeth to improve wear resistance, while the gear's core would benefit from greater ductility. Since induction heating is able to rapidly heat the surface of metal, this treatment is faster and more efficient than similar treatments with conventional heating [50].

Another application of induction heating is to use it for melting metals; one such furnace can be seen in Figure 2.11. This form of induction heating involves placing an induction coil near the crucible that contains the soon-to-be melted metal. While melting metals is normally the domain of conventional furnaces, the use of induction coils offers several benefits. One such benefit is the ability to cause electromagnetic stirring forces, which allow for improved composition and thermal parity throughout the molten metal. Induction melting furnaces generally offer superior power densities and can operate at very high power outputs, sometimes 20 MW [51].

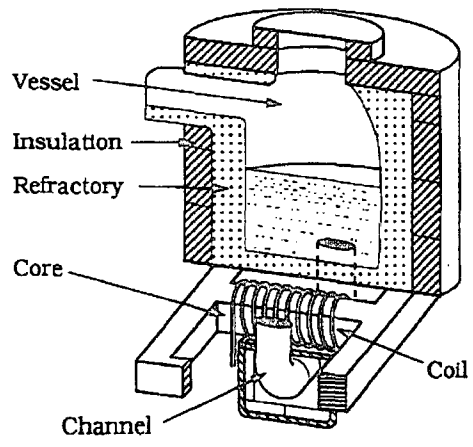

Figure 2.11 - Induction Melting [51]

Unlike the applications for metals, the use of induction heating on plastics is primarily focused on the welding of two thermoplastic or composite pieces together. The reason for this focus is mainly due to the lack of polymers' ability to absorb the electromagnetic waves and convert them into heat. This lack of absorption is overcome during welding by introducing a small metallic workpiece. In the case of implant induction welding, a thin metal part, or gasket, is placed in between the two pieces to be welded. When the weld joint is placed within an induction coil, the metal piece will absorb the electromagnetic waves and heat up, which is conducted to the adjacent thermoplastics. This arrangement is displayed in Figure 2.12. The high conductivity of the metal causes the adjacent plastic to melt while the rest of the part remains nearly unaffected. After a specified amount of time, the object is taken away from the induction coil and allowed to cool, at which time the melted plastic permanently bonds to the metal on each side. This form of thermoplastic welding is very effective at controlling the heating and cooling rates, which allows for low residual stresses, compared to other forms of bonding two plastics together. While this process does have the noticeable disadvantage of the metal workpiece remaining in the final part even after processing is complete, this buffer zone between the two plastics allows a wider variety of plastics to be joined compare to other welding processes [52].

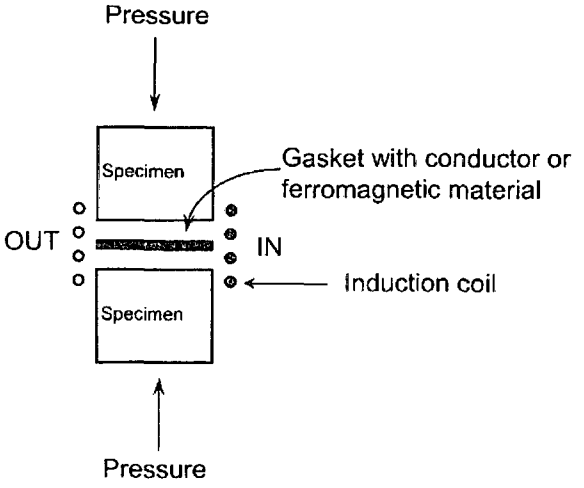

Figure 2.12 - Implant Induction Heating [52]

2.6.4 Adaptation of Induction Heating for Fibre Composite Rebar Production

The concept of implant induction heating has been adapted for this work. The implant material is in the form of a number of axially-oriented fine diameter stainless steel wires. During production, the electro-magnetic waves penetrate the uncured composite and excite the steel wires. The heat caused by induction heating would then propagate to the uncured composite. As mentioned in the previous section with the welding of two plastic parts with a gasket, the steel wires remain in the composite after production. Since these wires would occupy a small fraction of the total cross-sectional area of the composite, there is not a noticeable influence on the rebar's longitudinal mechanical properties. More information pertaining to the implementation of induction heating in the production process can be found in the following chapter.

Chapter 3

Experimental Setup

3.1 Composite Rebar Production Process

A modified pultrusion process was developed by a number of students to produce a pseudo-ductile composite rebar. In this work, the major hardware modification was the addition an induction heating station. The traditional pultrusion die was omitted because the desired shape of the product was a simple rod. Since the strong external heat flux from the die did not exist, two tunnel furnaces in series were used as a substitute heating source. In addition to these heating modifications, a braiding unit was set up to braid aramid fibres at a 45° angle on top of wetted carbon fibres prior to curing. A comprehensive description of the equipment follows.

For this production process, the creel carried eighty double tow spools and seven single tow spools of carbon fibre. The creel station without the tow spools of carbon fibre in position can be seen in Figure 3.1 and Figure 3.2. The double tow spools were placed near the centre of the creel while the single tow spools were placed on the outside of the double tow spools on the same rod as required. On eight creel rods where the single carbon fibre tow spools were not placed, a spool of stainless steel wire was attached. This wire resembles music wire and had a diameter of 0.5 millimetres. Helical compression springs and washers were used at the end of each rod to apply a controllable amount of tension in the carbon fibre tows.

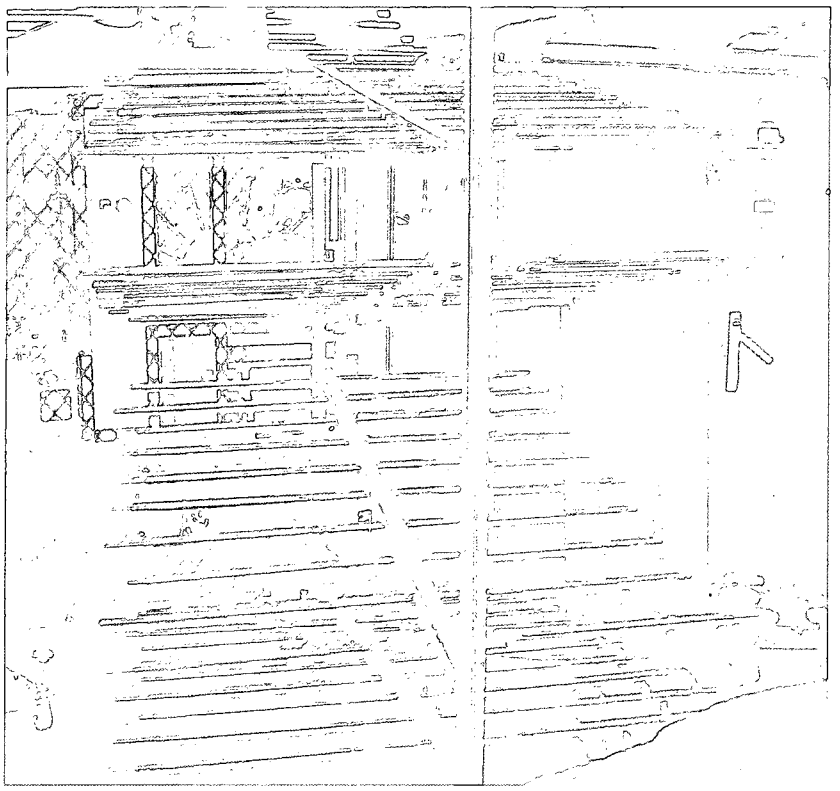

Figure 3.1 - Creel Stand

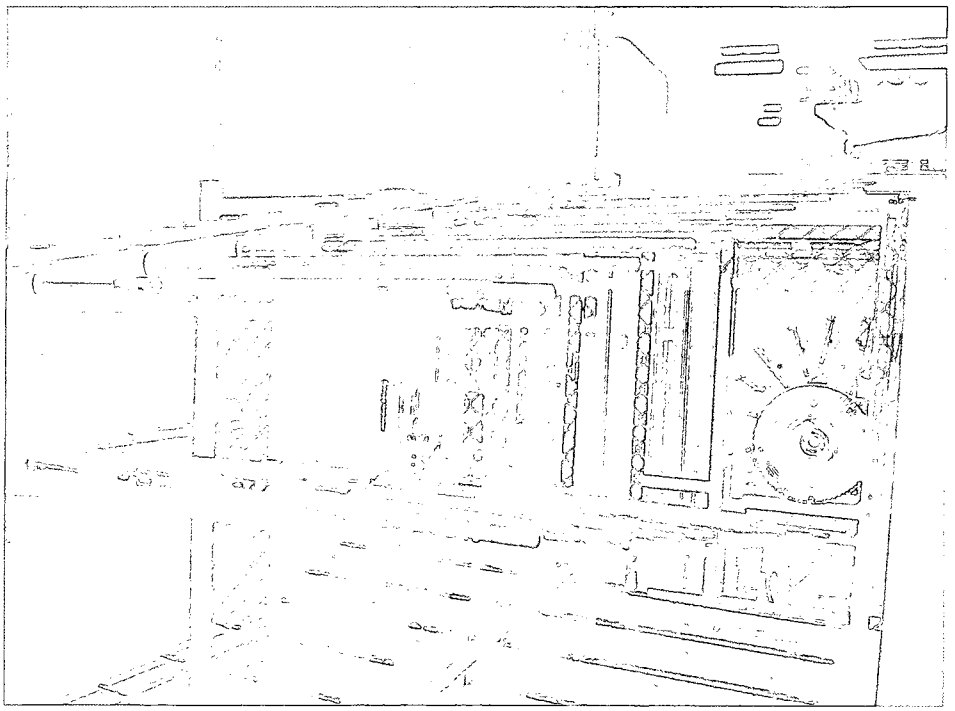

Figure 3.2 – Close up of Creel Stand

The carbon fibre and steel wire from the creel station were arranged by means of the Fibre Sorter. This device consisted of a wire mesh fan in which ninety-six copper tubes were placed in this mesh; either a strand of carbon fibre or a steel wire passed through each tube. This is seen in Figure 3.3. The fibres and wires would then pass through an annular impregnation ring. This ring had holes through which the epoxy resin and hardener mixture could drain through to impregnate the carbon fibre.

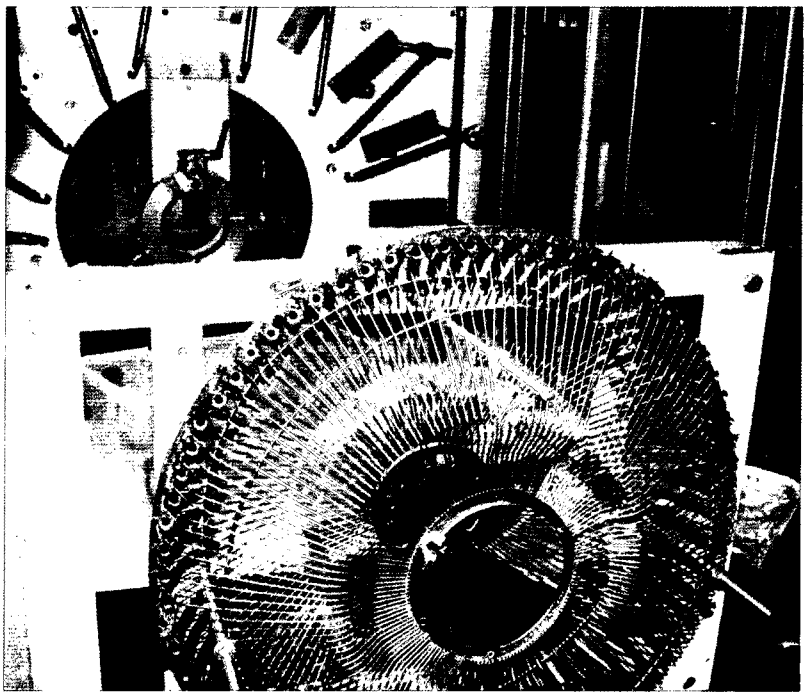

Figure 3.3 - Fibre Sorter

Once the carbon fibre has been impregnated with epoxy, the fibre bundles would pass through the braider station that applied the aramid fibres overwrap. The aramid fibres were braided in a 45° angle using eighteen spools of fibre. While automated and calibrated to operate at a fast rate, braiding is the slowest process of this production line. For the type of braid required, the braider can apply the overwrap at a maximum of 0.73 metres of composite rod per minute.

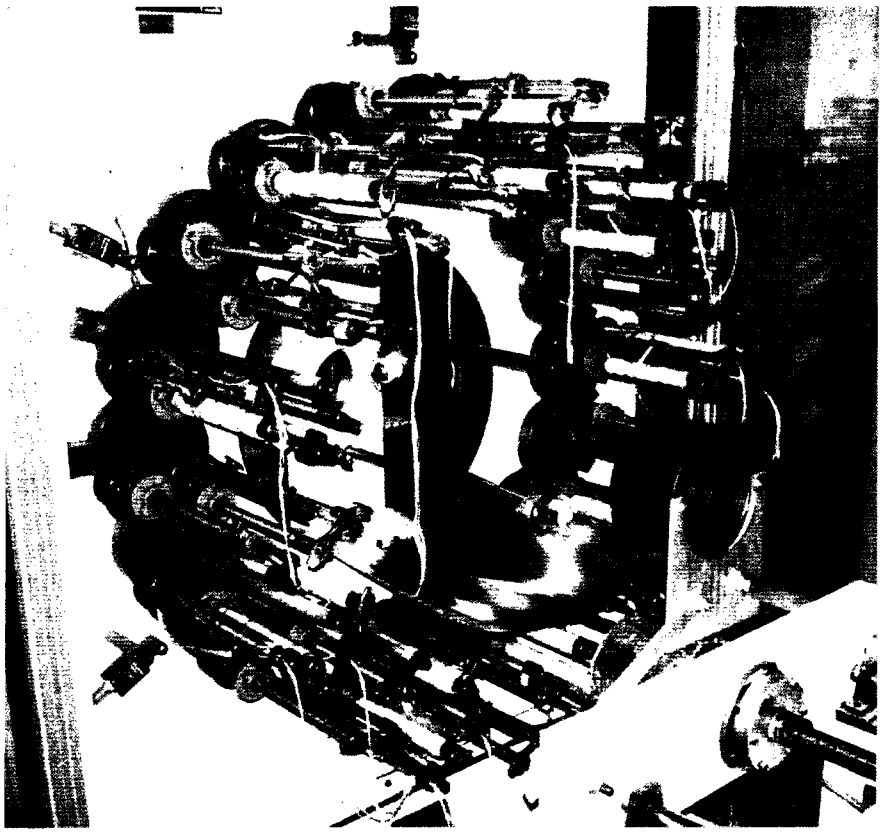

Figure 3.4 - Braider

Once the aramid fibres have been braided and applied to the carbon fibre core, the uncured composite passed through the induction coil. The induction coil was twenty-one centimetres long and generated an electromagnetic wave with a frequency of 140 kilohertz and a maximum work output of two kilowatts. This unit was custom-built by Ameritherm Inc. for the University of Ottawa. As the uncured composite rod passed inside the coil, the steel wires absorbed the electromagnetic waves and heated up. This allows the core to be heated directly. After the induction heating station, the outer layer of the composite rod is heated by passing through two furnaces. The induction heating coil and unit can be seen in Figure 3.5 along with the entrance of the furnace. To prevent any uncured epoxy from dripping on the furnaces, a steel tube was placed along the total length of the furnaces.

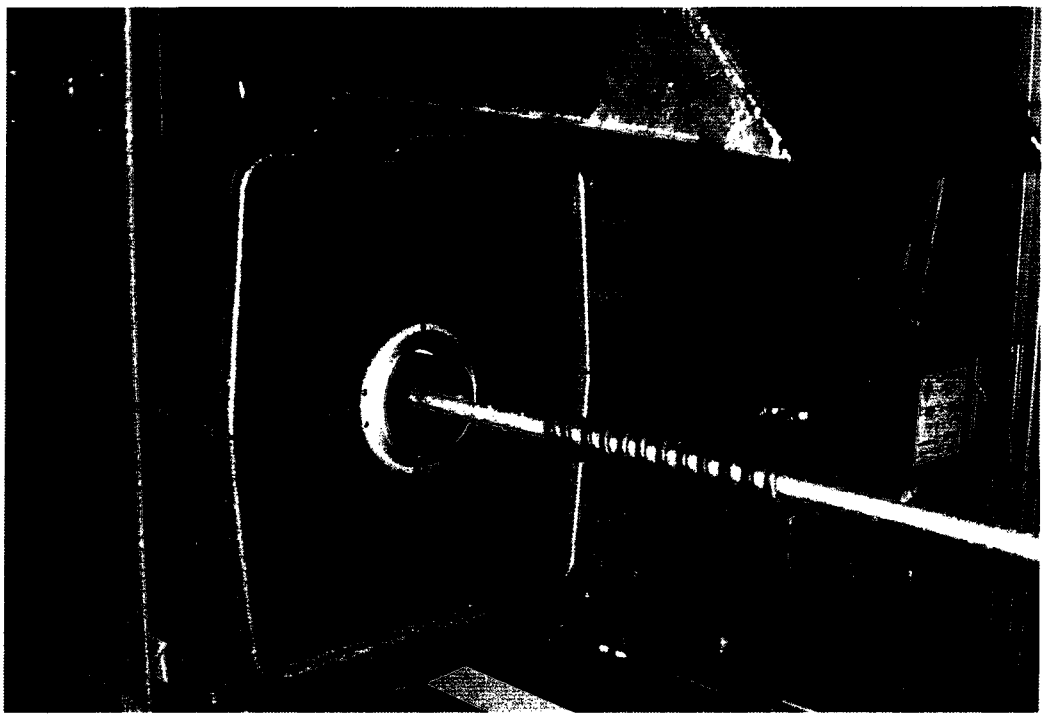

Figure 3.5 - Induction Heating and Furnace Entry

As the rod passes through the furnaces, the rod is subjected to temperatures typically between 200 and 240 °C. After exiting the second furnace, the rod passes through the puller. The puller which can be seen in Figure 3.6 is a caterpillar mechanism commonly used in pultrusion to move the rod at a constant rate. The rods are then cut to desired lengths by an overhead diamond saw. To ensure the process can continue while a section is being cut, the saw was placed on rollers to allow it to move with the rod.

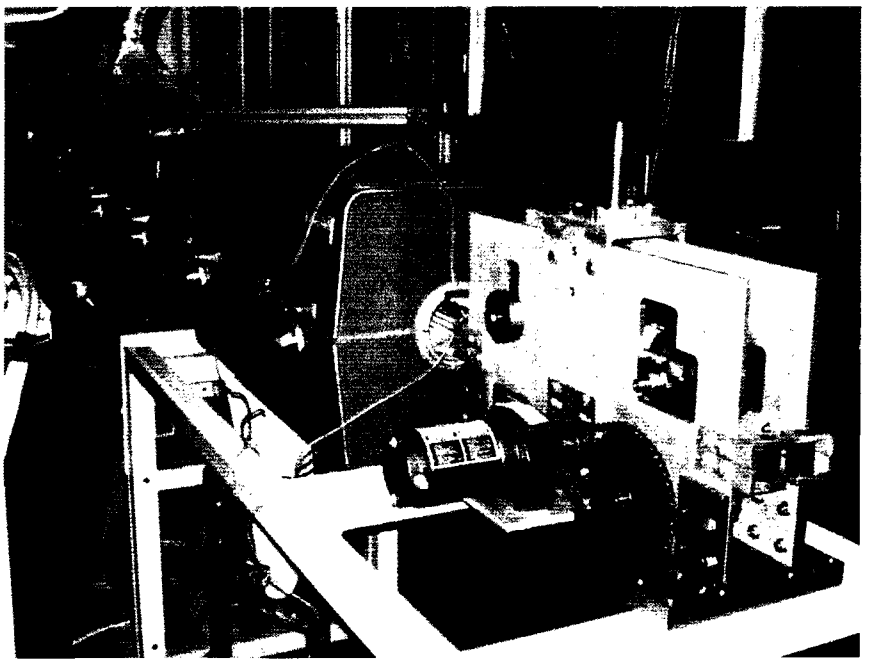

Figure 3.6 - Furnace Exit and Puller

3.2 Location of Steel Wires for Induction Heating

The heat generated by induction heating originates at the embedded steel wires and then propagates outwards into the carbon fibre core. Since induction heating is the primary method for curing the carbon fibre composite core, it is desirable that the heating is transferred as uniformly as possible and requires the minimum amount of heating from the furnaces. Furthermore, the location of each wire is important for a number of reasons. Firstly, the closer the wires are to the coil, the more heat is produced. Secondly, if the wires are positioned too near the aramid fibre braid, the heating profile would be similar to furnace heating and little benefit would be gained from using induction heating. Finally, if several wires are located too close to each other, the temperature in this region could be high enough to burn the epoxy resin. For these reasons, the proper location of the wires was selected based on symmetry, as shown in Figure 3.7. This diagram depicts a rebar with a diameter of twenty-five millimetres and the coordinates of the embedded wires in millimetres. Currently, the only apparatus to guide the steel wires to their desired position is the Fibre Sorter station.

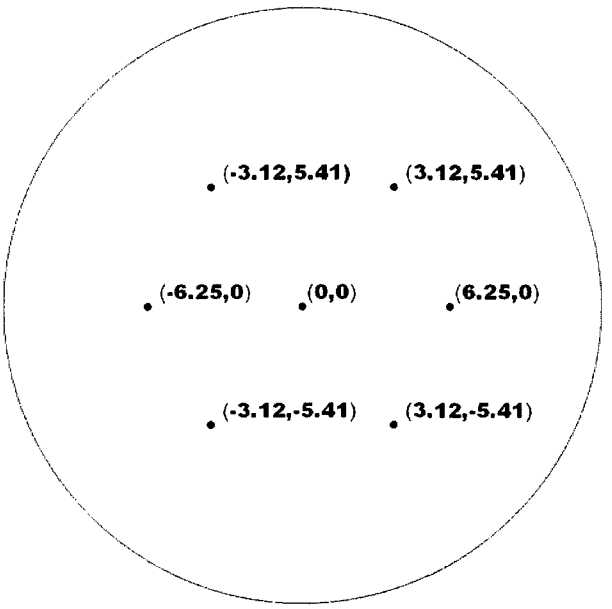

Figure 3.7 - Location of Steel Wires in Millimetres

During the use of the finite element model, other wires patterns were tested to understand the effects of the embedded wires location. These tests included one larger central wire or several wires clustered together. It was found that, while the heating profile was less desirable and overall the curing took longer, the effects were not as significant as originally predicted. The results suggested that if there was sufficient induction heating power to initiate the curing of the epoxy adjacent to the wires, the heat released from the exothermic reaction would result a cascading effect occurring in the curing of the neighbour regions. As such, only the results from the simulations based on the desired wire arrangement in Figure 3.7 are presented.

3.3 Measuring Induction Heat Output

While the location of the wires is important in determining the effectiveness of induction heating, it is the heat output of induction heating unit that determines the amount of time required to cure the carbon composite core. There are two methods available to determine the amount of heat transmitted by the induction coil; namely analytically or experimentally. It was decided that an experimental approach would be used. This alternative was selected in order to avoid the complexities of the electromagnetic shielding that the composite rod and other wires would provide when formulating how much heat was

released from the wires. Thus a simple experiment was designed to measure the amount of heat that would be generated in the steel wires during the induction heating phase.

For this experiment, seven steel wires were placed into a glass test tube filled with distilled water; the glass test tube had a similar diameter as the composite rod (approximately 20 mm diameter). These wires were heated by the induction unit and this heat was transferred to the surrounding water. This configuration can be seen in Figure 3.8. In order to maintain a constant wire configuration and to provide electrical insulation between the wires, plastic straws were placed around each wire. This configuration can be seen in Figure 3.9.

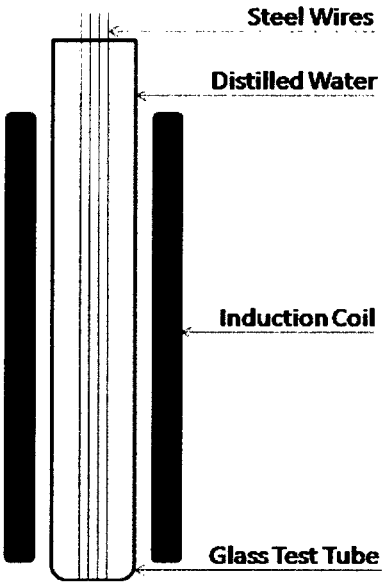

Figure 3.8 - Experiment to quantify Induction Heating

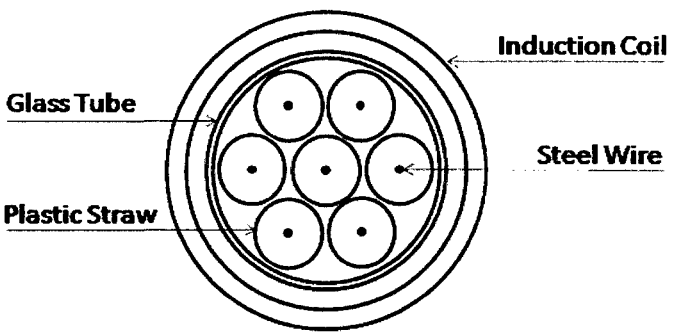

Figure 3.9 - Cross-section of Experiment to quantify Induction Heating

Various durations and currents were used in these tests, ranging from 20 to 40 seconds and 60 to 180 Amps, respectively. A K-type Thermocouple was used to record the water temperature at several points a few seconds after the heating was completed. The final recorded temperature was an average of these readings. It should be noted that any test that exhibited the water boiling – as some of the high duration, high power tests did – was ignored since it was not possible to record the amount of energy devoted to latent heat with the available facilities. After the temperature was obtained, a heat balance was created to determine the total power output. The heat lost to the surrounding air and glass tube was omitted from the calculation due to the low conductivity and convection values associated with these insulators. The results of these tests and the resulting calculations are presented in Section 4.3.

3.4 Epoxy Exotherm Testing

In addition to the furnace and induction heating, the composite rod is also heated by the energy released when the epoxy cures because the reaction that takes place is exothermic. As such, this heat must be quantified and added to the FEA model in order for the simulation to give accurate predictions. The goal of this section was to determine a method to formulate an equation that could be implemented into the Finite Element model. This equation would relate the temperature and percentage of the epoxy cured to the amount of heat that is released per time interval.

Typically, the polymerization of some epoxy resins will occur at room temperature but for higher performance fibre composites the epoxy resin is heated to cause the reaction to progress at a faster rate. However, for the epoxy used in the pseudo-ductile composite, the epoxy will only rapidly cure when it is above 80 °C. The existing testing standard (ASTM D2471) is used to evaluate the exothermic reaction of epoxy resin. Since these tests must be conducted at an elevated temperature to ensure that the curing reaction occurs, two approaches considered. To prevent the epoxy from draining out before curing, the wetted bundle was slid into a glass tube. The temperature was recorded by placing three K-type thermocouples in the furnace: one in the centre of the bundle, another between the aramid and carbon fibres, and the third in the middle of the furnace.

The first method involved placing the uncured epoxy and fibre bundle in a furnace and having it heat at a constant rate. As the bundle temperature approaches the point where the epoxy will start curing, the internal heating rate will increase. The difference in heating rates between the furnace and the curing bundle represents the heating that is generated by the exothermic reaction. Once the heating rate slows down and the rod starts to cool back down to the furnace temperature, the experiment is over. A sample of the results that this method would generate can be observed in Figure 3.10.

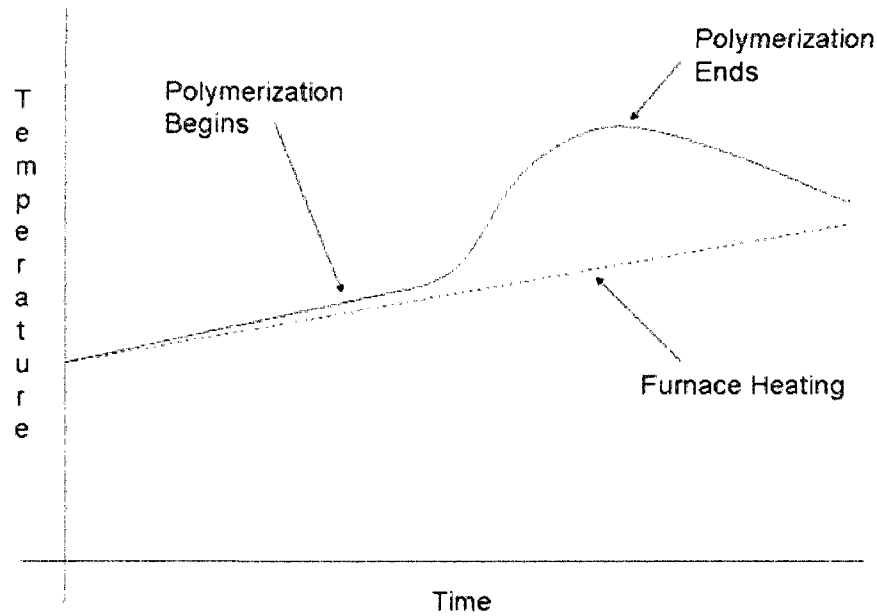

Figure 3.10 – Epoxy Reaction during a Controlled Furnace Heating Test

An alternative method was to control the furnace temperature at a specific value and have the uncured epoxy and fibre bundle, initially at room temperature, placed into the furnace. As the epoxy reaches a temperature near 80 °C, curing will commence and cause the temperature of the bundle to surpass that of the furnace. The test is complete when the rod cools back down to the furnace's set temperature. A sample of this heating profile can be found in Figure 3.11. To minimize any heating that might occur from the furnace's heating coils, a second heating cycle was run with the cured bundle. The difference in temperature between these tests was the result of the epoxy curing and thus can be quantified. This test must be conducted at several temperatures to develop the relationship between cure rates to both temperature and cure percentage. This method had an important

advantage over the one previously mentioned because the production process' furnaces were set to a specific temperature and, thereby, simulates how the production line heats the rod. However, this method required two experimental runs for one experiment which could create some error when the results are compared as there might be some small variance between them. One possible variance would be the temperature drop in the furnace when the bundle is inserted. If on one run it takes more time to position the epoxy than during another, the heating profiles will be different and the results must be altered to take this into account. Thus this method had a lower potential for repeatability.

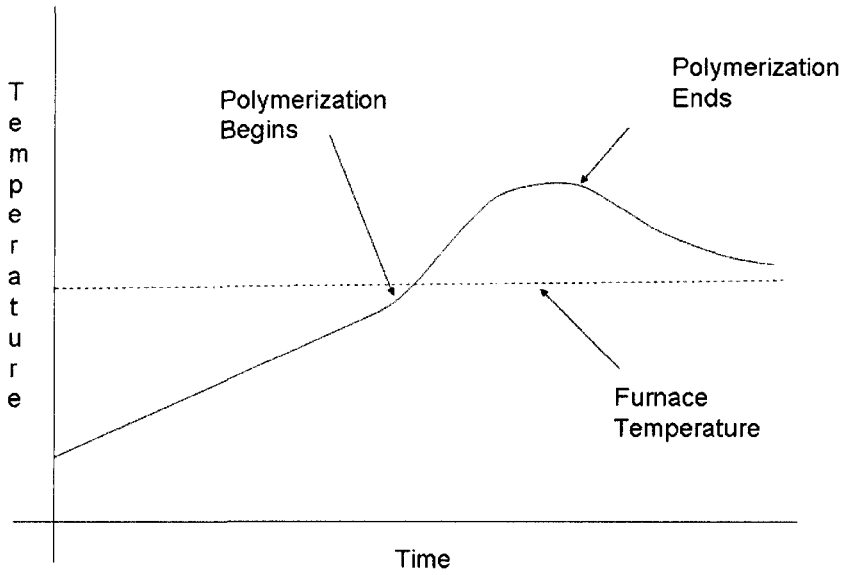

Figure 3.11 – Epoxy Reaction during a Controlled Temperature Test

Ultimately, it was decided that using a controlled temperature test would generate the best results because it was easier to model. Upon experimenting with both approaches, it was found that achieving a constant heating rate was difficult with the facilities at hand. In contrast, the experiments conducted under constant furnace temperature could record the difference between the furnace temperature during the two phases. The final testing procedure used to determine the exothermic heat generated by the epoxy used in this production process can be found in Appendix A. In total, fifteen experiments were conducted, at furnace temperatures ranging from 120 °C to 240 °C. The calculations derived from the lower temperature experiments can be found in Section 4.1. These results were interpolated to allow an equation to be implemented into the Finite Element model that was created in Chapter 5.

Chapter 4

Analytical Kinetic Models

4.1 Curing of Epoxy

The experiments conducted to model the exothermic reaction of the curing epoxy were performed as outlined in Section 3.4. These tests involved setting a furnace to a specific temperature and then placing a small piece of the composite bundle inside. The test consisted of two phases: the curing phase where the epoxy is uncured and the repeat phase where the epoxy has already been cured. A thermocouple is placed in the centre of the bundle as well as in between the carbon fibre bundle and aramid overwrap to record the temperature as the bundle heats up in the oven. Experiments were conducted between 120 °C and 240 °C, in 20 °C increments. A sample of the test results can be seen in Figure 4.1. The experimental results displayed in the diagram were gathered from a test conducted with a furnace temperature of 180 °C.

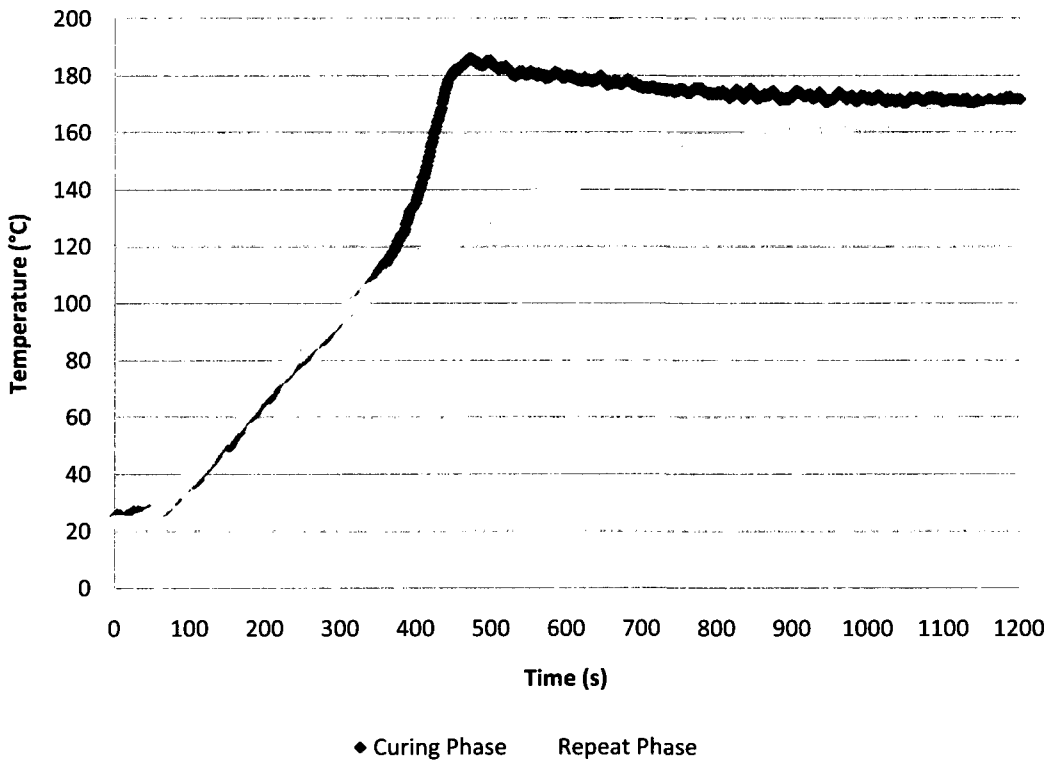

Figure 4.1 - Sample Epoxy Exotherm Test conducted at 180 °C

From the above diagram, it can be seen that bundle heats at a similar rate in both phases up until 110 °C. Above this temperature, the epoxy's exothermic curing reaction occurs fast enough to increase the temperature of the rod significantly. This temperature difference between the two curves peaks when the bundle temperature surpasses the furnace temperature. Past the temperature peak, the curing phase's temperature decreases slowly until it eventually reaches the same temperature as the repeat phase. For this experiment, the focus is primarily on the difference between the curing and repeat phase temperature, which is due to the exothermic reaction. Figure 4.2 displays this difference for the 180 °C test. As mentioned previously regarding the nature of the curve, the temperature difference remains close to zero up to 330 seconds; then becomes rapidly increases, achieving almost 60 degree Celsius difference around 450 seconds. The data obtained from the temperature difference curve allowed for the calculation of the total amount of heat released by the epoxy curing, as well as the rate of curing at different temperatures and cure fractions. The total amount of heat released was calculated by multiplying the maximum temperature difference by the mass of the bundle and the averaged specific heat of the bundle.

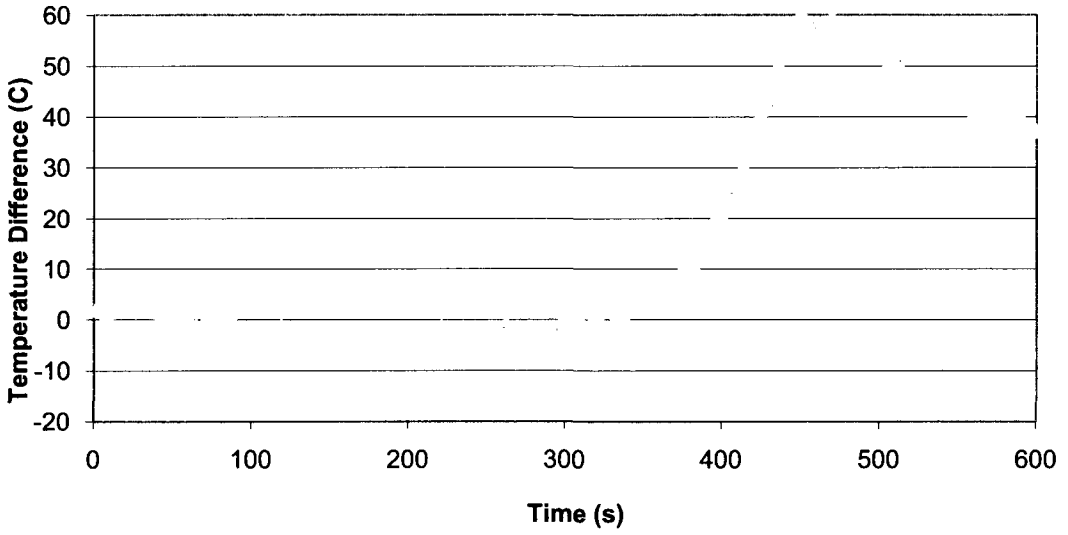

Figure 4.2 - Sample Temperature Difference from a 180 °C Test

The results obtained from the curing tests exhibited two sharp changes in heating rates which suggests that the curing has three phases. The first curing leg had the lowest increase and lasted for roughly one third of the total reaction. The longest and most rapid

phase of the cure was Curing Leg 2. Conversely, the final curing leg was the shortest, but due to the elevated temperature, the temperature rise was faster than the initial leg. An illustration of this trend is in Figure 4.3.

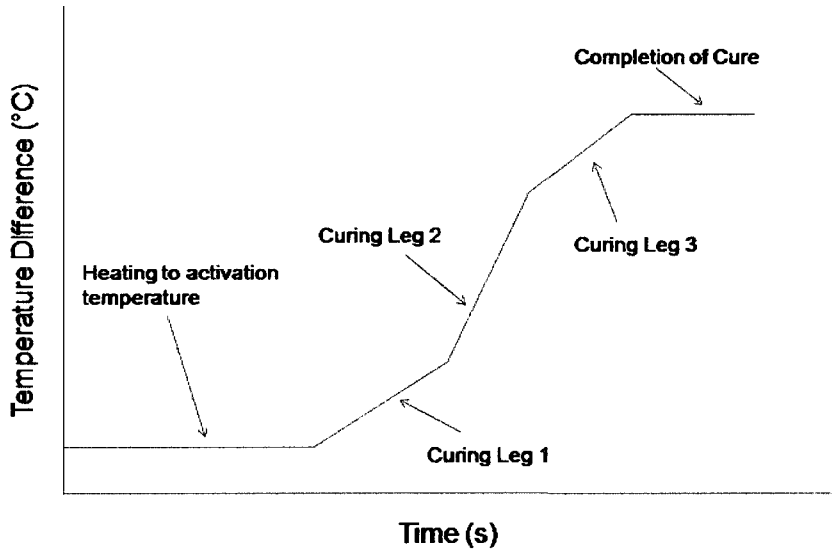

Figure 4.3 - Temperature Difference Profile

These curing phases occurred at similar cure fractions throughout the testing temperatures. This trend is displayed in Figure 4.4, which contains a sample of the exothermic test's heating rates. The fraction of cure was calculated by relating the amount of heat released compared to the total amount of heat released by the curing reaction. It can be seen that the changes in heating rates occur at similar cure fractions, roughly at 30% and 80%. Using this trend, the first heating leg was selected to dictate the heating rate between 0 to 30 % cure, 30% to 80% corresponded to the second leg, while 80% to full cure was controlled by the third leg. The observation of having the epoxy cure at a fastest rate around 30% cure fraction reflects well with other curing models. Several papers have reported that the epoxy reaches its maximum cure rate at 30% [26,28,29]. The motivation to split the curing into three parts was to simulate the cure rate slowing as the cure fraction reached unity. Since the exothermic heat released during the reaction increases the temperature that the reaction takes place at, the reaction rate increases as the curing progresses. With the addition of the third curing leg, the reaction slows down which coincides with what is seen in experiments.

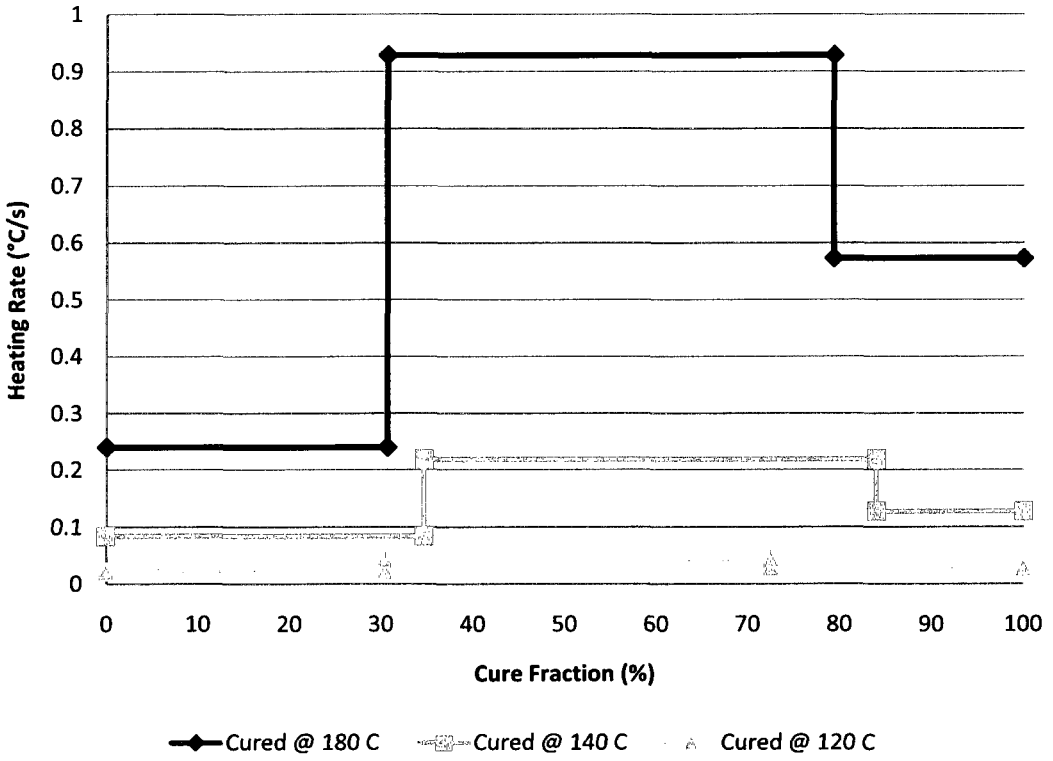

Figure 4.4 – Heating Rate as a function of Amount Cured for Selected Tests.

This curing data was input into the Arrhenius equation. Since the reaction rate varied greatly between legs, each leg was considered a separate reaction. Using an iteration method, a curve of best fit was determined by using the activation energy and scalar constants of each leg from the heating rate data. The Arrhenius equation is:

$$K = A \cdot exp\left[\frac{-E_a}{RT}\right] \tag{2.13}$$

It should be noted that the curing rate is displayed in Figure 4.5 in temperature rise per unit time for presentation purposes. The final rate constant and activation energy are given in Table 4.1. It can be seen in Table 4.1 that Activation Energy of the three legs does not vary much between legs; the greatest difference between legs is less than 7 %.

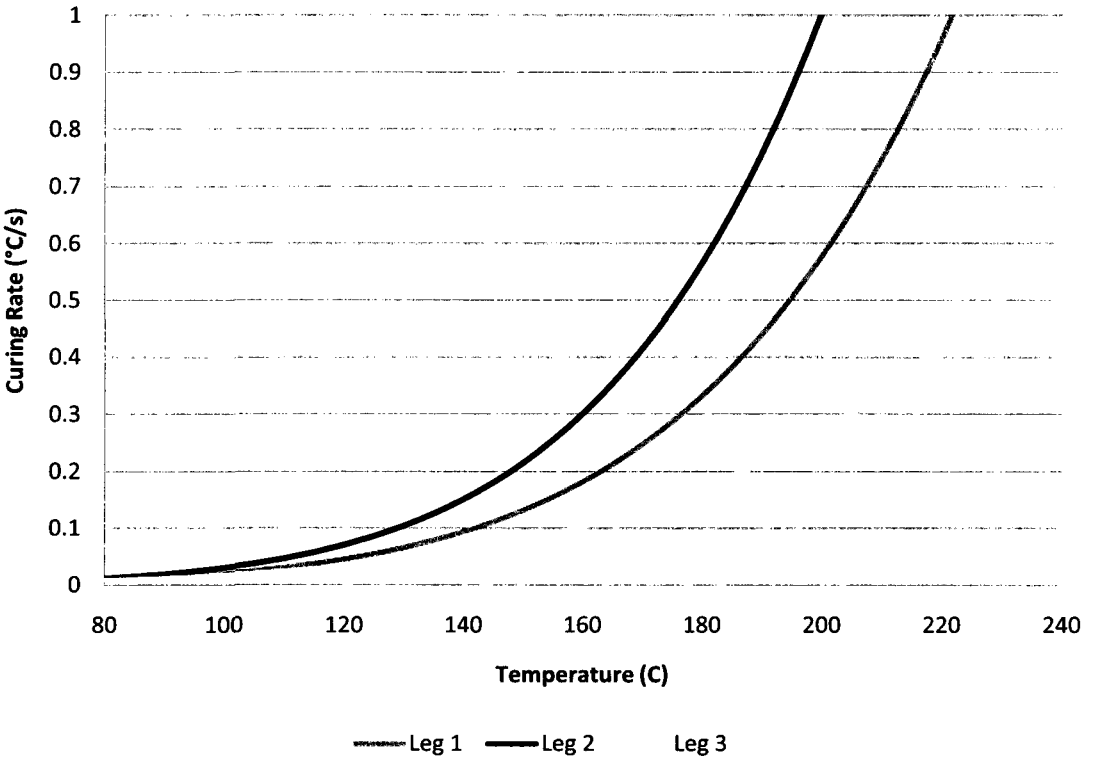

Figure 4.5 – Calculated Curing Rate of Epoxy as a function of Temperature

Leg	A (1/s)	E_a (J/mol)
1	96010	43010
2	110010	42010
3	92010	45010

Table 4.1 - Experimentally Derived Parameters for Epoxy Exothermic Reaction

4.2 Heat Transfer Modes for FRP rods in the Furnace Section

When the composite rod passes through the furnace, there are three ways that the heat can be transferred to the rod: conduction, convection, and radiation. The three forms of heat transfer are illustrated in Figure 4.6. These heat transfer modes are not mutually exclusive and usually all occur when one object is warmer than its surroundings. However, it is common for one or two of these heat transfer methods to be the dominant form(s) of heat transfer and thus the minor heating form(s) can be ignored with little loss of accuracy.

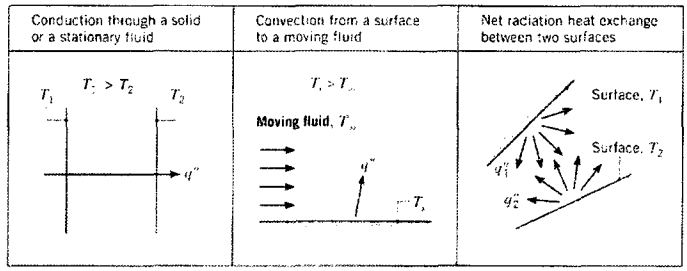

Figure 4.6 - Illustrations of Conduction, Convection, and Radiation Heat Transfer [53]

The transfer of heat by conduction occurs at the molecular level where the regions that possess a greater amount of heat transfer some of its thermal energy to adjacent regions that possess less heat. The rate at which the heat is transferred depends strongly on how the atoms or molecules interact with each other as quantified by the thermal conductivity (k). Metallic materials usually have a higher conductance value than non-metallic materials. The following equation is used to quantify heat conduction [53].

$$q_{conduction} = A \cdot k \cdot \frac{T_1 - T_2}{L} \tag{4.1}$$

Conduction heat transfer is not solely limited to transfer of heat within an object but can also be used to describe the heat being transferred from one object to another. In this situation, the conductivity of both materials influences the heat transfer rate. Additionally, this rate is also influenced by how these objects are joined, or specifically what type of interface is present. This interface is caused by gaps present at the contact, as objects are never perfectly smooth. Since these gaps are filled with air, or other gas, that has a very low conductance constant, it will impair the transfer of heat. Thus, for a given pair, the objects that have rough surfaces in contact will encounter a higher interfacial resistance compared to a smooth contact.

Similar to conduction, convection also deals with heat being transferred at the molecular level, but in this situation, a medium is responsible for transferring heat. As such, this mode of heat transfer deals with a fluid that flows over the object, thereby either heating or cooling is determined by the temperature difference. The amount of heat transferred is proportional to the convection heat transfer coefficient (h), which varies depending on several factors; these factors include the medium's thermal properties as well as the speed

and direction in which the medium travels. Equation 4.2 quantifies the rate at which the heat is transferred by convection [53].

$$q_{convection} = A \cdot h \cdot (T_{\infty} - T_S) \tag{4.2}$$

The effects of both conduction and convection on heating or cooling an object are greatly influenced by the medium that carries the heat. For a high transfer of heat to occur in conduction and convection, a medium with favourable material properties is required. In contrast, radiation occurs best when there is no medium present. Instead, the amount of heat that an object absorbs from thermal radiation depends on whether it absorbs the radiation or reflects it. This property is quantified by its emissivity value (ε), where a value of unity states that the object fully absorbs the radiation and null value indicates that all the radiation is reflected. While radiation can heat an object even without a medium to transfer the heat, the medium will absorb some of the heat as the radiation travels through it. The amount of heat that is transferred by thermal radiation is quantified with the following equation [54].

$$q_{radiation} = A \cdot \varepsilon \cdot \sigma_B \cdot \left(T_S^4 - T_{Sur}^4\right) \tag{4.3}$$

To predict how objects will heat up over time, numerical methods are typically used, as the discussed analytical methods are only suitable for straightforward applications.

4.2.1 Modeling Natural Convection

Convective heat transfer can be achieved by either natural or forced convection. Forced convection occurs when a fan or other device causes the heat transferring medium to move and thereby dictates the speed of the medium. When no mechanical device is present to influence the motion of the medium, the mechanics of natural convection take over. Natural convection occurs with hot gases or liquid having a buoyancy force which causes the medium to circulate.

For an object suspended in a furnace, conduction and forced convection contributes a minimal amount of heat exchange; instead, the object is heated by natural convection and thermal radiation. To take into account the natural – or free – convection that occurs in a furnace, the following equation can be used to determine the convection coefficient [55]:

$$h = \frac{Nu \cdot k}{x} \tag{4.4}$$

There are several equations that are available to quantify the Nusselt number, depending on the heating (or cooling) situation and which type of medium is undergoing convection. One such formula that can be used for the natural convection of air under a wide variety of temperatures follows [55]:

$$Nu^{1/2} = 0.60 + 0.387\left\{\frac{Gr\,\mathrm{Pr}}{\left[1+(0.559/\mathrm{Pr})^{9/16}\right]^{16/9}}\right\}^{1/6} \tag{4.5}$$

The Prandtl number can be readily obtained from published data of the gas film at a specific temperature. As for the Grashof number, it can be determined with the following equation [55]:

$$Gr_X = \frac{g\beta|T_0 - T_\infty|x^3}{\nu^2} \tag{4.6}$$

The values pertaining to the physical properties of gas film can be obtained from a table located in Appendix B. The specific film temperature that is used in Equation 4.6 is obtained by averaging the initial temperature with furnace temperature; the corresponding physical properties of the air for the film temperature will be used for the above calculations. For ideal gasses, the volume coefficient of expansion is defined as the inverse of the temperature. The model presented in this work assumed that the air within the gas film behaves as an ideal gas.

4.2.2 Modeling Thermal Radiation

The second major heating method that occurs in the furnace for the composite bundle is thermal radiation. In contrast with modeling natural convection which is influenced by several variables, thermal radiation depends upon the emissivity value of the source and target. However, the numerical methods that are presented in the next two sections only involve convection heat transfer. This limitation can be circumvented by the following equation which transforms thermal radiation into a similar form as the relationship for convection [54].

$$q_{rad} = h_R \cdot A \cdot (T_S - T_{Sur}) \tag{4.7}$$

$$h_R \equiv \varepsilon \cdot \sigma_B \cdot (T_S + T_{Sur}) \cdot (T_S^2 + T_{Sur}^2) \tag{4.8}$$

Thus, by applying this derivation, thermal radiation can be modeled under the same methods as typically used for convection. The benefit of having thermal radiation modeled as convection will be apparent in Section 4.2.5.

4.2.3 Semi-Infinite Approach

There are two common methods for analytically predicting how an object's temperature will change in a transitory situation: Semi-Infinite and Lump Capacitance. The Semi-Infinite approach makes the assumption that the object being heated (or cooled) is wide enough that no edge effects are present. Thus, the heat transfer occurs constantly in a single direction. Using the Semi Infinite Model for a cylinder, the amount of time required to heat up the rod to a given temperature can be obtained from the following equation [55]:

$$\tau = \frac{Fo \cdot R^2}{\alpha} \tag{4.9}$$

The thermal diffusivity combines the thermal conductivity, density, and specific heat into one value to relate how easily a material will transfer heat in transient conditions. The Fourier number can be found by using Figure 4.7 which relates the difference in temperature with the Fourier number for a given Biot number.

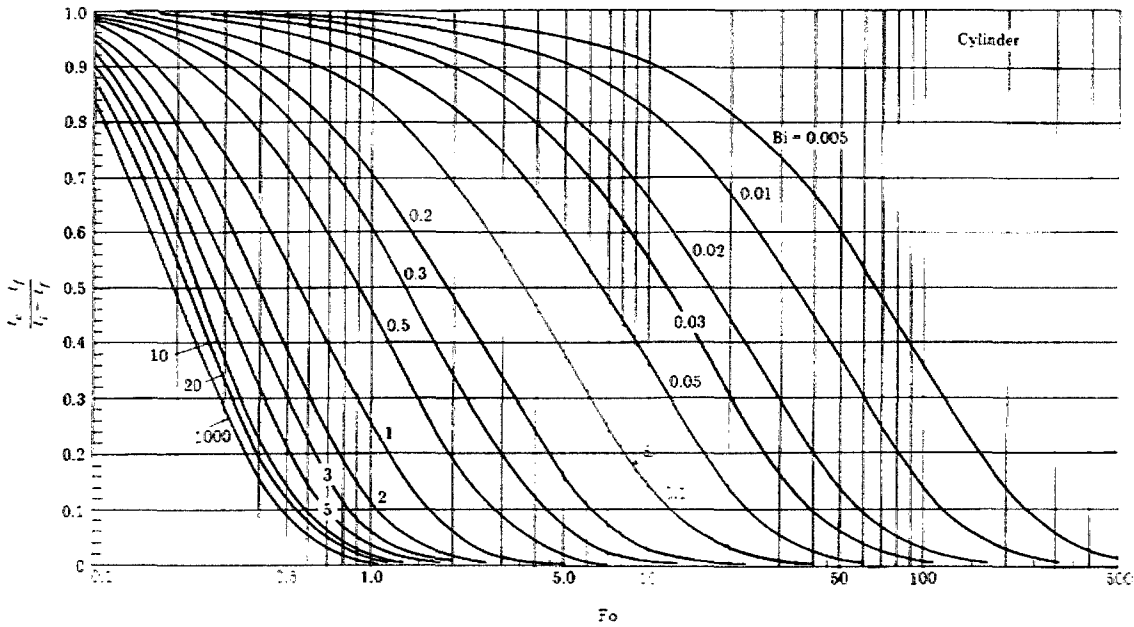

Figure 4.7 - Heat Transfer through a Semi-Infinite Cylinder [54]

The Biot number represents how slowly the object can transfer the heat in the surrounding fluid to the centre. A lower number means that the heat transfers readily from the external liquid to the centre while a higher value would represent that the centre would take a great deal of additional time to heat up compared to the surface. It can be calculated by the following equation [54].

$$Bi = \frac{hR}{k} \tag{4.10}$$

While the above discussion has been focused upon determining the object's centre temperature, the Semi-Infinite method is by no means limited to only evaluating this region and can be used to predict the temperature at other locations. The temperature at other various radii can be obtained by the use of Figure 4.8, which relates the radius temperature with the temperature of the centre. As can be seen in the graph, at very low Biot values, the heat transfers readily within the object and possesses a nearly uniform temperature profile. Conversely, at higher Biot values, the temperature profile is more prominent.

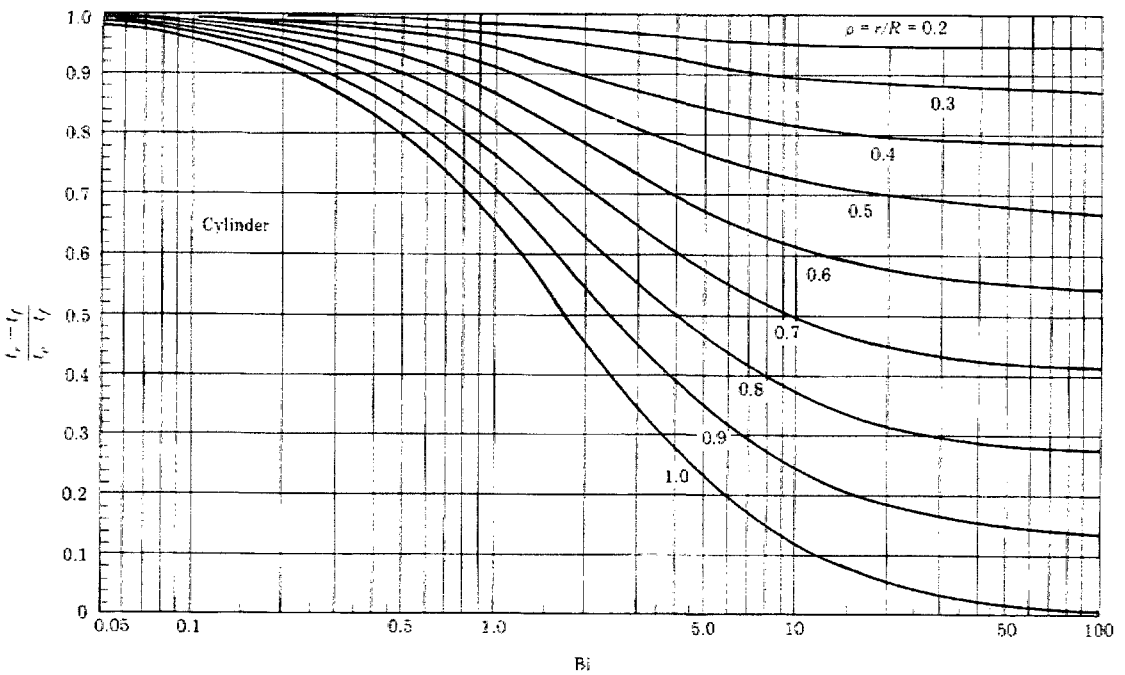

Figure 4.8 - Temperature Profile of a Semi-Infinite Cylinder [54]

4.2.4 Lumped Capacitance Approach

An alternative transient analytical heat transfer model is the Lumped Capacitance model. This approach relates the change in temperature of an object to the time it is heated or cooled. At first the difference between the object and the environment is quite large, causing a larger heat flux. However, as the object being heated or cooled spends more time subjected to a different temperature, the heat flux is greatly reduced and the object's temperature gradually moves closer to that of the environment. This approach relates the time (τ) taken to achieve a desired temperature (T) through the following formula [54].

$$\frac{T - T_\infty}{T_0 - T_\infty} = \exp - \left\{ \left[\frac{hA}{\rho c V} \right] \cdot \tau \right\} \tag{4.11}$$

Before the Lump Capacitance approach can be used to predict the heating or cooling of an object, it must be calculated whether the above assumptions are valid. The following equation evaluates whether this is the case [54].

$$\frac{h(V/A)}{k} < 0.1 \tag{4.12}$$

For a finite rod length, the volume to surface ratio is highest when the length is at a minimum. However, due to the very low conductivity of the epoxy matrix and the natural efficient volume to surface ratio that the cylinder shape has, the above test fails at lengths above two micrometres which is a length that is unable to be duplicated in practical terms. As such, the lumped capacitance method is inappropriate to be used as an analytical model for the heating of the composite rod and thus will not be considered further.

4.2.5 Validation of Analytical Model

To ensure that the finite element model that will be described in Chapter 5 is accurate, an analytical model was derived; this model was compared with the finite element model and experimental data. Of the two analytical approaches that were discussed previously, the most appropriate is the Semi-Infinite approach. For simplicity, this approach was applied to heating a carbon fibre composite rod and thus ignored the aramid overwrap. Since the carbon fibre composite thermal properties are similar to the properties of aramid fibre composite, this simplification does not contribute a significant amount of error. These calculations were made for the heating of the composite rod, originally at 22 °C, with a furnace at 200 °C and 220 °C, and being heating solely by convection or by both convection

and radiation. To integrate thermal radiation in the semi-infinite model, radiation was modeled using a derivation that was discussed in Section 4.2.3, where the total heat transfer coefficient (h_T) is sum of its convection (h_C) and radiation (h_R) components. The accuracy of this data was evaluated by comparing it with the experimental results obtained from furnace heating curves using a similar process as the exotherm experiments described in Section 3.4. For this validation test, the glass tube was omitted and only the repeat (non-curing heating run) was recorded. A set of sample calculations for a 220 °C furnace test is located in Appendix C. A comparison between the experimental results and the analytical methods can be seen in Figure 4.9.

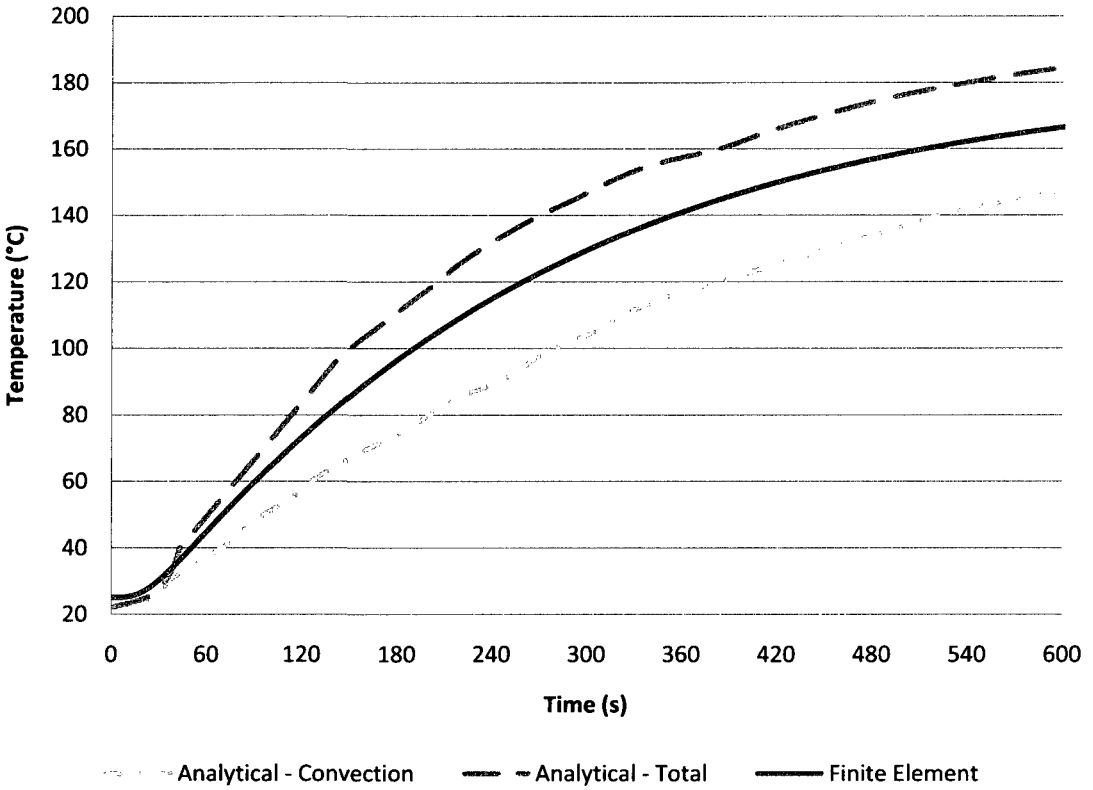

Figure 4.9 - Comparison of Analytical Model with Experimental Results obtained at 200 °C.

4.3 Induction Heating

In Section 3.3, a method was presented to determine experimentally the amount of heat produced by the induction unit. This experiment involved the induction coil heating a glass tube filled with water and several steel wires. Neglecting the small amount of heat that is lost to cooling, a temperature reading of the water was obtained which permitted the total heat released to be determined. The induction coil's power was determined by a simple heat balance, where the increase in temperature of the contents in the glass tube over a given time corresponded to the overall amount of heat transmitted by the induction unit. In this section, the results of the experiments are briefly presented to provide insight on how the final formulation was achieved.

The induction coil experiments had two parameters, current and heating time, which ranged from 60 to 180 Amps and 20 to 40 seconds, respectively. A sample of the results recorded from an experiment can be seen in Table 4.1. The displayed experimental results were from an experiment that had the induction unit set to heat the wires for half a minute at 60 Amps of current. Performing a heat balance of the water, steel wires, and polystyrene tubes, the power was obtained.

Current			60	A
Time			30	s
Displayed Power			133	W
	Polystyrene	Steel	Water	
Mass	2.5	0.5	46.0	g
Specific Heat	1.30	0.50	4.18	J/g K
Start Temperature	23.3	23.3	23.3	C
End Temperature	39.0	39.0	39.0	C
Heat Absorbed (J)	51	4	3020	J
Total Heat			3080	J
Power			**103**	**W**

Table 4.2 – Sample of Data gathered from an Induction Heating Test

The induction unit that was used in these experiments displayed the total input power. This value is included in Table 4.1 so that it could be contrasted with the calculated wattage. These experiments were conducted at currents ranging between 60 and 180 Amps

in 20 Amp intervals while the heating occurred for durations of 20, 30, and 40 seconds. A condensed sample of the recorded data is located in Table 4.2. These results demonstrated that increasing time does not have a noticeable effect on the amount of power obtained from the induction heating. The results from the test involving 180 Amp and 40 second test did not have their values recorded because a noticeable amount of the distilled water had boiled during the heating phase. Since the equipment available is unable to determine the amount of latent heat that was absorbed during an experiment, these values were discarded.

		Amperage			
		60	120	180	
Time	20	95	340	460	
	30	100	270	425	
	40	95	280	----	
Average		97	297	445	Watts

Table 4.3 – Sample of Power Released from an Induction Heating Test

While running the tests, the console displayed the amount of input wattage. These values ranged from 130 Watts at 60 Amps to 520 Watts at 120 Amps to 1070 Watts at 180 Amps. This trend agrees with that of Equation 2.26.

$$Power = I^2 \times R \tag{2.26}$$

From the test results which are displayed graphically in Figure 4.10 it was found that varying the duration of did not noticeable effect the resulting power. The effective power did, however, depend on the current, as can be seen Figure 4.10. While Equation 2.26 suggests a square power curve, a linear relation – or more accurately a slightly less than linear relationship – was obtained. This observation can be explained by several losses that occur because of the nature of induction heating. While a very efficient process, the amount of heat absorbed depends on the relative resistance of the work piece and coil. In order to maximize the efficiency of the process, the copper coil must be cooled, in order for it to maintain a low electrical resistance; this causes some cooling losses to occur. The amount of heat absorbed by the work piece is also limited by the shielding that occurs from the surrounding composite itself as well as the neighboring wires.

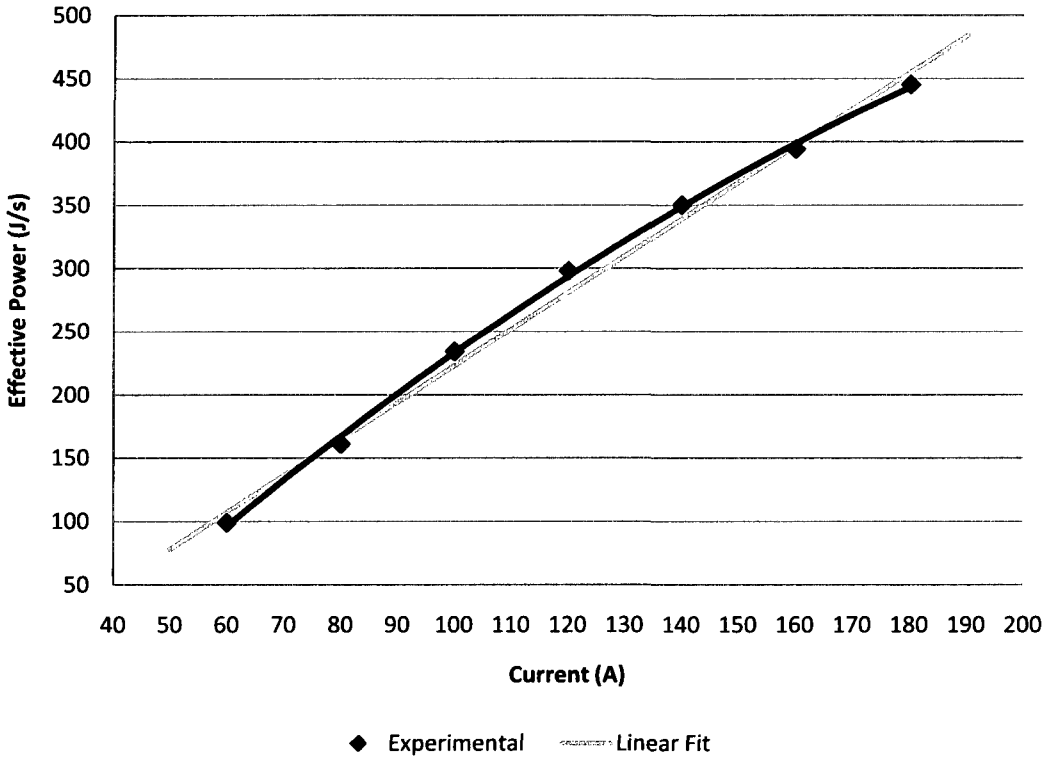

Figure 4.10 - Amount of Heat Released by Induction Heating as a function of Current

The final relationship that was selected to be used in the finite element model was a linear relationship. This type relationship was selected for its simplicity to interpolate the values in between the values obtained experimentally as well as be able to determine the power at greater currents. While the data from experiments with higher current do not have their corresponding power values rise as fast as the linear relation suggests, it is believed that some of this trend is caused by some heat being lost from a minor amount of boiling, in addition to the higher cooling losses that occurred from heating the water more. The linear relationship is displayed in Figure 4.10 alongside the experimental values; the linear equation used is:

$$Power = 2.9 \times I - 67 \tag{4.13}$$

Chapter 5

Finite Element Model of Heat Transfer and Cure

5.1 Model Requirements

The purpose of the Finite Element model was to determine the highest production rate possible for the production process outlined in Section 3.1 while still ensuring that the epoxy was cured properly. This model was required to take into account the chemical reactions that occurred within the epoxy while the rod passed first through induction heating and then the conventional furnaces. Thus the model would simulate the production process between after the braiding station and before the puller. After each simulation run was calculated, the results were analyzed to determine the heat distribution at different time intervals and at what point different elements reached a fully cured state. It is desired to have the composite leave the furnaces at 100% cure because of two reasons. First, the rod is rapidly cooled after leaving the furnace to prevent thermal degradation. Therefore, curing is expected to cease after the rod leaves the rod. Secondly, the puller subjects the rod to a strong compressive force as it pulls the rod along its caterpillar track. During experiments where the composite rebar only possessed a moderate cure fraction, it was found that the rebar experienced notice deformation after passing through the puller.

5.2 Choice of Finite Element Package

In order to meet the requirements described above, the Finite Element program ABAQUS was selected. ABAQUS is a powerful software package that can be used to simulate a wide variety of engineering problems, including heat transfer. This product is the flagship software of ABAQUS Inc. and can be used either in standard or explicit modes and offers better compute time efficiencies when compared with similar packages [56].

ABAQUS has three methods to create a Finite Element model. The first and most common way is to use the Computer-Aided Engineering (CAE) program that allows the user the ability to use a graphical interface to program the model, its various features, and loads applied. This method is very similar to Computer Aided Design (CAD) software, except that it takes the design further and allows the user to determine how a design will fare with

different loads. While the CAE allows for a wide variety of tasks to be controlled, some ABAQUS features are unavailable to the CAE, in order to simplify the interface and make it easier to use. Instead, the user can create a model by writing an input file (.inp) to code the model and its features. These approaches to creating a model are not mutually exclusive, as the CAE can create an input file that can then be modified. Likewise, input files can be loaded in the CAE and edited. The third way that one can create a model in ABAQUS is by writing a Python script. Python is a high level open source programming language that can be used to script programs like ABAQUS or create standalone applications [57]. By using Python, one gains even more control over the creation of the model. However this additional control comes at the price of having to know the programming language, as well as having to create some of the functions that are already set up for the CAE and input file paths.

To allow property changes (material property changes, different loading conditions, etc.) as the model is being calculated, ABAQUS allows user subroutines to be added to the model. By using a programming language, in this case Fortran, a user subroutine can be written to have modifications made to the model based on variables that change as the model is calculated. Thus, in addition to the ABAQUS software, a Fortran compiler was also required to implement the user subroutines that are mentioned in the next section. For this thesis, Compaq Visual Fortran 6 was used, as it was the most compatible with ABAQUS. The Fortran code was attached to ABAQUS through the CAE interface. At the beginning of calculating a model, the Fortran code is compiled by ABAQUS and then accessed when needed.

5.3 Construction of the Model

The first step in constructing the Finite Element model was to determine the proper length of the rod that would be modeled. The model could not encompass too long a rod since that would require a large amount of elements and therefore make the solution either less accurate than a smaller rod or more cumbersome to compute. However, using too short a rod can also cause some problems. Ideally only the cross-section of the rod would be used as a model to maximize the amount of radial elements, but this setup would require knowing in advance the amount of lateral heat that is transferred as the rod passes through different heat sources. Instead of calculating this heat transfer, it was felt that the most accurate

solution would be to use a reasonably long rod. The modeled length was obtained through a simple convergence study, with lengths ranging from one centimeter to twenty-four centimeters. While the two ends of the cylinder were considered insulate, elements halfway between the two ends would have longitudinal heat transfer able to occur in both directions. It was found that at a length of twelve centimetres, or eight times the rod's diameter, was sufficient long enough to have a negligible effect on the longitudinal heat transfer. This length was also approximately the distance between the end of the induction heating coil and the entrance of the furnace. With the mesh size selected in Section 6.1, the total computation time of the model took slightly over one hour.

The physical features, material properties, and interfacial data were all input into ABAQUS by the use of its CAE interface. Table 5.1 contains the basic material properties that were used. While both the carbon and aramid fibres are anisotropic in behaviour – where they having a higher conductivity in the longitudinal direction – it was found that longitudinal heat transfer had only a minor influence on the model. This was because the heat is locally generated and therefore there is only a significant difference in temperature between the two ends during the induction heating stage. Along with the material properties, there were also interfacial properties that were needed when heat transferred between the steel and carbon elements, as well as between the inner and outer layers of the composite. Since the same uncured epoxy coated both the aramid and carbon fibre, there is minimal interfacial resistance expected. Likewise, the epoxy fully wets the steel wires during the epoxy impregnation stage and therefore a large conductivity value for the interface was achieved. The final values used in the model were obtained by comparing the model with experimental results. It was found that that making moderate changes the interface values of the model had relatively minor effect. The interfacial conductivity values are presented in Table 5.2. To control the heat released by the polymerization of epoxy, the user subroutine HETVAL was used.

Material	Specific Heat ($J\ kg^{-1}\ K^{-1}$)	Radial Conductivity ($W\ m^{-1}\ K^{-1}$)	Axial Conductivity ($W\ m^{-1}\ K^{-1}$)	Density ($kg\ m^{-3}$)	Emissivity
Aramid + Epoxy	670	0.12	0.4	1270	0.85
Carbon + Epoxy	855	0.4065	400	1470	–
Steel	500	50	50	7800	–

Table 5.1 - Material Properties [11]

Interface	Conductivity ($W\ m^{-1}\ K^{-1}$)
Steel – Carbon	200
Carbon – Aramid	800

Table 5.2 - Interface Properties

The subroutine, HETVAL, was used to record when the element obtained a fully cured state, as well as calculating how much heat was released as the curing took place. Figure 5.1 is a flow chart that illustrates the logic used when determining how much heat to release. When computing the model, this flow characteristic is activated at the end of every iteration for each element of carbon or aramid composite. If the subroutine determines that the composite element is curing, it increases the temperature of the element by an amount determined by the formula. This temperature increase is then propagated to the rest of the rod during the next iteration.

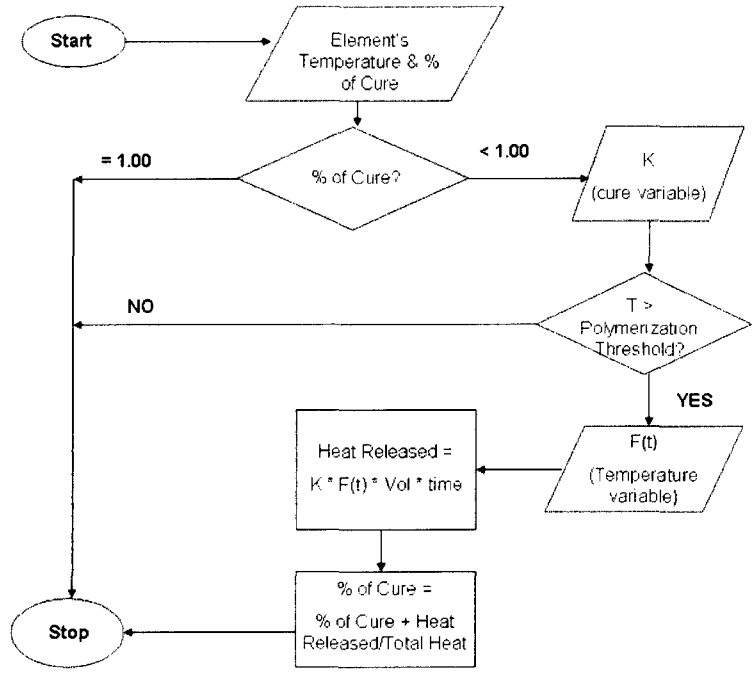

Figure 5.1 - HETVAL Process

The user subroutine DFLUX was used to designate the proper elements that were to be heated during both the induction heating and the furnace stage. Figure 5.2 is a simple sketch of how the process changes as it moves towards the rod, where leftmost portion of the rod was used as the reference point for all distances. For the heating to correspond to the rod's progress, both the coordinate of the element and the time were required. By inputting a production speed into DFLUX, the location of the element in relation to the process was calculated by ABAQUS so it could be heated or cooled accordingly.

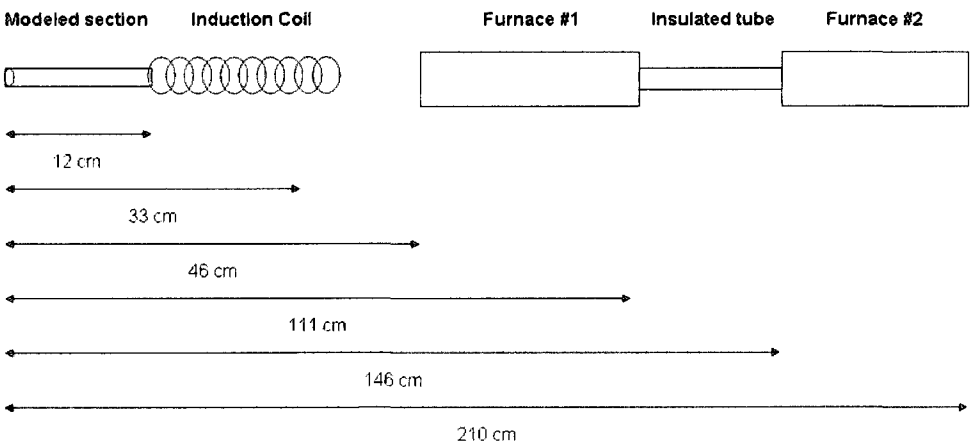

Figure 5.2 - Region Modeled by ABAQUS. Not drawn to scale.

The final portion of constructing the Finite Element model was to divide the rod into elements. The element type was DC3D8, an eight-node linear heat transfer brick; this is the standard heat transfer element used in ABAQUS. A screen shot of a rod that has been meshed can be found in Figure 5.3. A sample of FEA model used in this thesis can be found in Appendix D as an input file created by the CAE program. Along with the input file, both subroutines are also located in Appendix D.

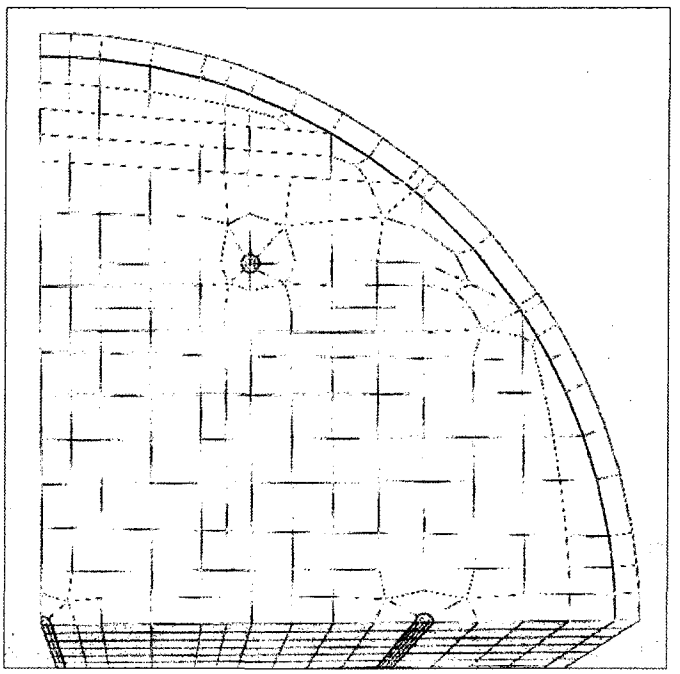

Figure 5.3 – Rod Broken Down into Elements

5.4 Assumptions and Simplifications

As this is a heat transfer model, some physical characteristics of this process would require a separate Finite Element model to quantify their effects. As such, the mechanical stresses placed on the fibres by the puller are assumed to have no influence on the curing process or local fibre density. More importantly, the model also assumes that there is a uniform distribution of epoxy within the layers prior to curing. As mentioned in Section 3.1, the impregnation station between the creel and the braider applies epoxy resin to the carbon fibres as they pass through. In order for this assumption to be correct, all the carbon and aramid fibres must be completely impregnated before they pass through the induction coil.

As there was uncertainty present in data used in the development of the model, the resulting data obtained from a simulation also contained some error. Therefore it was not expected to obtain 100% accuracy with the FE model but instead to better understand how the epoxy cures as it passes through the production process. The model was deemed successful if it could accurately predict trends when modifying the parameters and allow the production process to operate with greater confidence in the final product without having to conduct several costly test runs.

Chapter 6

Discussion

6.1 Convergence Study of the FEA Model

The purpose of the finite element model was to analyze how the fibre composite rebar cured as it passed through the induction coil and furnaces. Before its results are displayed, a proper mesh size must be obtained. The selection of a proper mesh size is important since the ultimate results of FE model depend on having enough elements to fit the behaviour sufficiently. Typically the finer the mesh, the more accurate the results are, however there are exceptions. Thus, the results of various meshes must be compared to determine the pattern of the results delivered by the model.

For this study, four meshes were utilized. The coarsest mesh was dubbed "Lowest" while the finest mesh was referred to as "Highest". Each mesh increment resulted in roughly double the number of cross-sectional elements, thus the "Highest" mesh had eight times the elements that the "Lowest" mesh. The results of the convergence study can be seen in Figure 6.1 and Figure 6.2. It was found that only the Low mesh results diverged somewhat from the other three meshes; however, the discrepancy from all meshes was fairly minor. Nevertheless, the High mesh was selected for this study.

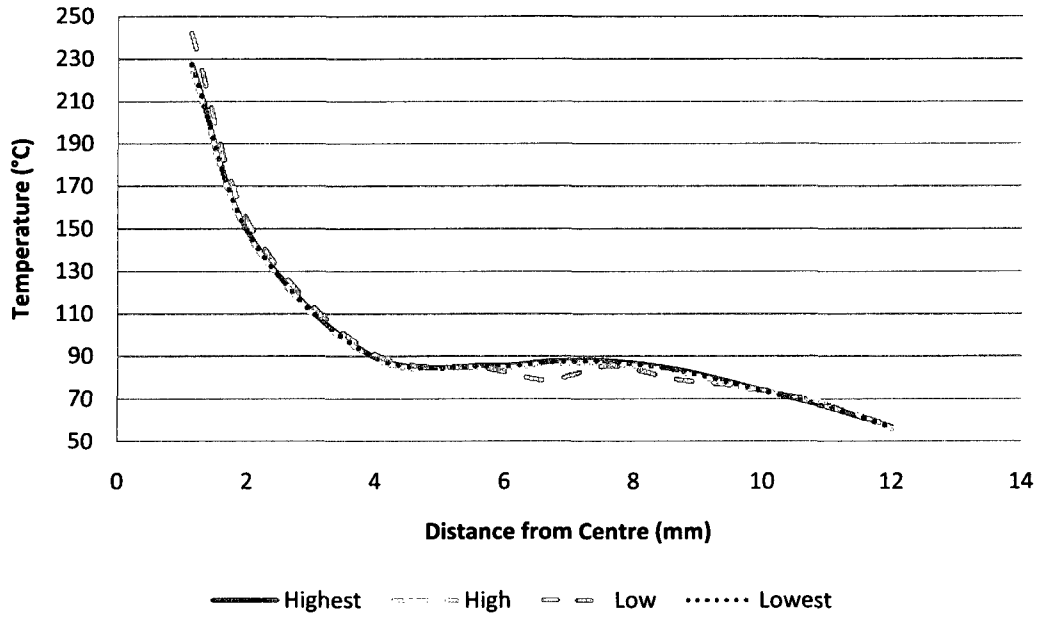

(a)

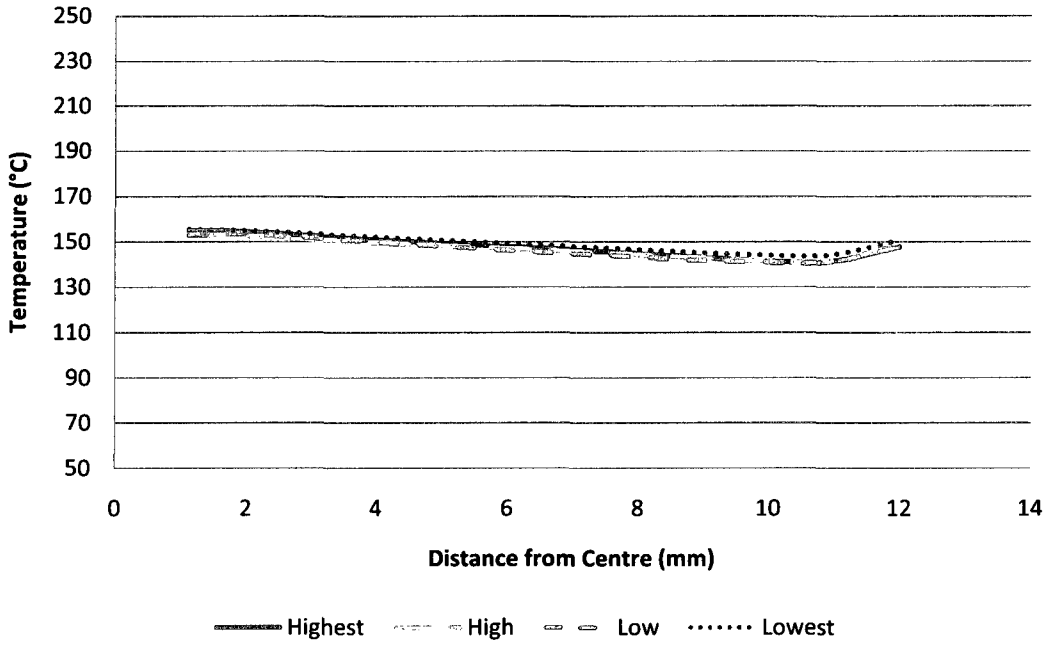

(b)

Figure 6.1 – Temperature Convergence Study
a – 30 seconds; b – 60 seconds; c – 90 seconds; d – 120 seconds

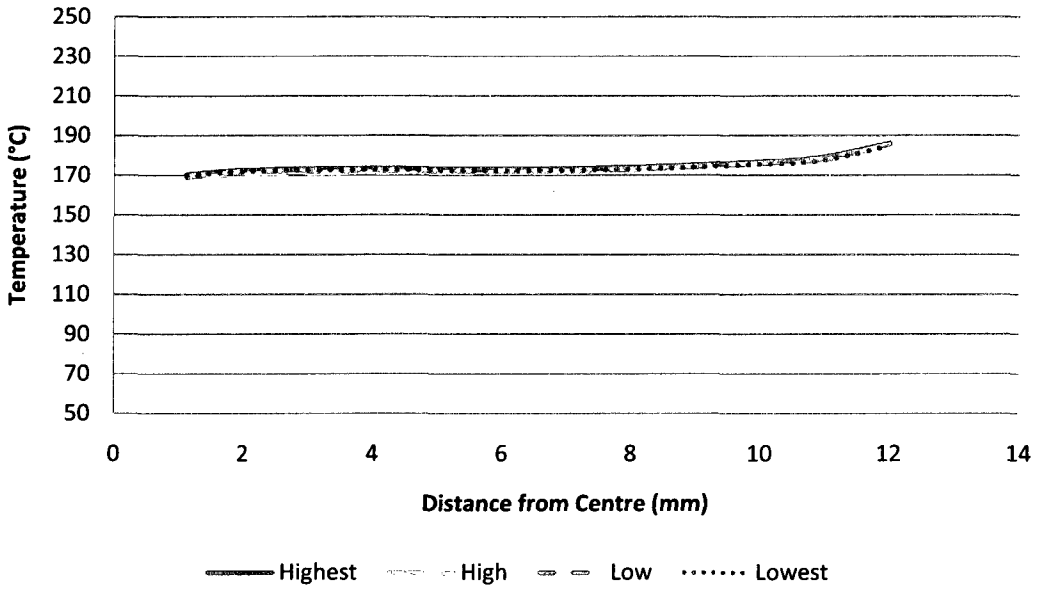

(c)

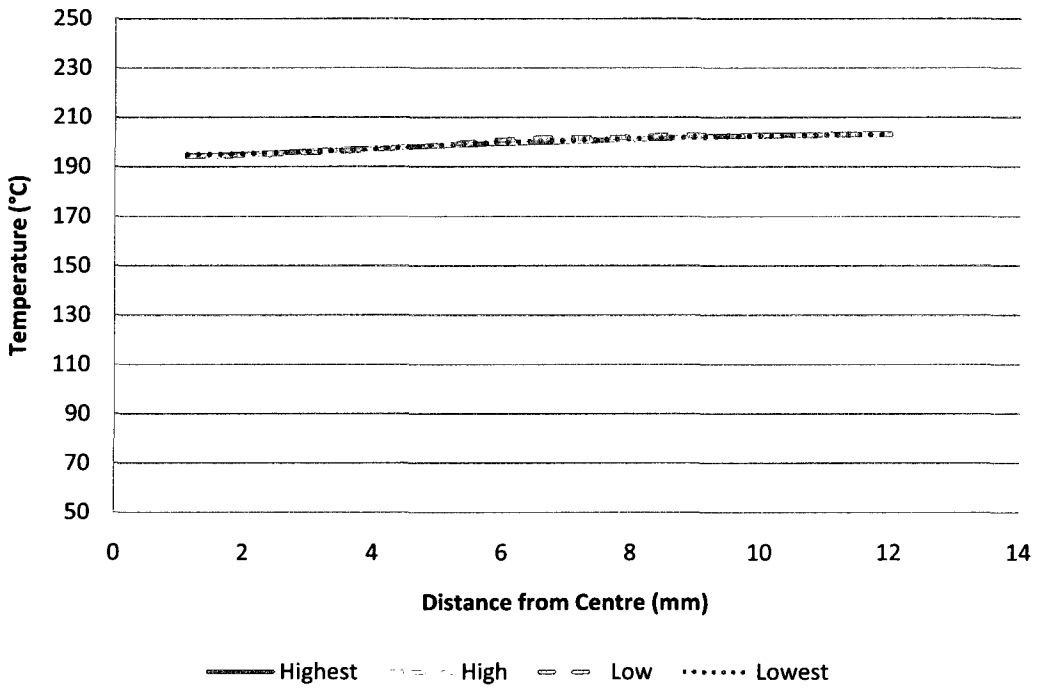

(d)

Figure 6.1 – Temperature Convergence Study
a – 30 seconds; b – 60 seconds; c – 90 seconds; d – 120 seconds

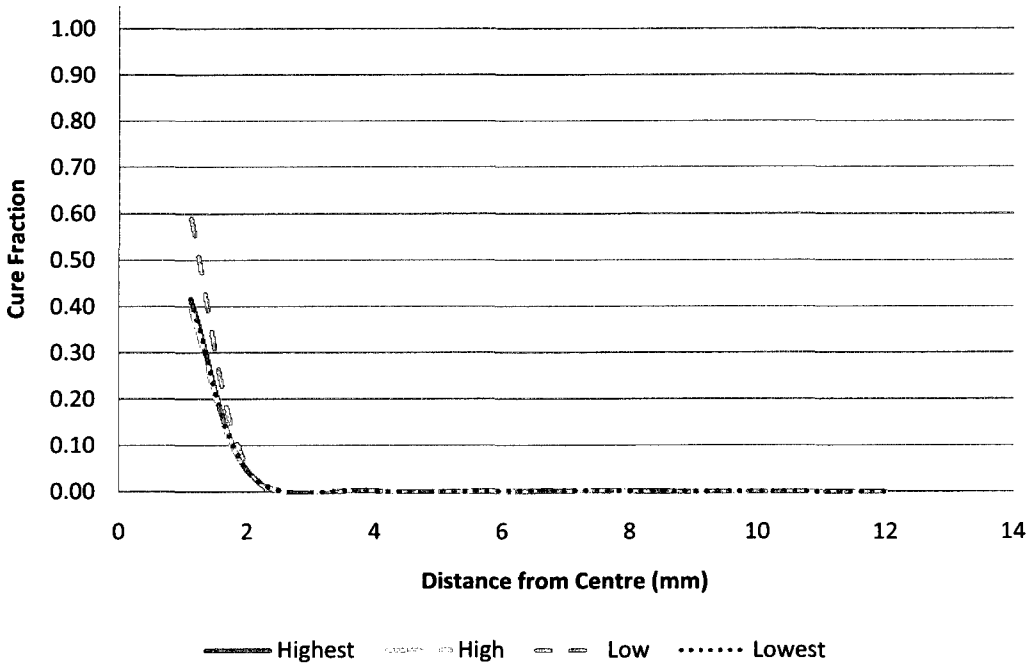

(a)

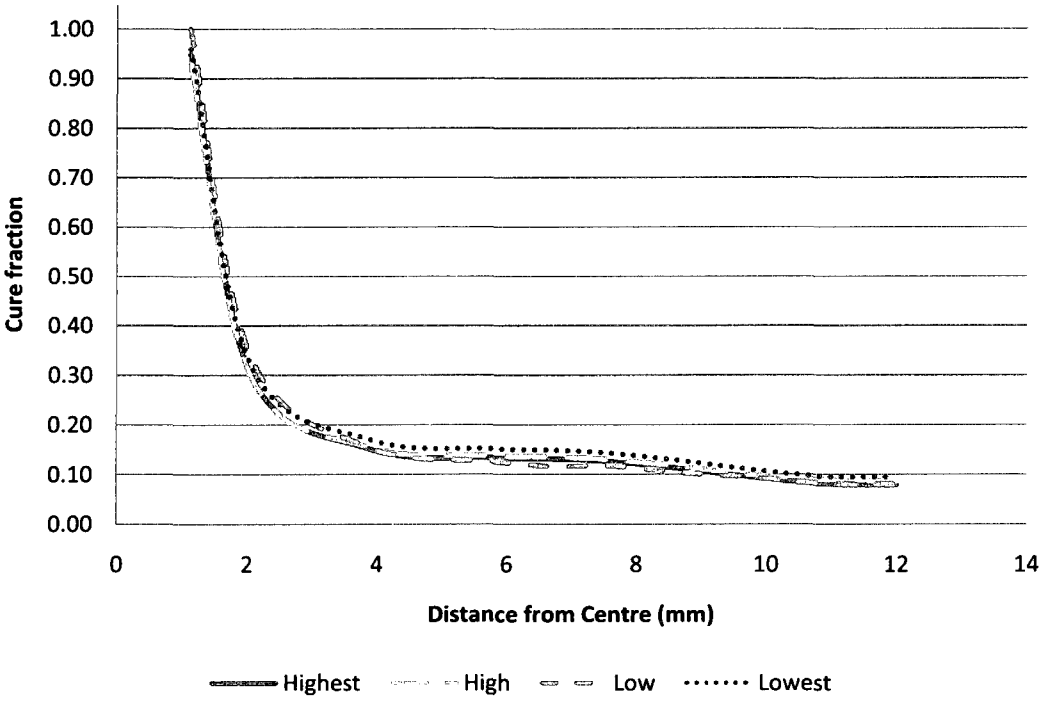

(b)

Figure 6.2 – Cure Fraction Convergence Study
a – 30 seconds; b – 60 seconds; c – 90 seconds; d – 120 seconds

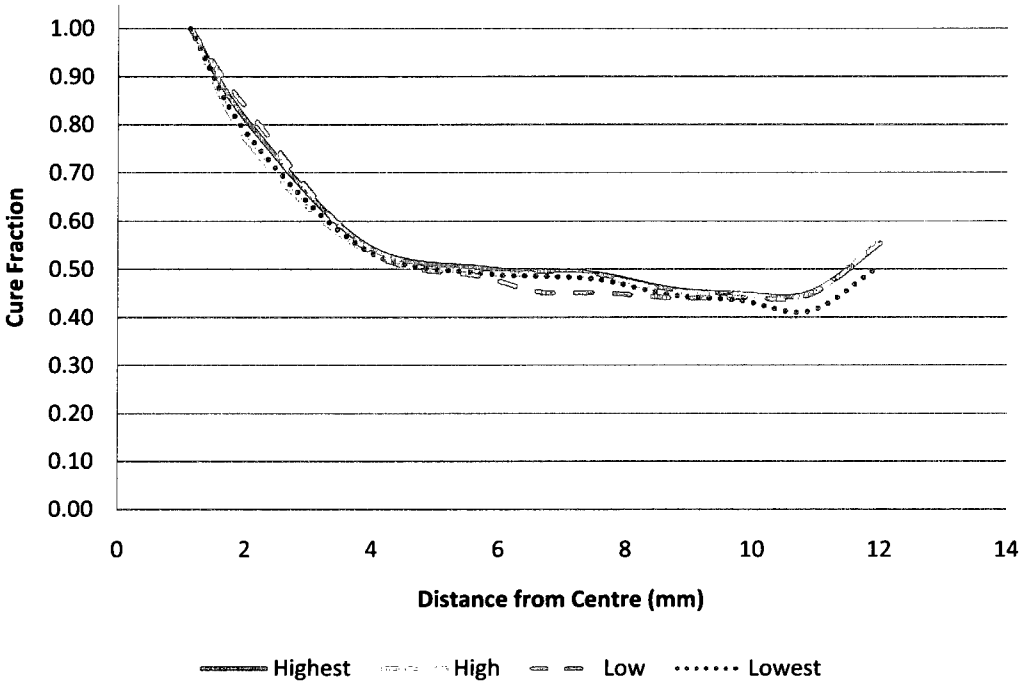

(c)

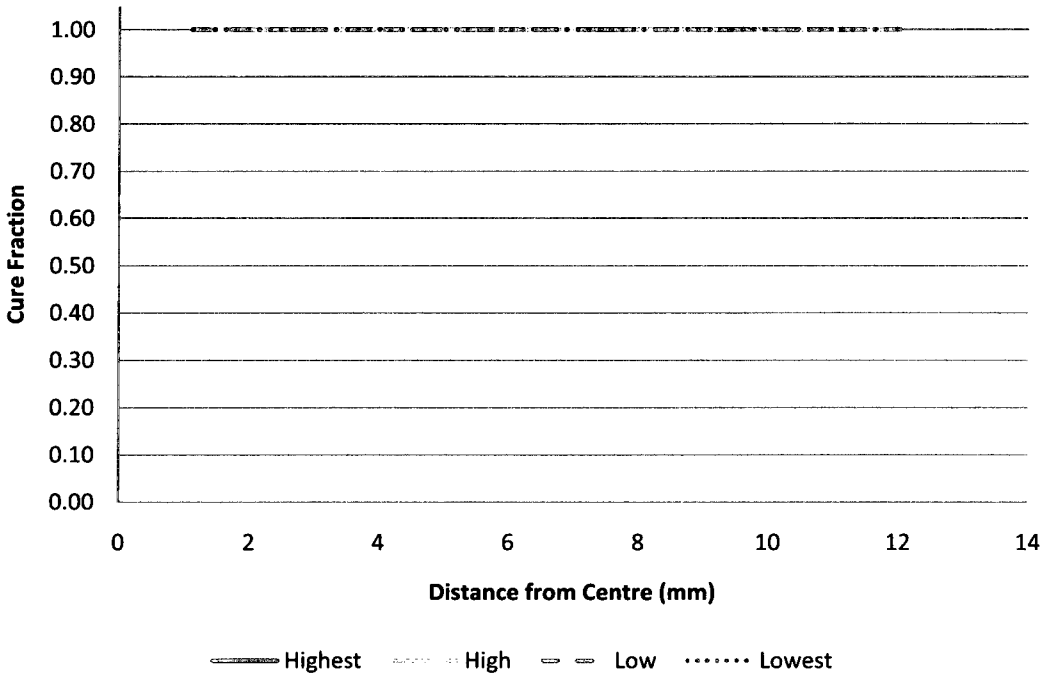

(d)

Figure 6.2 – Cure Fraction Convergence Study
a – 30 seconds; b – 60 seconds; c – 90 seconds; d – 120 seconds

6.2 Validation of FEA Model

In addition to the convergence study, a validation study was performed with the finite element model to ensure the results resembled experimental data. By removing the epoxy formulations from the FE model, a simple comparison could be made between experimental, analytical, and FE model when a cured rod is simply heated by a furnace at 200 °C. The value gained from this validation test was to ensure that the basic materials properties are correct, along with determining whether satisfactory interfacial values were used. The results of such simulation are displayed in Figure 6.3 along with the content of Figure 4.9.

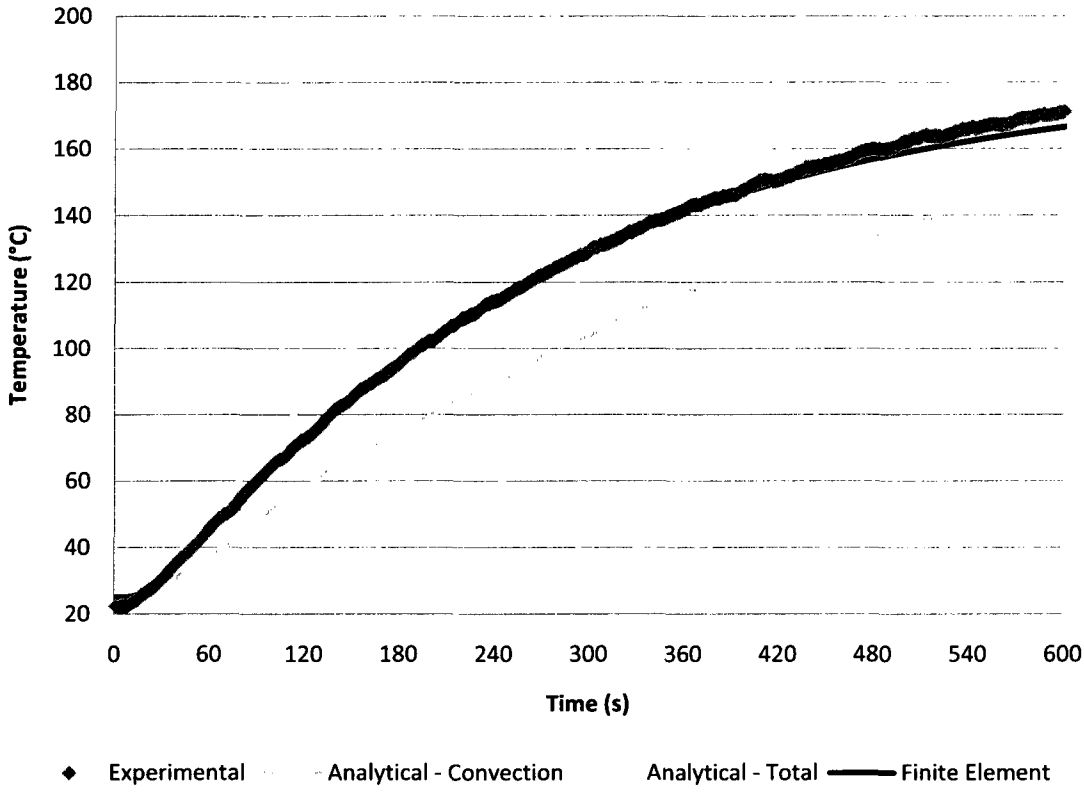

Figure 6.3 - Comparison of Analytical Model, Experimental Data, and FEA Model on Heating the Composite Rod at 200 °C

The results seen in Figure 6.4 and 6.5 display a comparison of Finite Element results and experimental data when the composite rod is curing. Just as in Figure 6.1, the results seen are for centre of the rod. Overall, the results show that the Finite Element results underestimate the amount of time required to cure the composite, with the model predicting that the rod would completely cure in 240 seconds, or approximately 50 seconds less than what was actually observed in the experiment; this translates into roughly 17% error. Other

simulations conducted at different furnace temperatures yielded comparable error values, though there was a trend with higher temperatures resulting in greater error. In all cases, the current curing formulation over-estimates the rate of cure, as it can be seen in Figure 6.5 that the FE results predict that the epoxy cures very quickly once curing is initiated. Thus the results presented in the following sections should be viewed as optimistic.

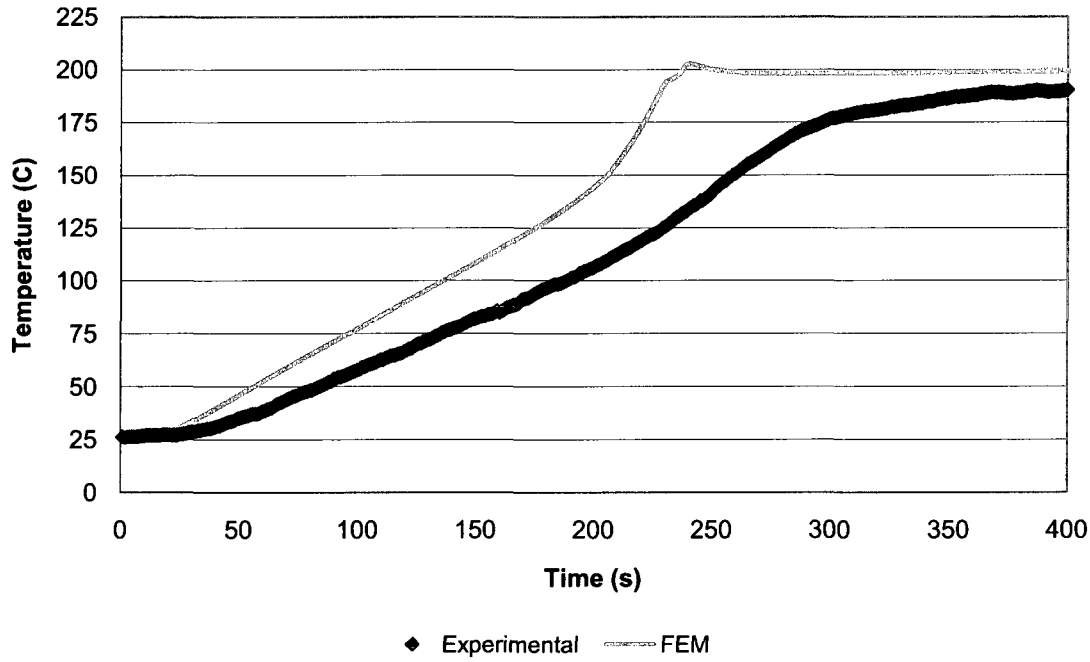

Figure 6.4 – Temperature at Centre of Rebar comparison between FEA Results and Experimental Data when cured at 200°C

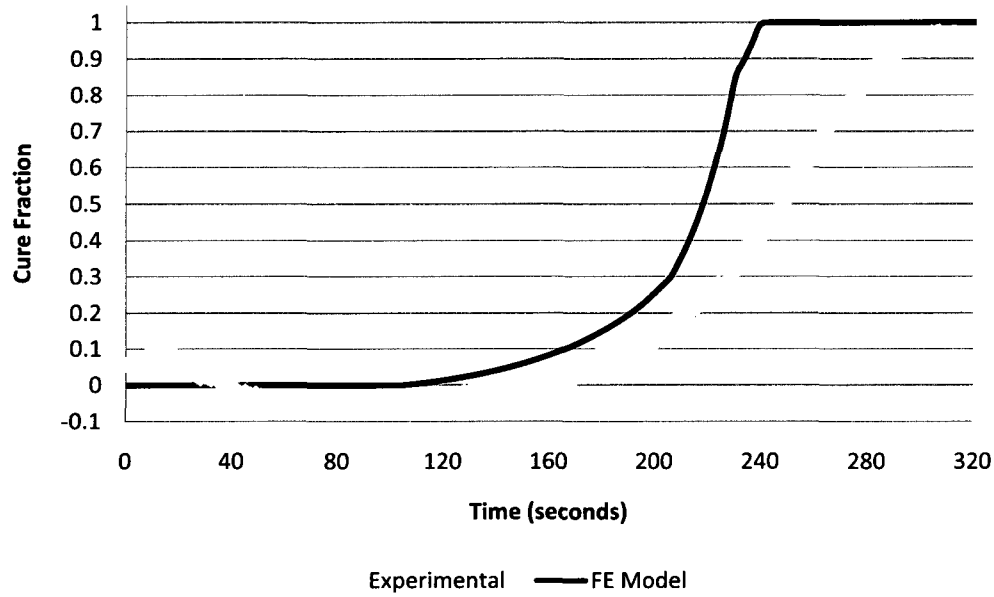

Figure 6.5 – Cure Fraction Comparison between FEA results and Experimental Data when cured at 200 °C

6.3 Comparison between Furnace and Induction Heating

To further explore the effect of curing epoxy with induction heating and to compare its results with traditional furnace heating, a set of cross-sectional profiles of temperature and cure fraction were created. These profiles were created at two different settings for both forms of heating; induction heating used 115.5 and 231 Amps while the furnace was set for 200 and 240 °C. It should be noted that the overall heat flux for the induction heating tests was higher than for the furnace. The purpose of this comparison is not to determine which method can cure the composite faster but instead to evaluate the progression of the cure fraction. A fibre composite rebar diameter of 25 mm was chosen for the simulations because it represented the maximum diameter that this production process would produce; this size is difficult to cure uniformly even by pultrusion. The location of the nodes that were selected can be seen in Figure 6.6. The first two tests were conducted with induction heating while the remaining tests were run with furnace heating.

Figure 6.6 - Location of Nodes used in the Cross-Section Profile

The first test used an induction heating setting of 115.5 Amps. The data presented in Figure 6.7 and 6.8 displays the cross-sectional profiles for temperature and cure fraction, respectively. The effects of induction heating demonstrate that the placement of the wires influences how elements heat up. It can be seen in Figure 6.7 and Figure 6.8 that a local maximum is reached around the 7.5 mm radial position, corresponding to the intersection of heat fluxes generated from the two nearby wires.

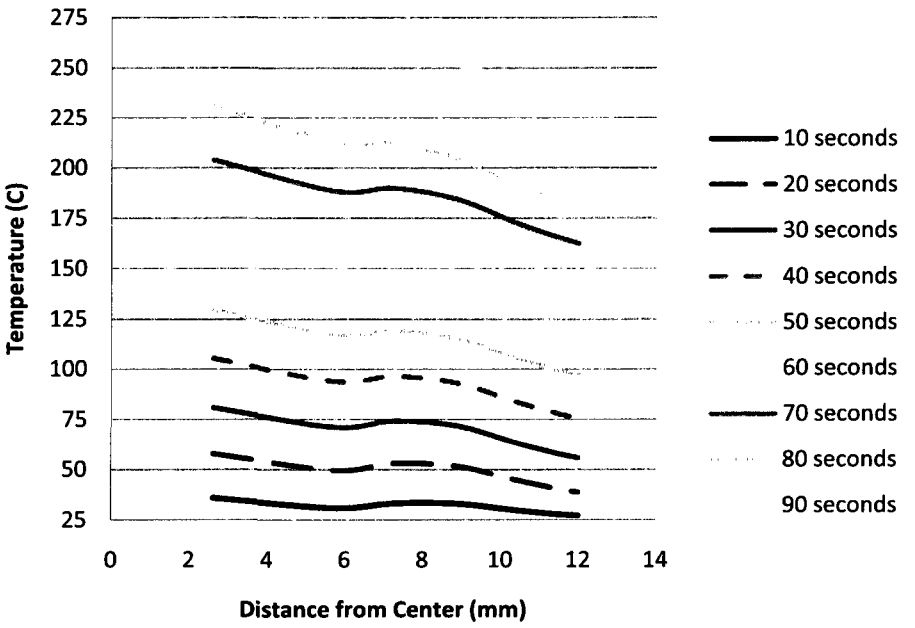

Figure 6.7 - Temperature Cross-Section of a 25 mm rod cured at 115.5 Amps

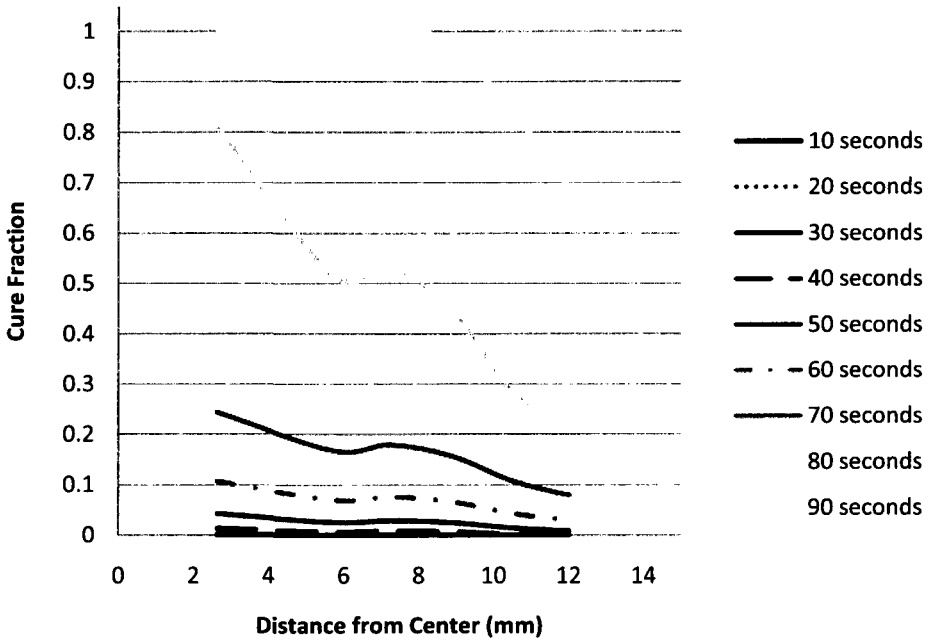

Figure 6.8 – Cure Fraction Cross-Section of a 25 mm rod cured at 115.5 Amps

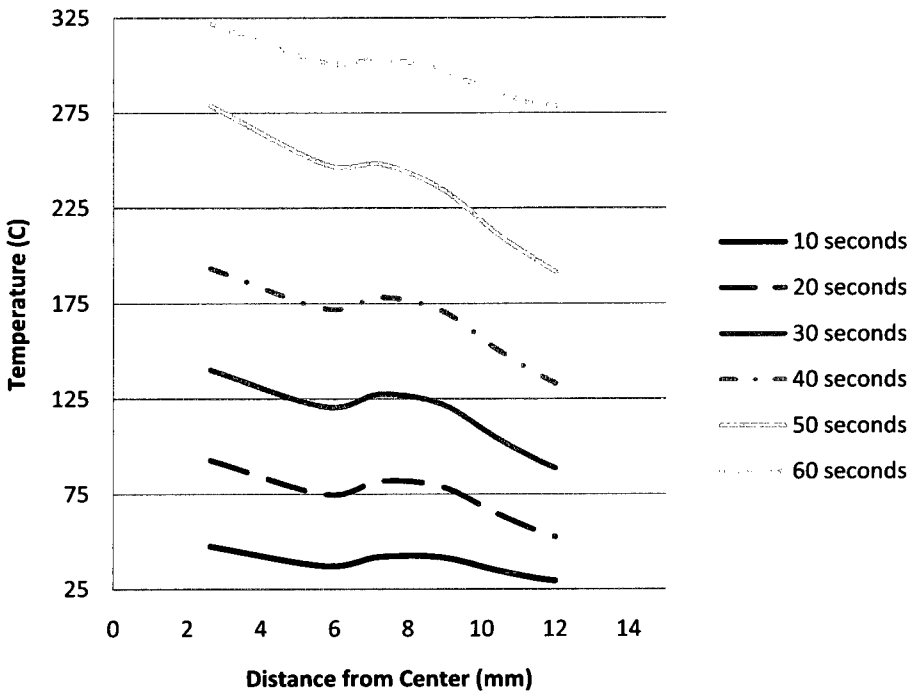

Figure 6.9 - Temperature Cross-Section of a 25 mm rod cured at 231 Amps

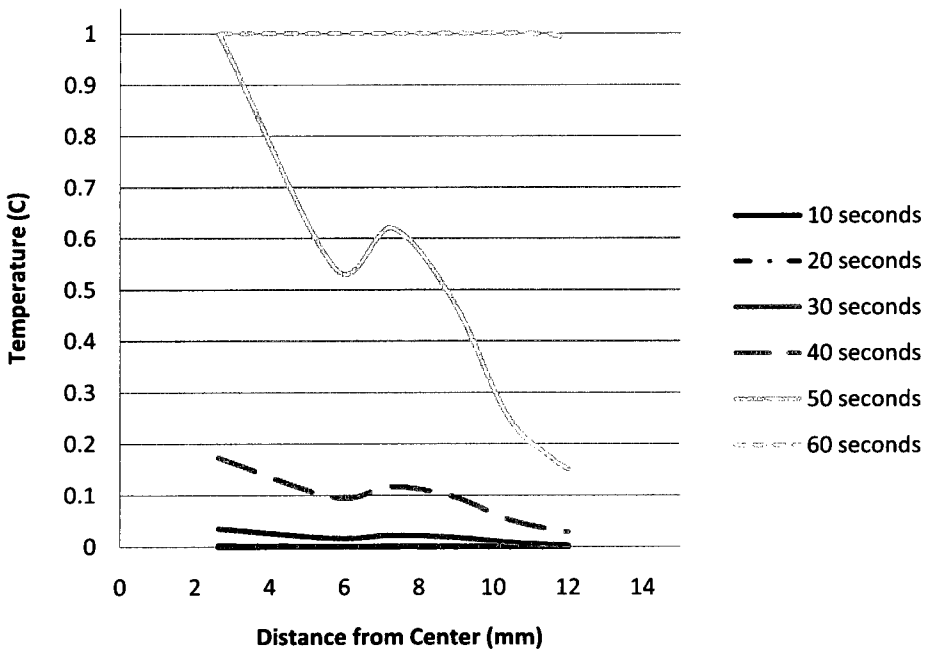

Figure 6.10 - Cure Fraction Cross-Section of a 25 mm rod cured at 231 Amps

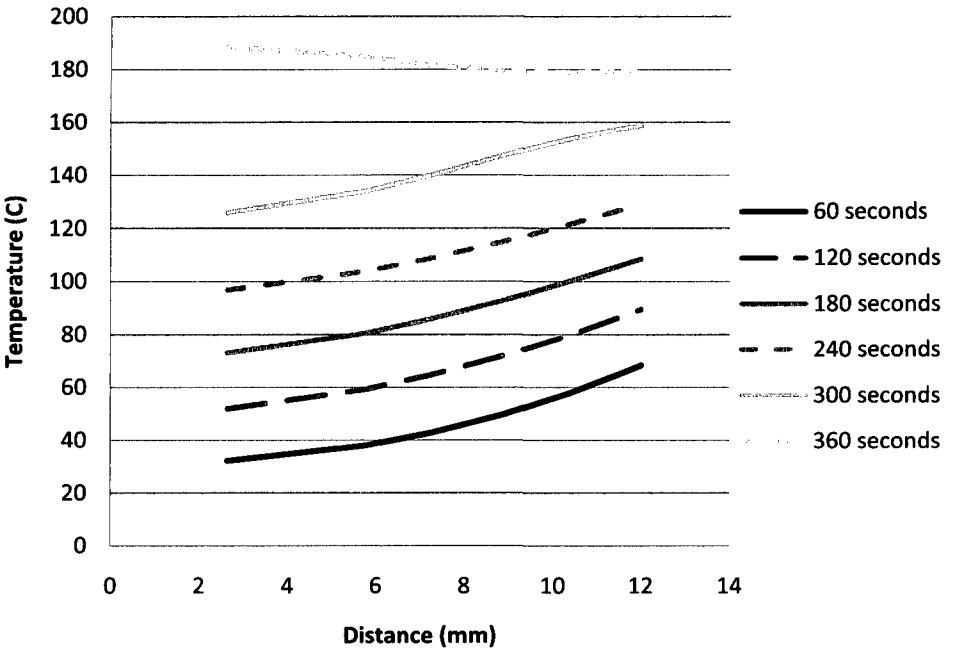

Figure 6.11 - Temperature Cross-Section of a 25 mm rod cured at 200 °C

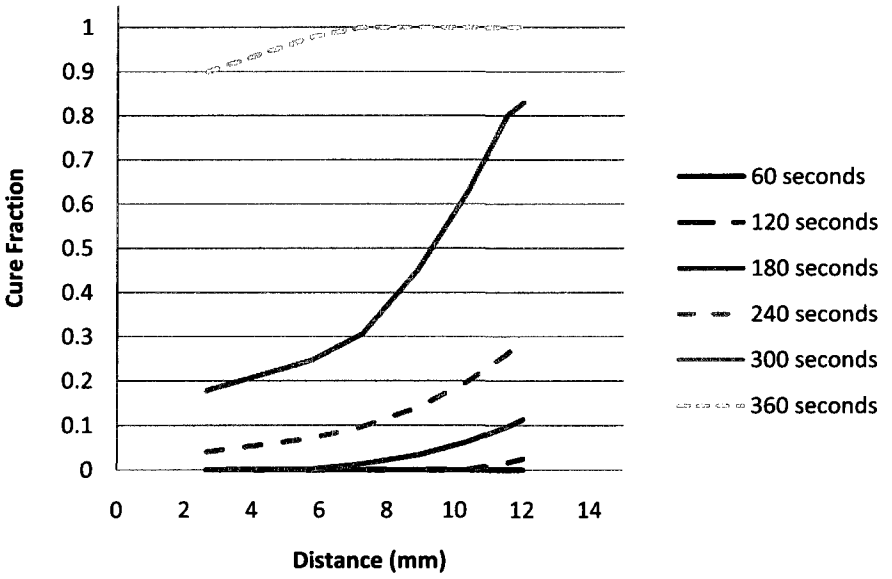

Figure 6.12 – Cure Fraction Cross-Section of a 25 mm rod cured at 200 °C

In Figure 6.12, there is a large difference in cure fraction at the 300 second mark, with the centre being approximately 20% cured while the region near the overwrap is at 80%. This difference is due to outer elements being at a higher temperature and therefore

curing much faster. It should be noted that at the end of the test, in Figure 6.11 the results show that the core temperature is about ten degrees Celsius above the outer elements. It appears that the core's temperature rises very rapidly at the end when it reaches sufficient temperature to cure rapidly. As such, while curing at 200 °C, when the centre temperature equals the surface temperature, it can be inferred that the rod is almost fully cured.

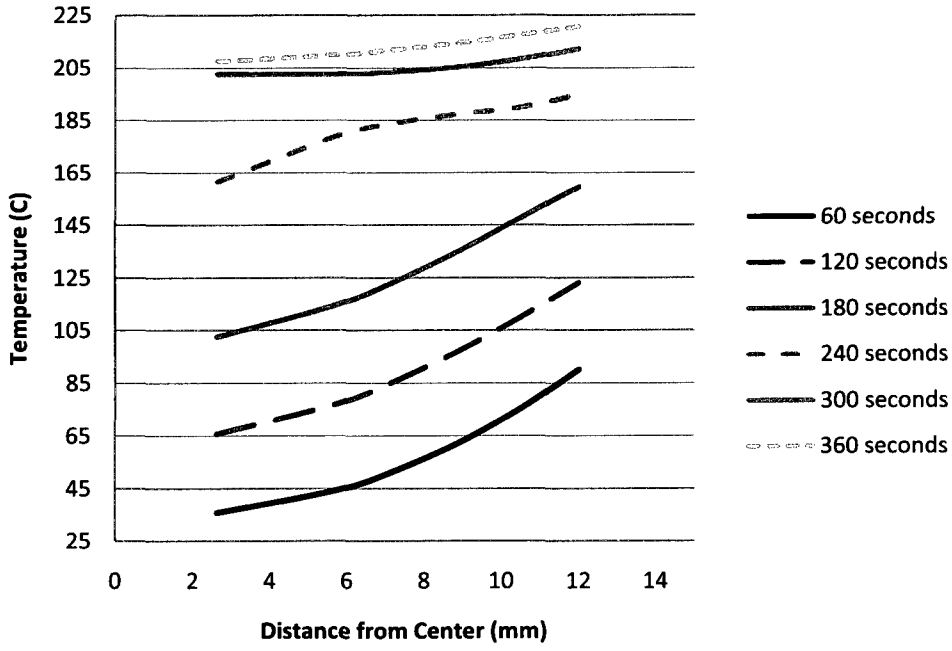

Figure 6.13 - Temperature Cross-section of a 25 mm rod cured at 240 °C

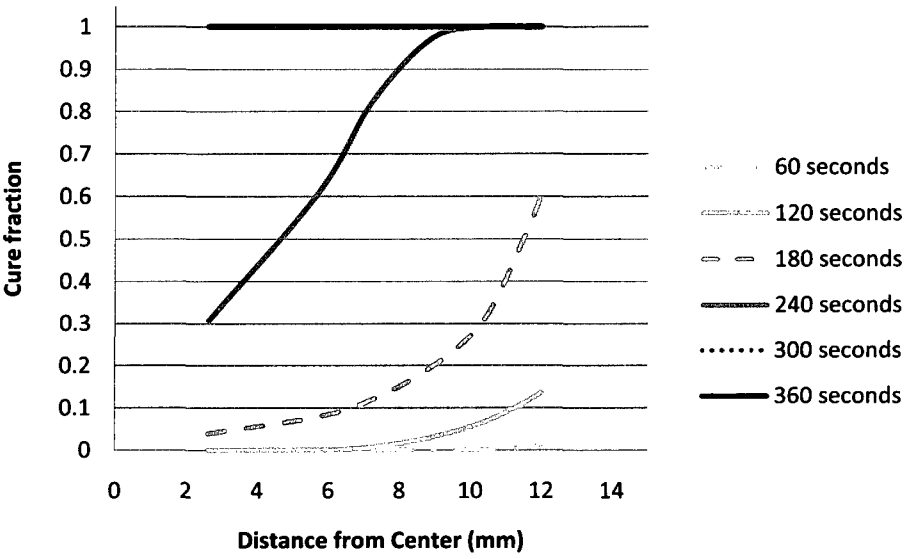

Figure 6.14 - Cure Fraction Cross-Section of a 25 mm rod cured at 240 °C

In Figure 6.13, the temperature rises consistently throughout the heating stage until reaching the 240 second mark; once past this point, the temperature does not change much near the surface. This is partly due to the lowering heat flux from having a hotter surface but also results from having much of the composite already cured around this area. The center area behaves differently than the outer region after 240 seconds since the epoxy there has more epoxy to cure and therefore has its temperature rise from the exothermic heat.

Overall, the results generated from the furnace heating tests show the epoxy fully cured on the surface of the core before the center is half-cured. This is a predictable result since the heat is applied from the outside and propagates in. As the epoxy reaction rate depends strongly on the temperature at which the reaction is occurring at, the elements near the surface cure at a faster rate. This simple principle works well for induction heating, where the source of heat – wires – is embedded inside the core and disturbed through several wires.

The weakness of using induction heating, however, is that the input heat is concentrated where the wires are located. Thus, as seen in Figures 6.9 and 6.10, the temperature is much lower near the surface of the core and the elements cure at a far slower rate than what is observed in the centre. Thus, in order to meet the requirement of curing the composite consistently through the thickness, the placement of wires is critical to ensure that

roughly equal temperature rise occurs. To achieve this, furnace heating could be used to complement induction heating and thereby eliminate the need to place wires near the surface. If the requirement is to simply cure the inner portion of the composite before the overwrap, then placing wires near the centre is sufficient.

6.3 Parametric Study using FEA Model

The finite element model was used to calculate the temperature and cure fraction profiles at three different production speeds: 50, 75, and 100 centimeters per minute. The lowest speed (50 centimeters per minute) was chosen because it represented the current speed, whereas the highest production speed was an upper limit. The amount of heat released from the induction and furnace stages was also a parameter. These simulations were conducted at two different induction current and furnace temperatures, 115.5 or 231 Amps and 200 or 240 °C, respectively. These values had been determined experimentally, by trial and error, as being reasonable values to cause curing in a short period of time. The purpose of the parametric study was to find the combination of induction heating setting and furnace temperature that would result in a uniform cure through the thickness to reduce residual stresses and thermal cracking. A list of the simulations and the parameters used can be seen in Table 6.1. Once the computations were complete, nodes of interest from the middle of the simulated rod were selected. The location of the nodes, along with their designated number can be seen in Figure 6.15. The nodes that were picked represented the behavior of specific key areas of the cross-section. The temperature and cure fraction graphs created with this data can be seen in the remainder of the chapter.

Processing Speed	Simulation	Induction setting	Furnace Setting
50 cm/minute	**1**	**115.5 A**	**200 °C**
	2	**115.5 A**	**240 °C**
	3	**231 A**	**200 °C**
	4	**231 A**	**240 °C**
75 cm/minute	**5**	**231 A**	**200 °C**
	6	**231 A**	**240 °C**
100 cm/minute	**7**	**231 A**	**200 °C**
	8	**231 A**	**240 °C**

Table 6.1 - Parameters Modified in the Finite Element Model

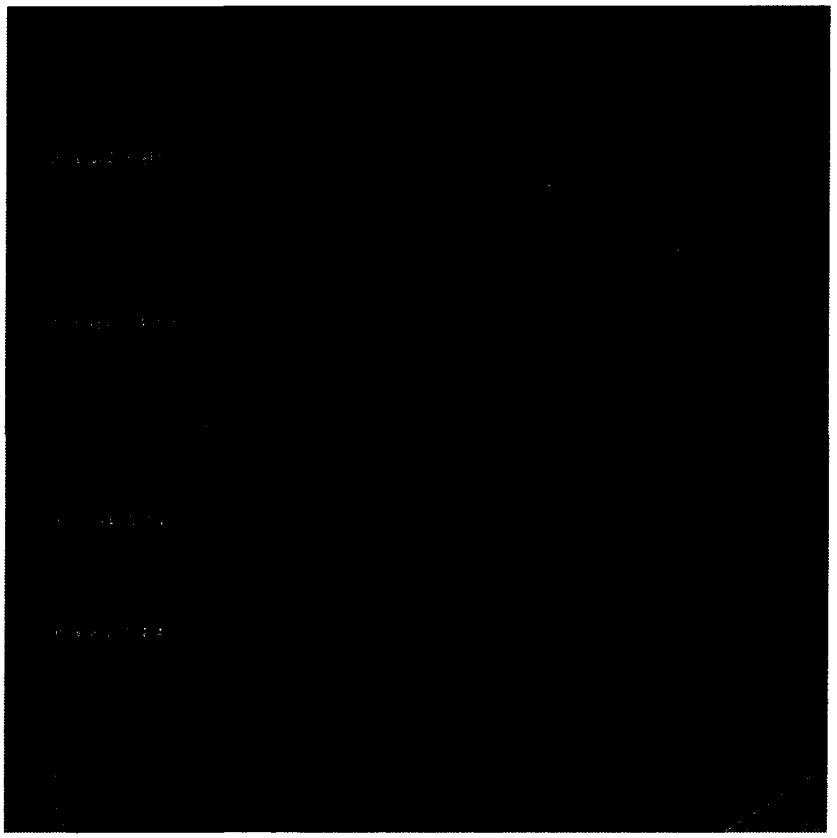

Figure 6.15 - Location of Selected Nodes

6.3.1 Processing at 50 centimetres per minute

For this type of production, a process speed of 50 centimeters per minute was considered to be an acceptable speed that is commercially viable. When processing at this speed, the centre of the modeled rod completes the induction heating stage in 40.8 seconds, while the total production line finishes at 222.8 seconds. While the finite element model computed the model until 280 seconds, only a minimal cooling heat transfer was calculated and thus the data after past the end of the furnace should be taken as only a suggestion of what happens after the rod leaves the furnace. The results of Simulation 1 can be seen below in Figure 6.16.

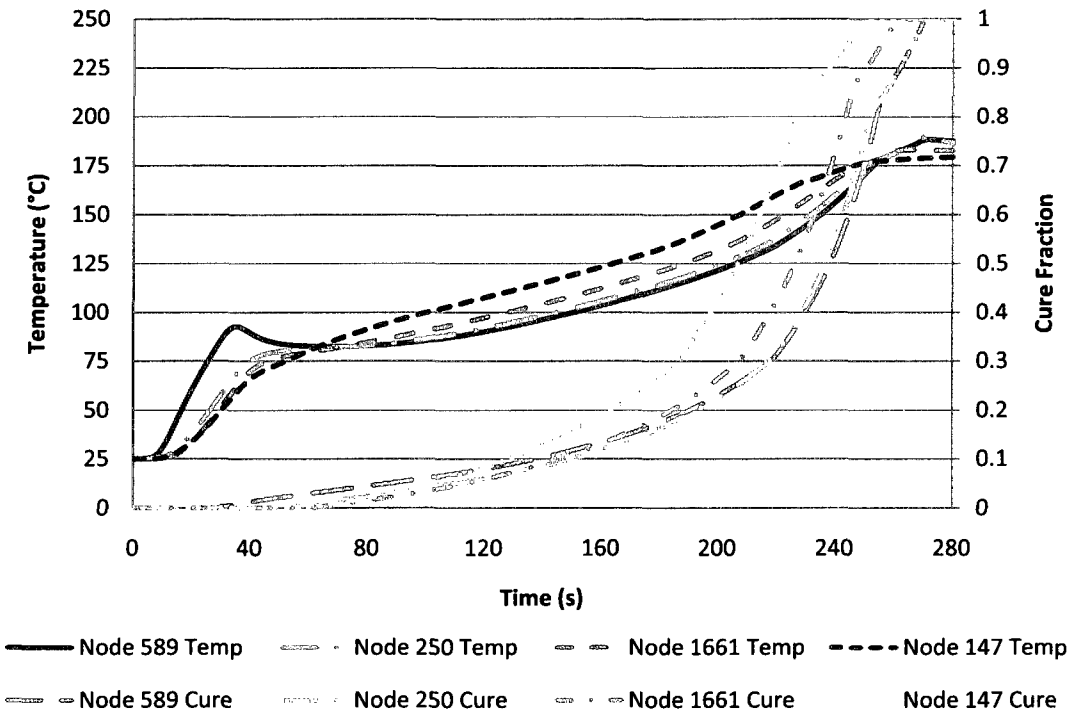

Figure 6.16 – Sim 1: Induction 115.5 Amps, Furnace Heating 200 °C

The data seen in Figure 6.16 demonstrates the effectiveness of induction heating to heat the interior, though it appears that it does not generate enough heat to initiate the curing reaction. This can be seen around the 40 second mark where the temperature peaks, just at the cusp of a rise in cure fraction. Because of this deficiency, it is the outer node that heats up over 80 °C the fastest and therefore cures the quickest. At the end of the production line, only the outer-most node is cured sufficiently.

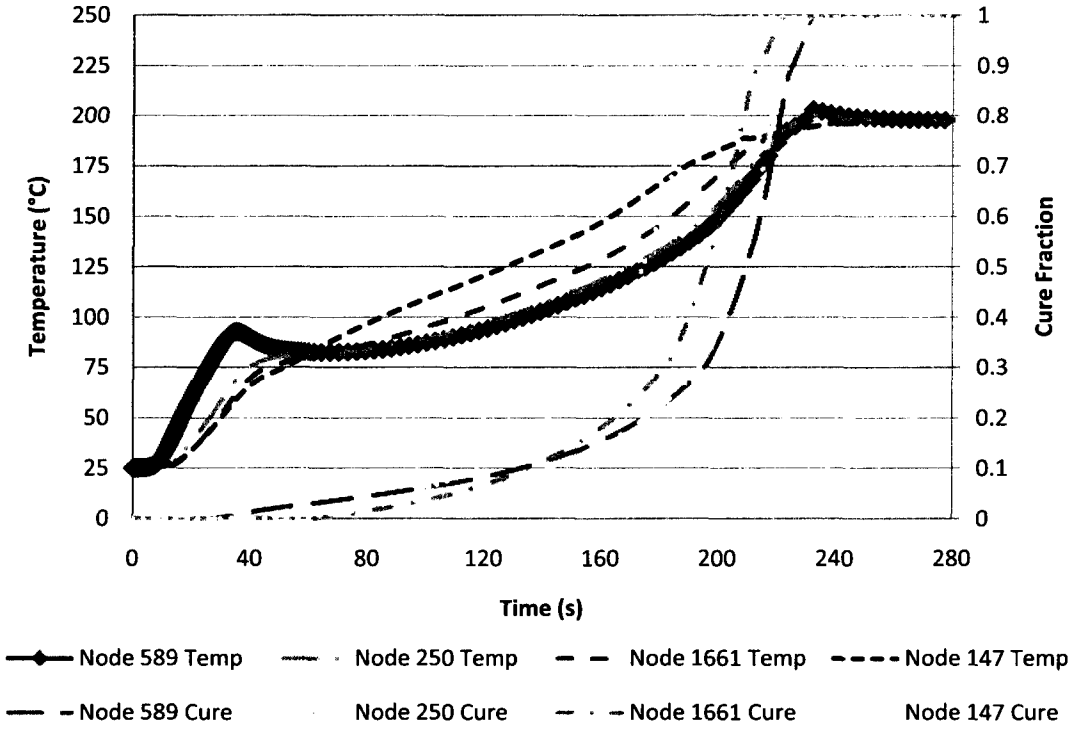

Figure 6.17 – Sim 2: Induction 115.5 Amps, Furnace Heating 240 °C

The above graph, Figure 6.17 displays Simulation 2, which has a higher furnace temperature than the previous test. This increase of the furnace temperature seems to have a profound effect on curing the composite, with the last node curing before the first node cured in Simulation 1. While all nodes cured before the completion of the production line, the nodes cure in the opposite order than desired. It should also be noted that the final temperature of the composite is only 200 °C, which means that the furnaces could be set to an even higher temperature or the furnace length increased to improve the curing rate. However, these changes would have a much more noticeable impact on the outer nodes, such as Node 147, than the centre nodes, such as Node 589. Since Node 147 already cures very quickly compared to Node 589, a more effective improvement would be to increase the amount of induction heating.

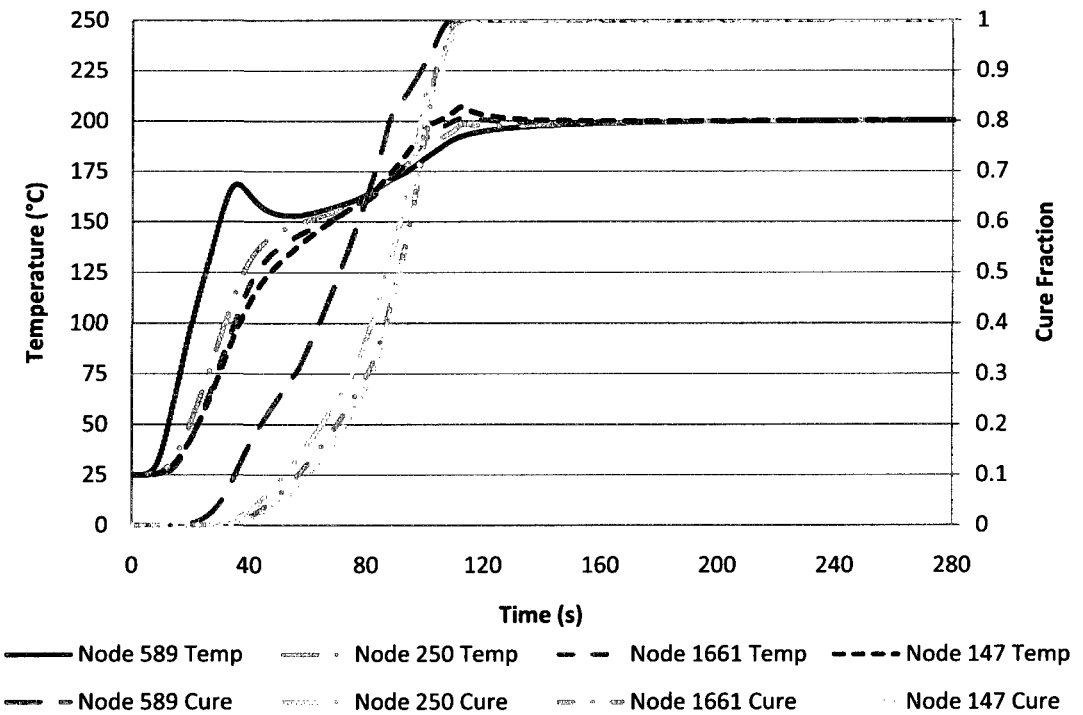

Figure 6.18 – Sim 3: Induction 231.0 Amps, Furnace Heating 200 °C

In Simulation 3, the induction heating amperage was doubled, while keeping the furnace temperature the same as in Simulation 1. As can be seen in Figure 6.18, the stronger induction heating stage has a key impact in how the rod cures, with all the nodes curing a roughly the same time. Despite the outermost node cure rate lagging behind the nodes closer to the induction wires, the heating from the furnace stage makes up for this lag and ensures that this node cures at the same time as the others. The rod is completely cured in less than 120 seconds, which is almost half the total production time.

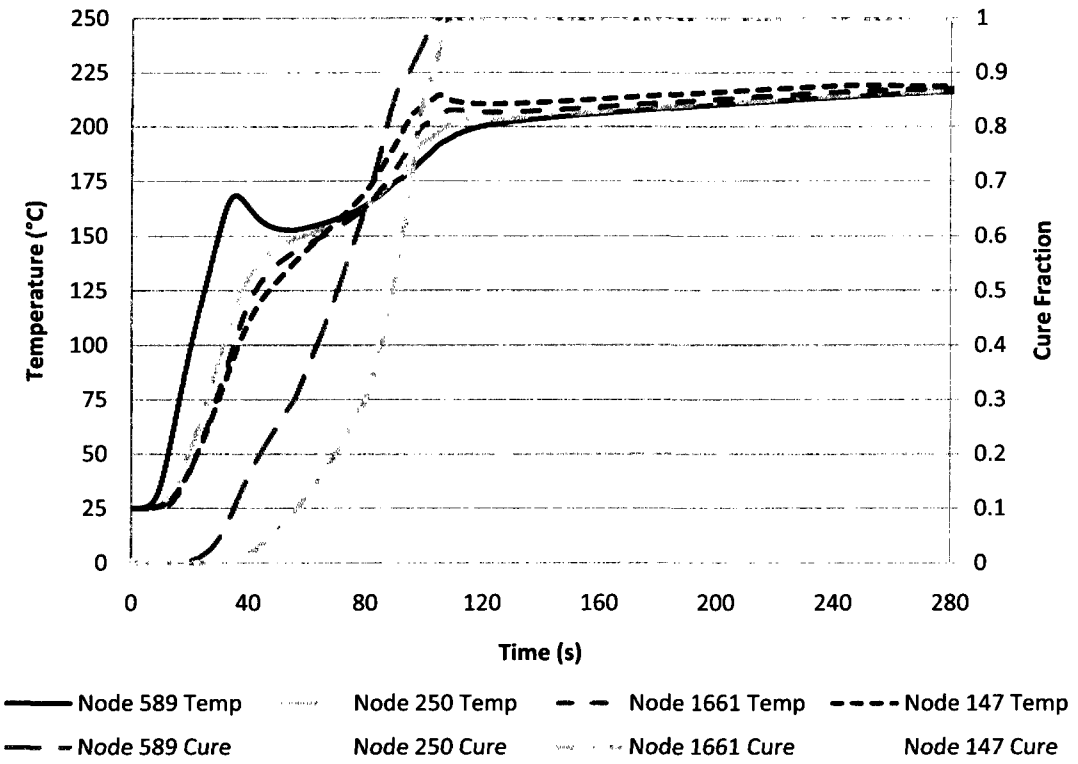

Figure 6.19 – Sim 4: Induction 231.0 Amps, Furnace Heating 240 °C

By raising the processing temperature in Simulation 4, seen in Figure 6.19, the cure rate of the outer nodes increases and therefore causes these nodes to cure first. However, this discovery might not be a problem since the other nodes have already cured to approximately 85%, and would probably not gain any noticeable residual stress. Overall, the rod seems to cure roughly 10% faster, with the model predicting a solid rod at just over 100 seconds.

6.3.2 Processing at 75 centimeters per minute

For the current arrangement, the production speed is limited at 75 centimeters per minute due to the braider. When processing at this speed, the total production line is completed in 163.2 seconds, while the induction heating stages ends at 30.6 seconds. This finite element model computed step until 220 seconds, though the only the data from the production process are of interest. The results of Simulation 5 can be seen below in Figure 6.20.

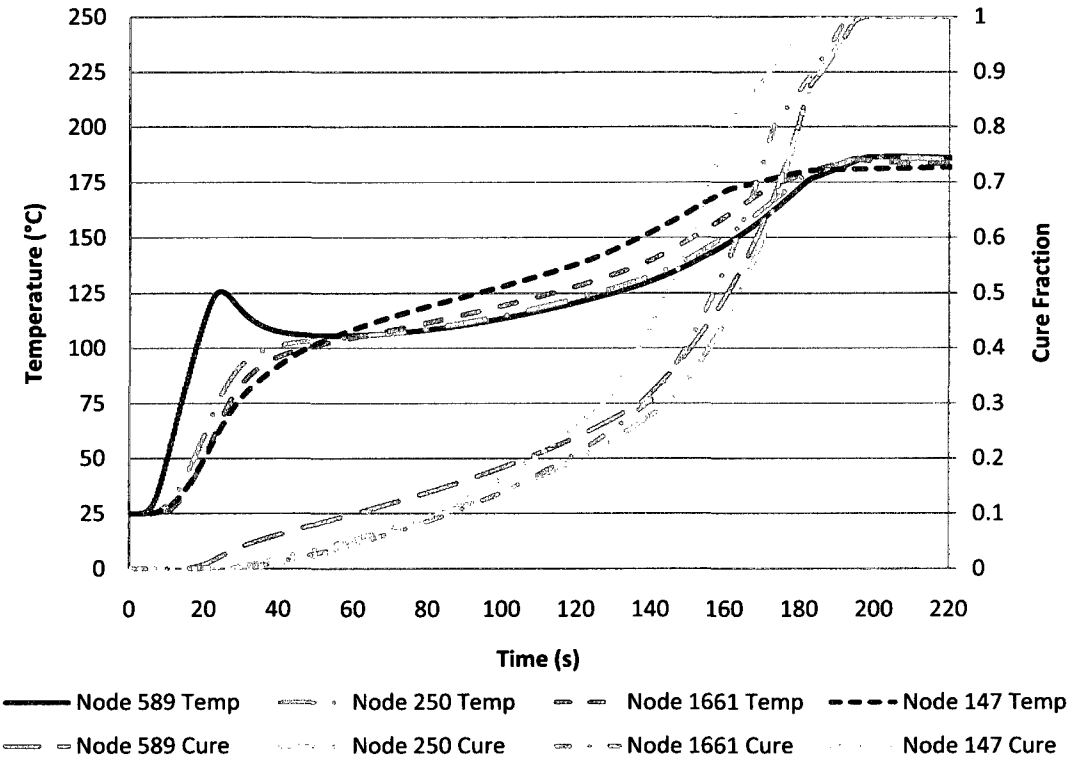

Figure 6.20 – Sim 5: Induction 231 Amps, Furnace Heating 200 °C

In Simulation 5, at the exit of the furnace, 163.2 seconds, the cross-section cure fraction profile ranges from between 40 to 90% cured and the fibre composite was not cured successfully; furthermore, it appears in Figure 6.20 that the outer nodes were the nodes that cured a greater amount which is not desirable. The cause for this lack of curing can be seen at the 30 second mark at the point where the rod completes the induction stage. While some curing occurs, the temperature is not great enough to cause enough of the epoxy to cure and therefore does not increase the temperature further. Instead, any heat that is generated from the exothermic reaction is conducted to the cooler outside, which is then heated by the furnace stage. The end result is that only the overwrap is sufficiently cured at the end.

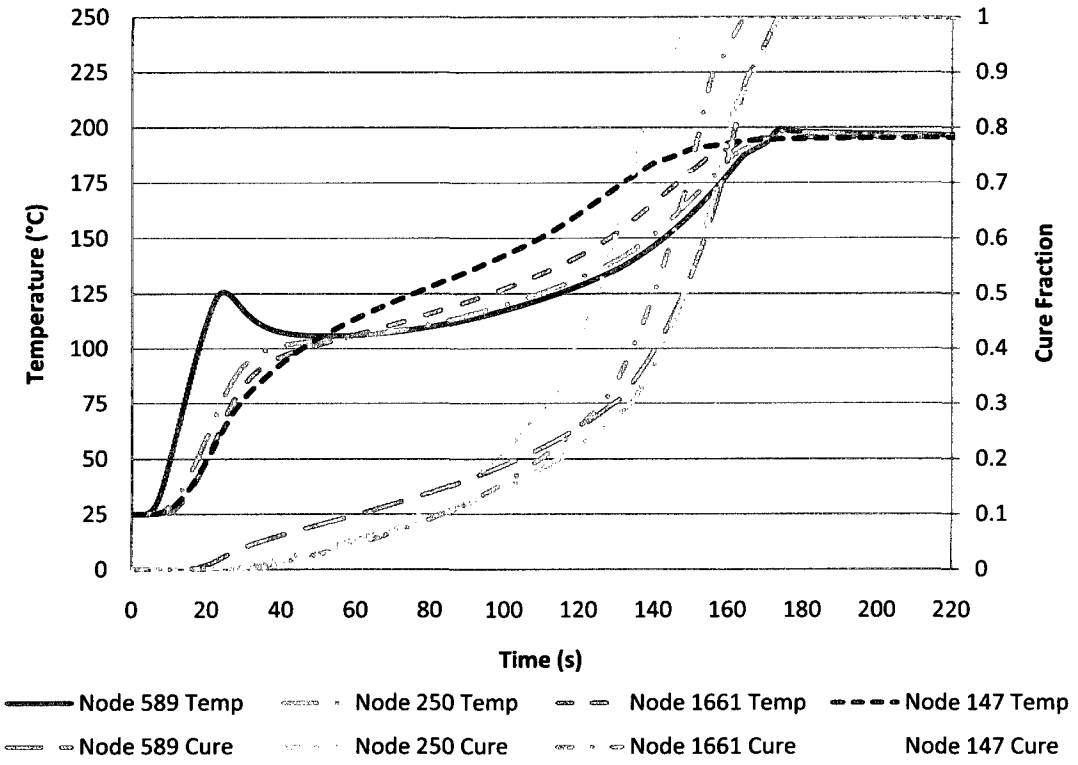

Figure 6.21 – Sim 6: Induction 231 Amps, Furnace Heating 240 °C

In Simulation 6, seen in Figure 6.21, the entire rod is cured before the composite finishes exiting the furnace; however, the order that the nodes cures is in the opposite order than desired. Since the inner node, Node 589, is just under 30% when the outer node cures, a composite rod might not behave mechanically as intended. It should be also noted that despite the furnace being set for 240 °C, the composite rod never raises much above 200 °C, indicating that the furnace's length could be further increased without causing the epoxy from experiencing thermal degradation.

6.3.3 Processing at 100 centimeters per minute

The final group of tests was conducted at processing the composite rod at 100 centimeters per minute. At this production speed, the induction heating station occurs for 20.4 seconds and the furnace station finishes at 122.4 seconds. As with the previous groups, the finite element model was computed past the end of the process, with only minimal heating attached to those increments.

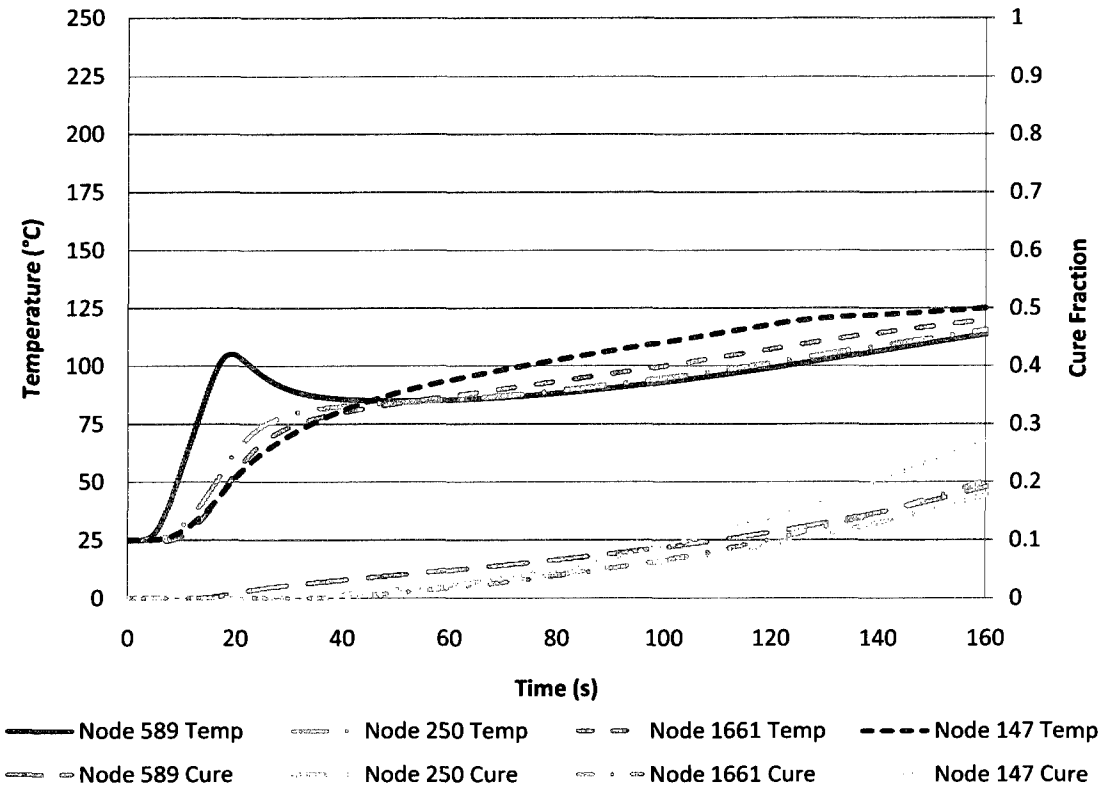

Figure 6.22 – Sim 7: Induction 231 Amps, Furnace Heating 200 °C

The results from Simulation 7 display that the amount of heat is insufficient to cure the composite at this production rate. Indeed, at the instance when the rod leaves the furnace, the epoxy had only cured approximately ten percent. This data indicates that under the current heating settings, processing at this speed is not possible. It should be noted that, even under the fast production speed, the induction heating is still able to bring the core to a temperature hot enough to cause the epoxy to begin, albeit not hot enough to cure it at more than a very slow rate.

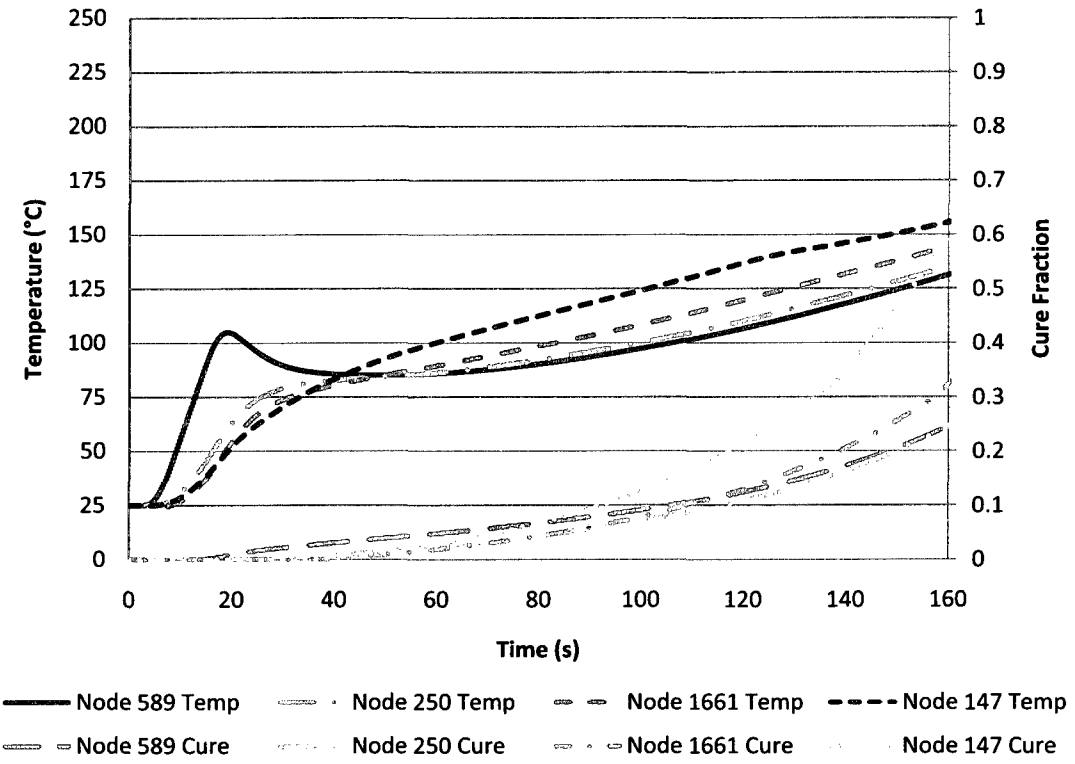

Figure 6.23 – Sim 8: Induction 231 Amps, Furnace Heating 240 °C

In the final test, Simulation 8 seen in Figure 6.23, the results show a similar conclusion as the previous test, that none of the nodes had fully cured before the composite left the furnace station. In the figure it can be seen that, although the furnace heating ends after 122.4 seconds, the rod continues to heat up due to the exothermic heat released from the curing of the epoxy. The outermost node, Node 147, cures especially fast during this period.

6.4 Cross-Sectional Profiles

To better analyze how the different regions within the rod cure, cross-sectional profiles of both temperature and cure fraction were constructed. These cross-sectional profiles are generated at various points in time to determine how the composite was heated and thus how it cured. As mentioned earlier, uniform temperature and cure profiles across the radius are the ideal case. These diagrams were constructed by taking seven nodes along the radius of the rod. The location of these nodes can be seen in Figure 6.24.

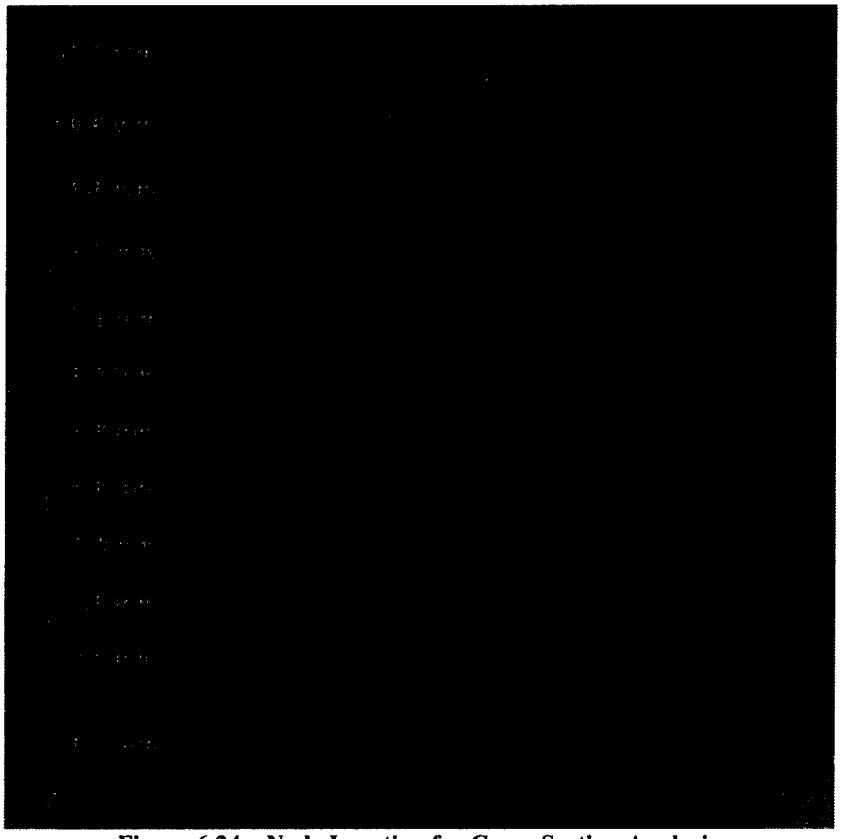

Figure 6.24 – Node Location for Cross-Section Analysis

6.4.1 Processing at 50 centimetres per minute

The cross-sectional diagrams for Simulation 1 displaying temperature and cure fraction can be seen in Figure 6.25 and 6.26 respectively. It can be seen that although the rod's temperature rises fairly uniformly – in many situations there is only a 25 °C difference between the core and the overwrap – the cure fraction increases dramatically for the outer nodes. This observation underlines the curing reaction's strong link to temperature. Figure 6.25 also shows how strongly the induction heating raises the core's temperature, yet once this stage is complete, the temperature only rises near the end of the line. Within 60 seconds, the innermost node obtains a temperature of 80 °C, yet it takes 90 more seconds to rise to 100 °C. Using the previous observation, a moderate increase in the temperature of the core would greatly improve the reaction rate.

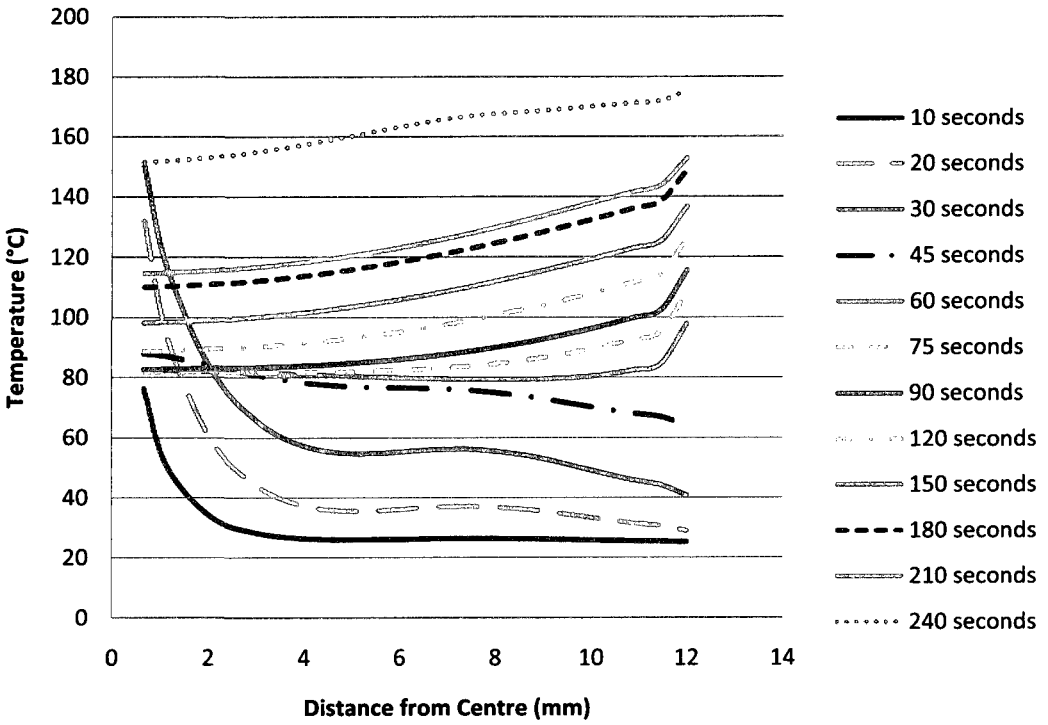

Figure 6.25 - Temperature Cross-Section profile for Sim 1 (115.5 Amps, 200 °C)

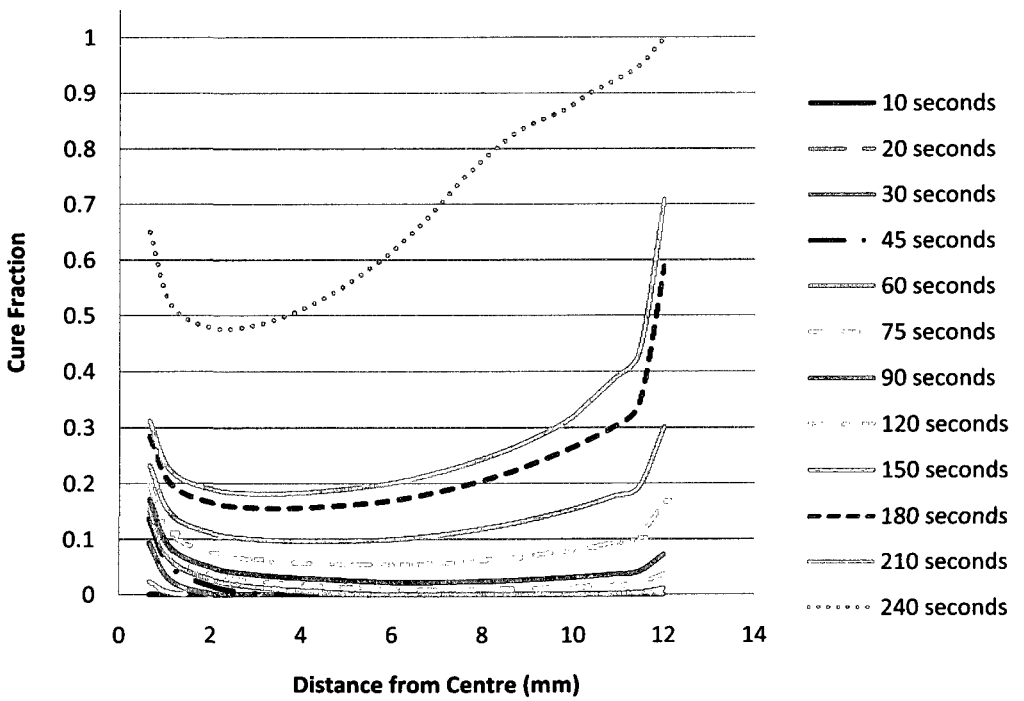

Figure 6.26 - Cure Fraction Cross-Section profile for Sim 1 (115.5 Amps, 200 °C)

The results for Simulation 2 are seen in Figure 6.27 and 6.28. Like Simulation 1, Simulation 2's cross-section indicates that more induction heating is required to rapidly cure the carbon fibre core. While the increase in furnace temperature does cure the composite faster, much of the overwrap is cured after 150 seconds of curing, even though the carbon fibre portion of the rebar is only 20% cured. The effects of this difference between the cure fractions would result in some residual stresses forming in the composite.

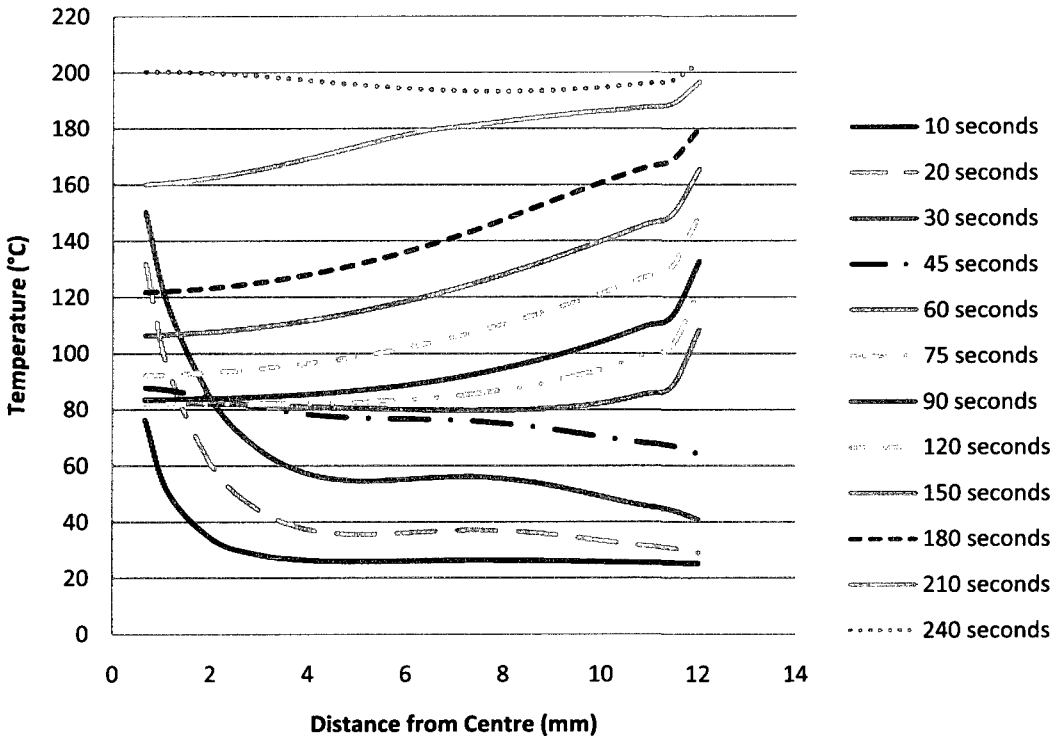

Figure 6.27 - Temperature Cross-Section profile for Sim 2 (115.5 Amps, 240 °C)

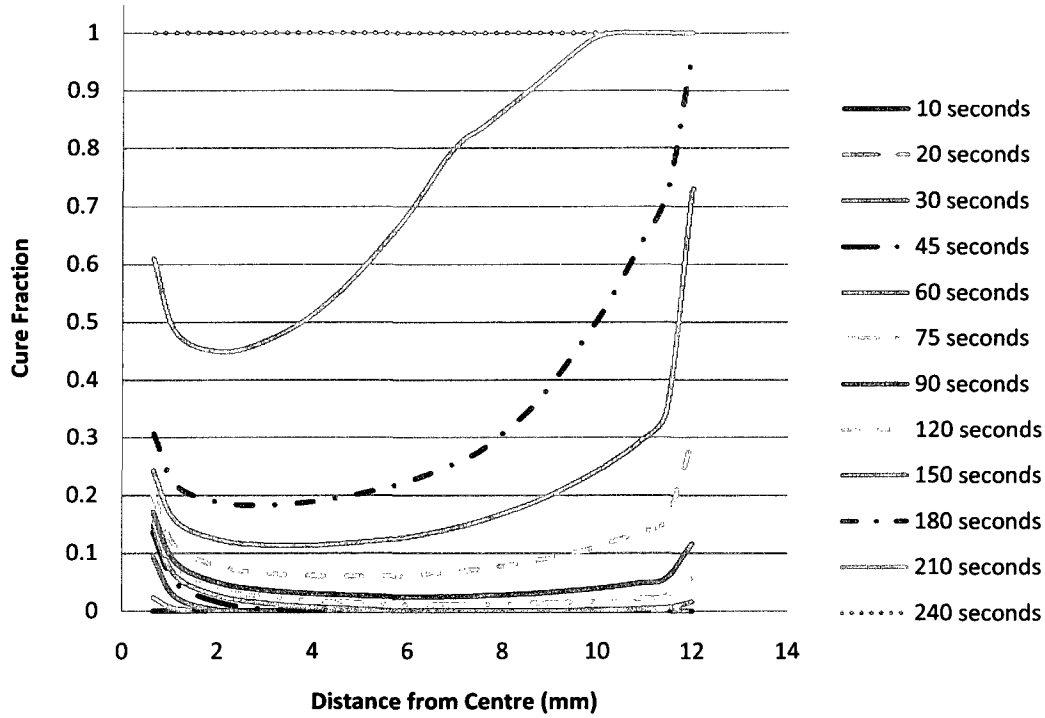

Figure 6.28 - Cure Fraction Cross-Section profile for Sim 2 (115.5 Amps, 240 °C)

For Simulation 3, the power level of the induction unit is double, providing the core with a substantially greater amount of heat. As can be seen in Figure 6.29, the center nodes reach a temperature of almost 200 °C after only 20 seconds, which is almost double than what was found in the previous two tests. The importance in this difference cannot be seen at initially in Figure 6.30, as when the section completes the induction stage, the core has only been cured a few percent in both tests. Instead its effects become more prominent as the composite passes though the furnace stage with its elevated core temperature. This causes the rod to be cured very quickly with the rate of cure accelerating from the exothermic heat released from the reaction. This addition of heat is so prominent that the temperature profile of the rod during the furnace stage rises almost consistently. This is the desired result of using induction heating and provides the ability to completely cure the composite in less than two minutes.

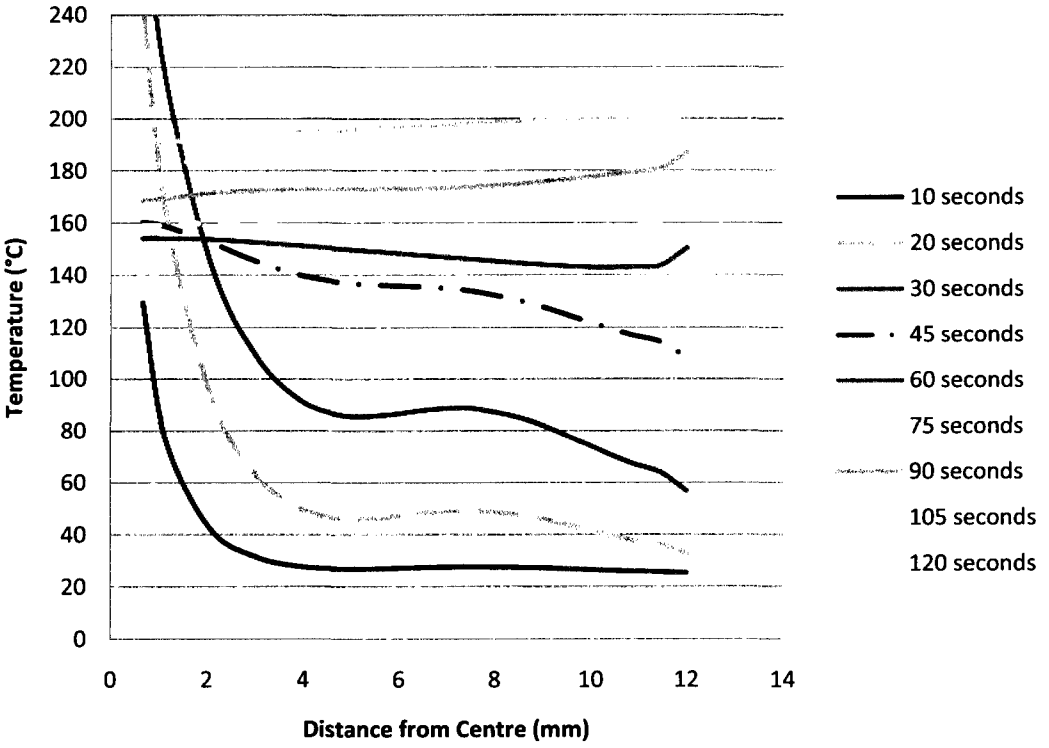

Figure 6.29 - Temperature Cross-Section profile for Sim 3 (231 Amps, 200 °C)

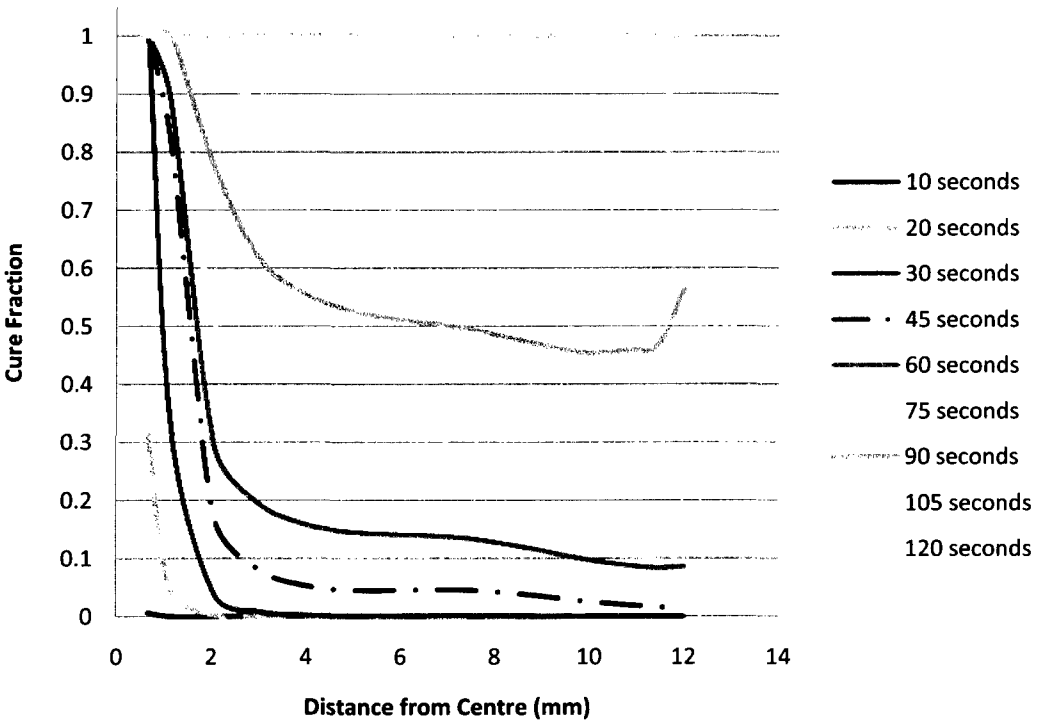

Figure 6.30 - Cure Fraction Cross-Section profile for Sim 3 (231 Amps, 200 °C)

The cross-sectional profiles for the final test conducted at 50 centimeters per minute can be seen in Figures 6.31 and 6.32. As seen with Simulation 1 and Simulation 2, the increase in furnace temperature has only a modest increase on the cure rate. However, as can be seen in Figure 6.32, the rod is nearly cured in 105 seconds, indicating that this composite can be cured with a very short furnace stage. While the curing is not completed as uniformly as in Test 3, the core nodes are cured sufficiently, resulting in a negligible residual stress gained during the final seconds of curing.

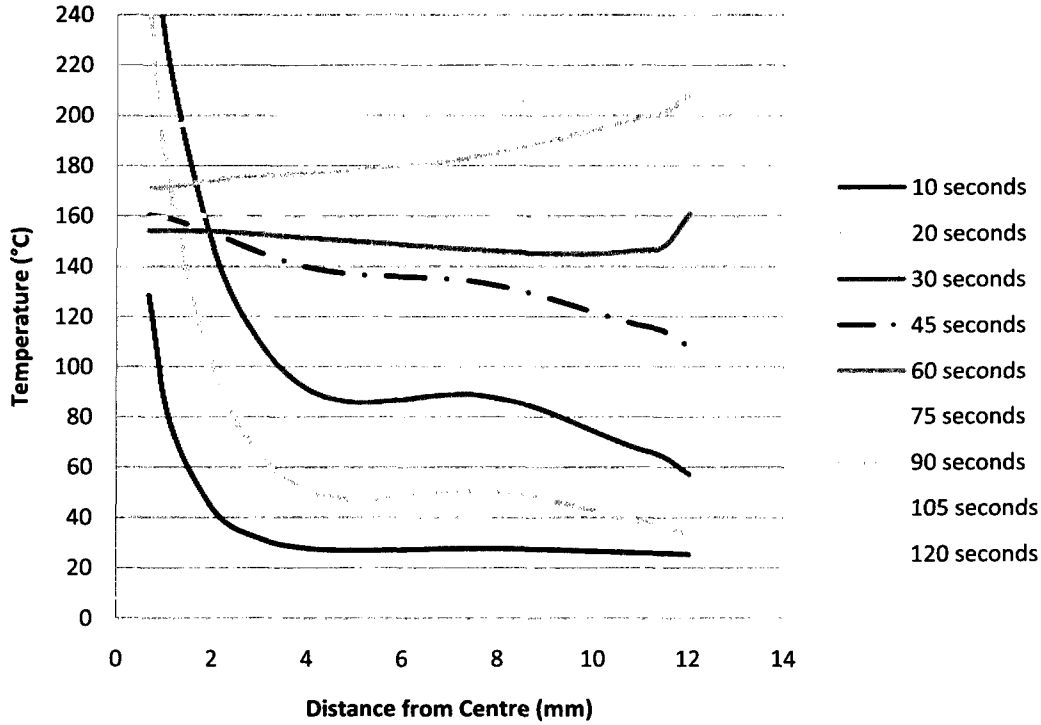

Figure 6.31 - Temperature Cross-Section profile for Sim 4 (231 Amps, 240 °C)

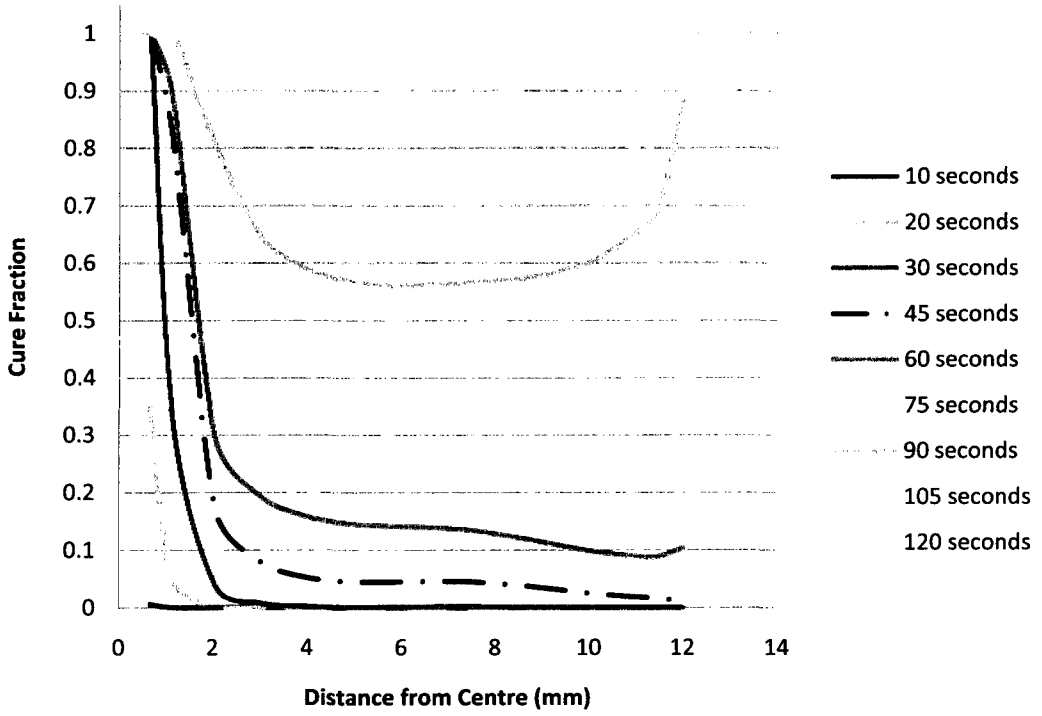

Figure 6.32– Cure Fraction Cross-Section profile for Sim 4 (231 Amps, 240 °C)

6.4.2 Processing at 75 centimetres per minute

The cross-section profiles for Simulation 5 are seen in Figure 6.33 and Figure 6.34, while Simulation 6 results are in Figure 6.35 and Figure 6.36. Of the two simulations, only Simulation 6 was able to cure in the given time. For Simulation 5, it can be seen in Figure 6.34 that the core is only half cured at the end of the production process. This is in great contrast with the results from Simulation 3, which the only parameter that was changed was increasing the production speed. It appears that the long induction heating stage was responsible for much of the heating seen in Simulation 3 and 4 which is lacking for these models.

One interesting feature of Figure 6.35 is that the final temperature has the inner most node having the highest temperature. This is caused by the rapid amount of curing that occurred in the core over that time interval, which is displayed in Figure 6.36. It might be possible to use this phenomenon to cure the composite without increasing the amount of heat delivered by the induction heating. This idea would involve creating a denser wire pattern to heat the center of the composite to a result in very rapid curing to occur in a small region.

With this method, the hope would be that the core's temperature would not be high enough to cause thermal degradation but still hot enough to cause nearby nodes to also cure very quickly, thus resulting in a chain reaction that would cure the carbon fibre rod efficiently.

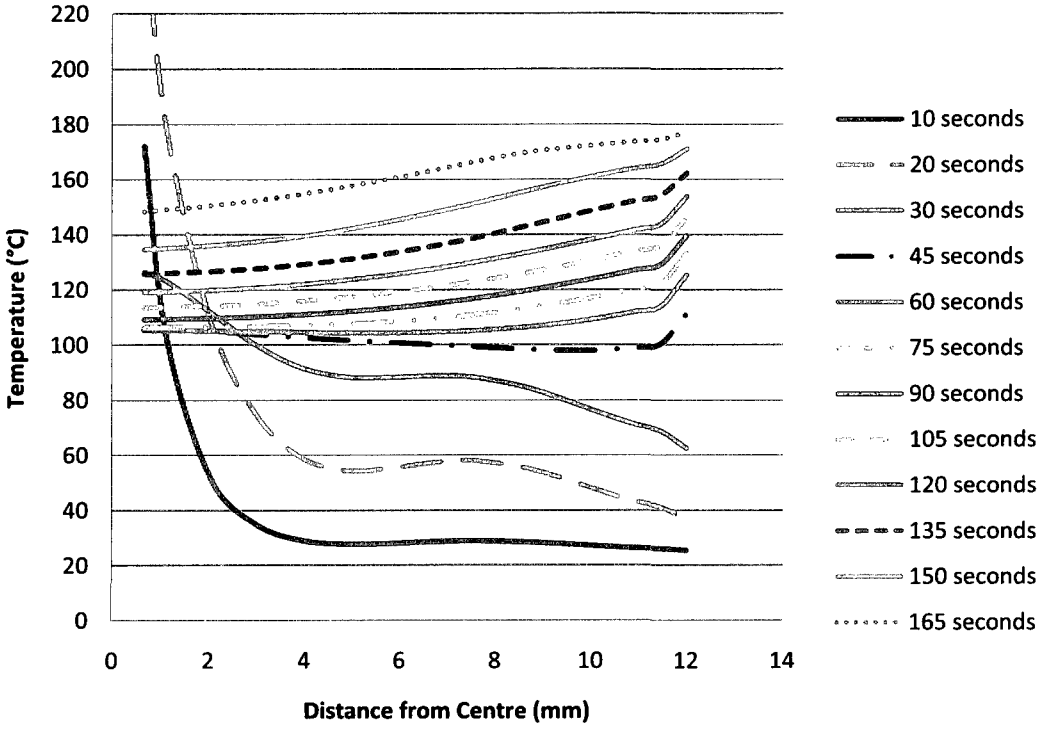

Figure 6.33 - Temperature Cross-Section profile for Sim 5 (231 Amps, 200 °C)

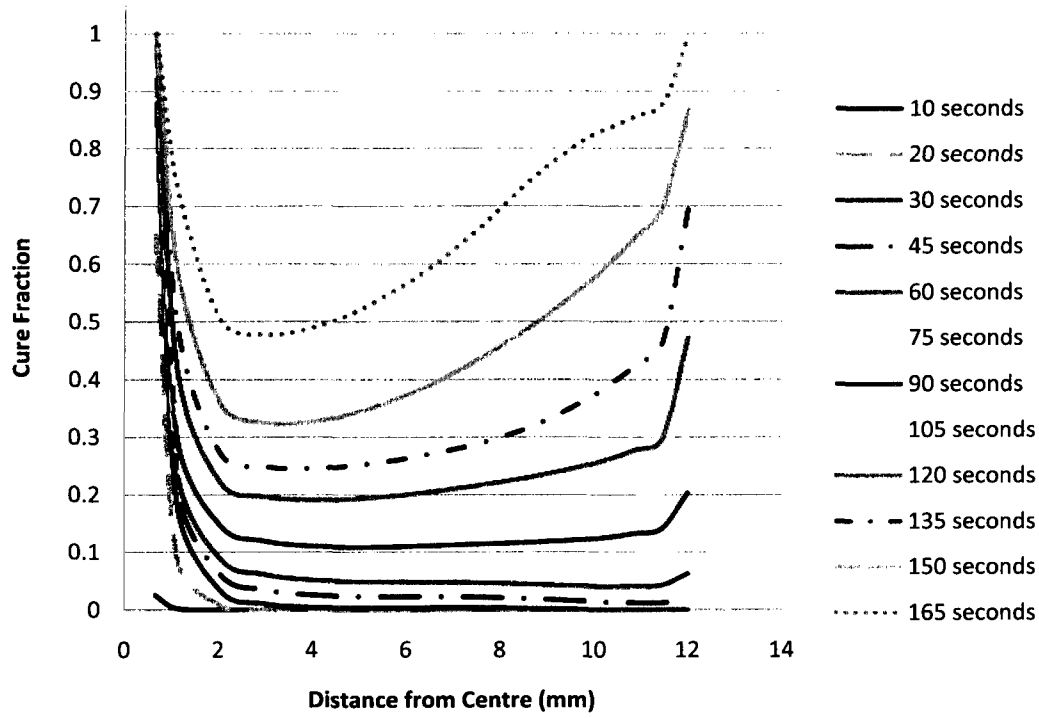

Figure 6.34 - Cure Fraction Cross-Section profile for Sim 5 (231 Amps, 200 °C)

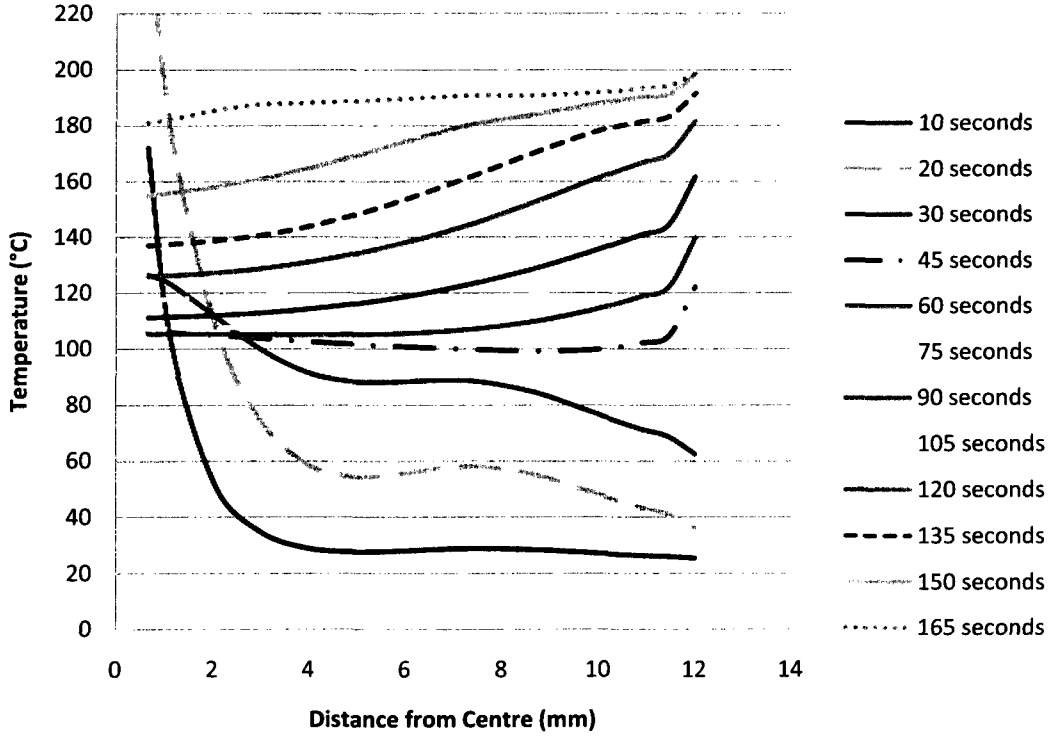

Figure 6.35 - Temperature Cross-Section profile for Sim 6 (231 Amps, 240 °C)

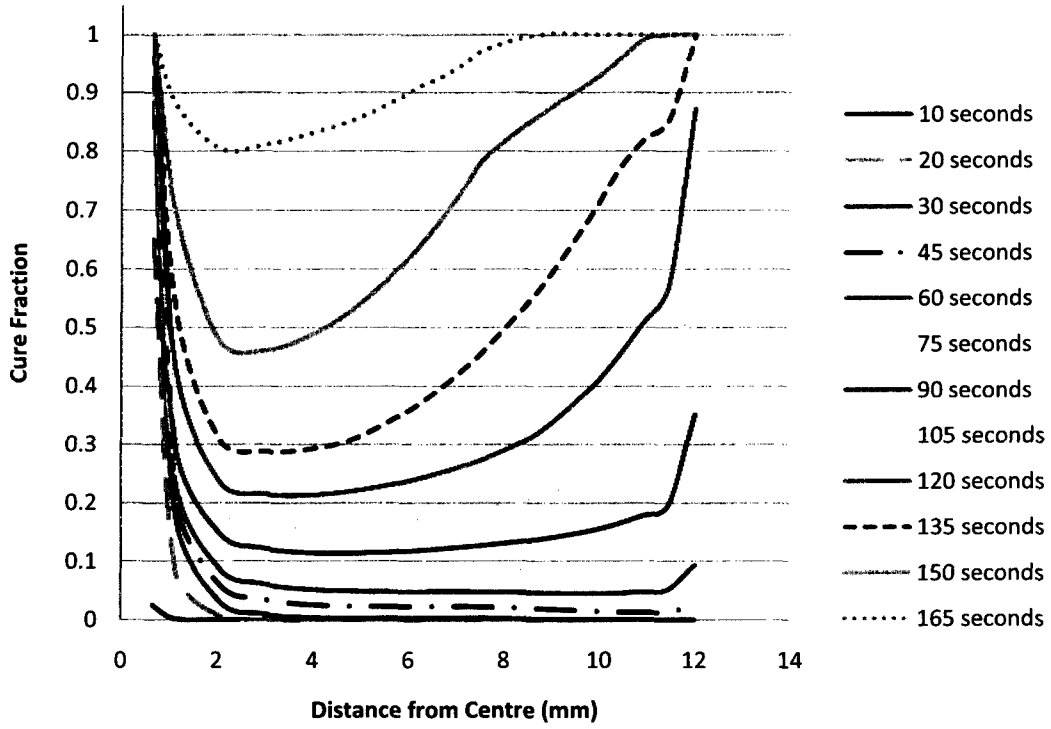

Figure 6.36 - Cure Fraction Cross-Section profile for Sim 6 (231 Amps, 240 °C)

6.4.3 Processing at 100 centimeters per minute

From the results in Figures 6.37 – 6.40, it is apparent that the level of heating is insufficient to cure the rod. As mentioned in the Section 6.3.3, the main difficulty of producing at a faster rate is that the induction heating stage is greatly reduced. This can be seen in Figures 6.37 and 6.39 where the core only reaches approximately 120 °C despite being heating for over two minutes. Thus either a current higher than 231 Amps or a second induction unit is required to produce at a rate of 100 centimeters per minute.

While Figure 6.40 demonstrates that the composite rod does not cure properly during its processing time, it can be seen that the outer two nodes reach a high degree of cure. This is in contrast to Simulation 7's results seen in Figure 6.38 where the same nodes achieve roughly one third the degree of cure. This observation suggests that the furnace temperature required to properly cure the composite at 100 centimeters per minute would be close to the 240 °C used in this test. However, FEA simulations that successfully cured the composite before the outside would require an increase in the amount of current directed to the

induction unit. Since even a small increase in temperature has a large effect on curing, a moderate temperature increase in the core would provide a great deal of curing to occur during the furnace stage.

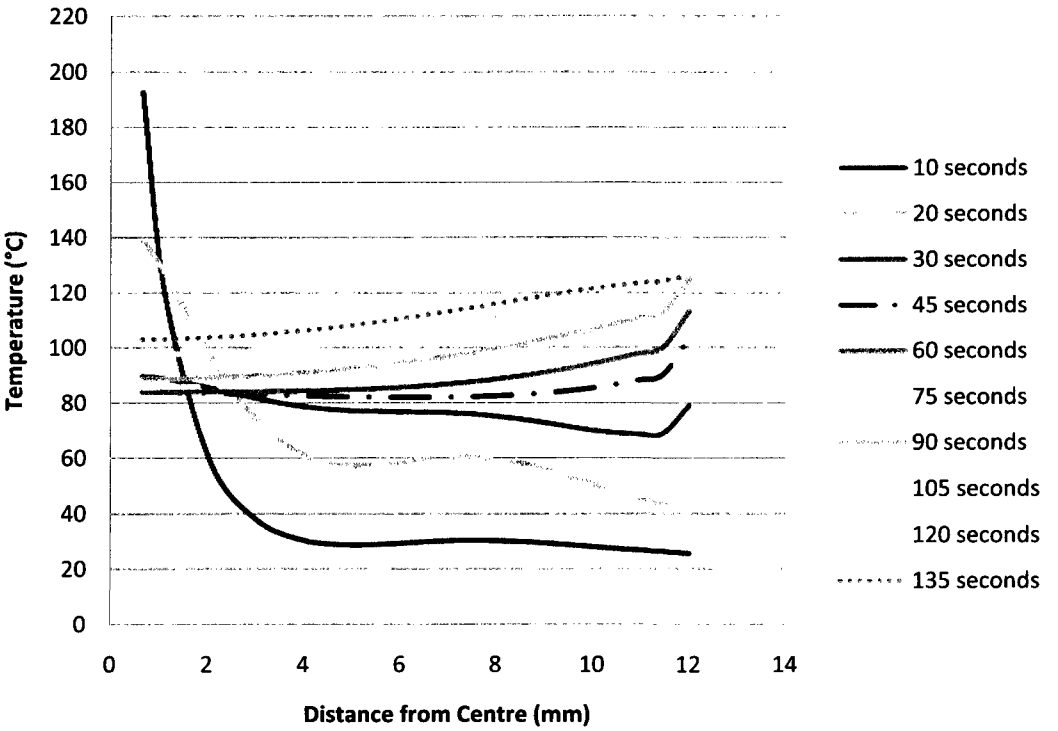

Figure 6.37 - Temperature Cross-Section profile for Sim 7 (231 Amps, 200 °C)

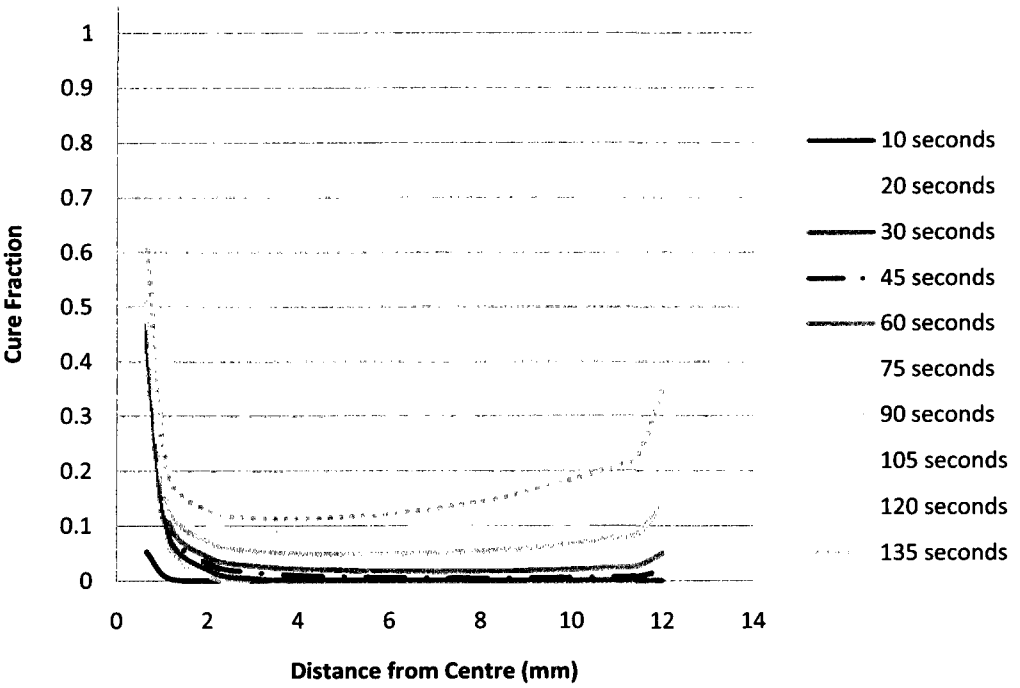

Figure 6.38 - Cure Fraction Cross-Section profile for Sim 7 (231 Amps, 200 °C)

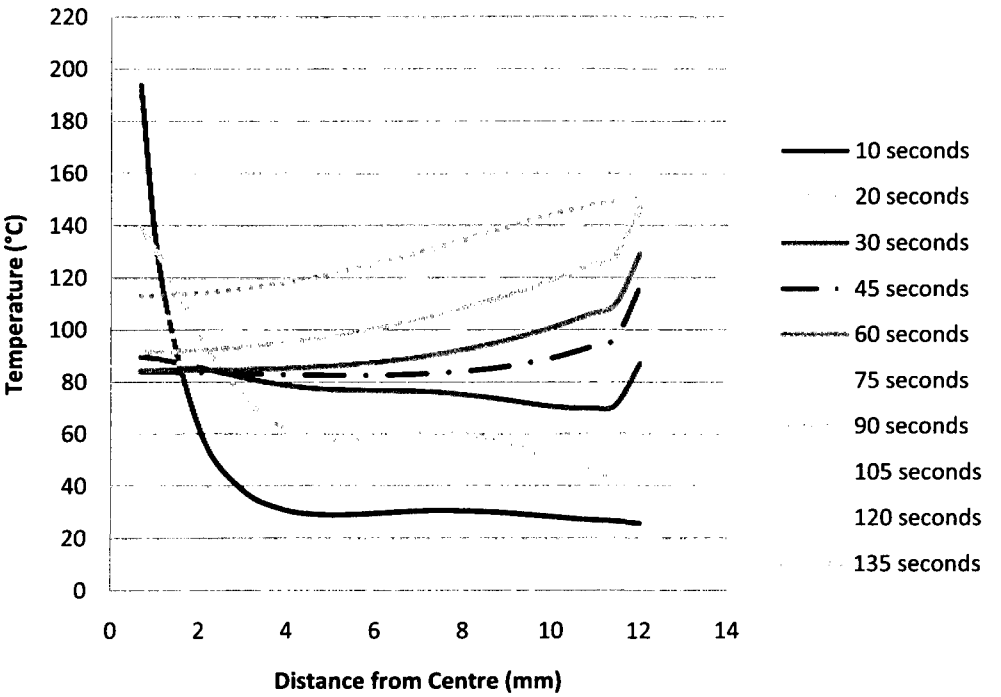

Figure 6.39 – Temperature Cross-Section profile for Sim 8 (231 Amps, 240 °C)

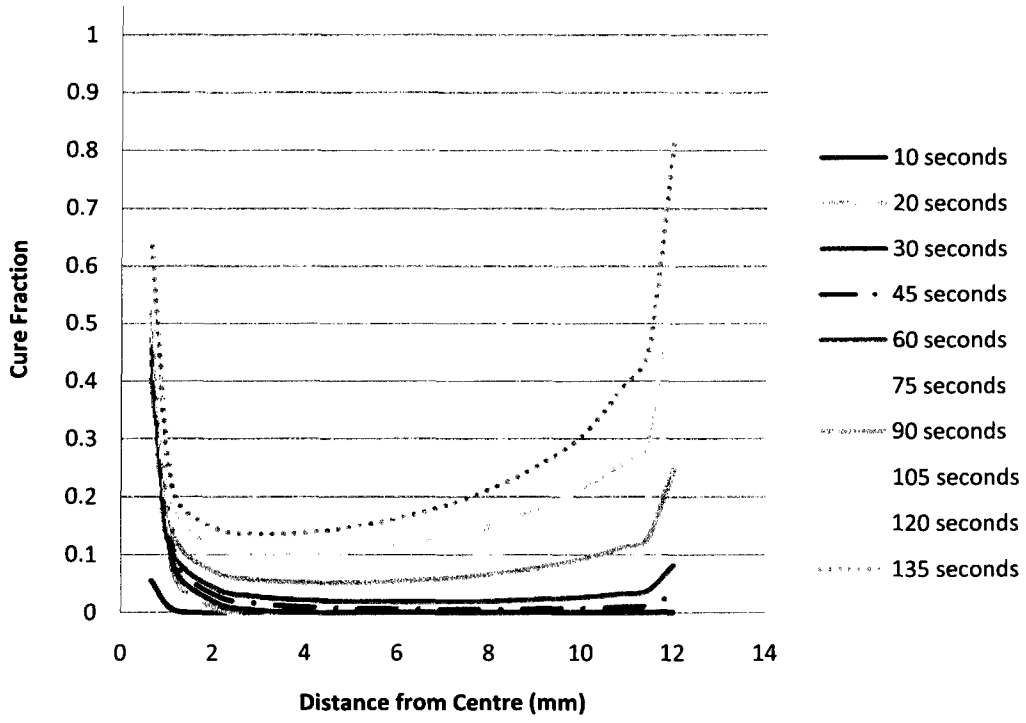

Figure 6.40 - Cure Fraction Cross-Section profile for Sim 8 (231 Amps, 240 °C)

Chapter 7

Conclusions

7.1 Final Results

In this thesis, an analysis was conducted to evaluate the curing of a fibre composite rebar in which a uniform cure would occur through the thickness. This analysis involved the development of a finite element model that determined the spatial and temporal cure distributions. The model was validated with experimental data and compared with an analytical analysis of heat transfer. It was found that, given the unique processing requirements, induction heating cured the rod in an effective and timely manner. This control is emphasized by the data that suggests that the entire cross-section can complete curing almost simultaneously.

With the introduction of induction heating, curing the inner portion of the hybrid composite is achievable and effective. Having both the induction stage as well as a later traditional furnace heating is necessary for curing at a reasonable production rate. This heating arrangement has the additional benefit of having the entire cross-section cure at approximately the same time, as some tests demonstrated. Out of all the tests conducted, Simulation 3 generated the best results and demonstrated that induction heating can properly cure the composite rebar. For higher speeds, Simulation 6 generated some promising data, suggesting that the composite could be produced at a faster rate if greater induction amperage was used. Neither of the simulations conducted at 100 centimeter per second proved to be successful at curing the composite within the designated time. With a specific combination of induction and furnace heating, the composite can be produced at a wide range of production speeds, with the option of curing the inside first or the whole rod at the same time. As such, while more investigation is required to develop the ideal settings and wire pattern, this Finite Element model has yielded encouraging results suggesting that the pseudo-ductile composite, with its unique production challenge, can be properly produced at a commercial production rate.

7.2 Proposed Production Settings

From the Finite Element simulations conducted in Chapter 6, it is believed that the following parameters would develop a suitable composite rod, which possesses the desired mechanical properties but produced in a timely rate.

Parameter	Setting
Production Speed	50 cm/minute
Induction Current	231 Amps
Furnace Temperature	200 °C

Table 7.1 - Proposed Settings

7.3 Suggested Future Work

The production settings proposed in Section 7.2 are believed to be adequate to sufficiently cure the hybrid fibre composite. While it has been demonstrated that the Finite Element model does compare well with the experimental results, a discrepancy remains. Further work can be implemented:

1. Develop a mathematical model for induction heating, one that encompasses electrical resistance and shielding. Currently, the finite element model treats all the wires as the same, though the induction heating literature relates the power released in induction heating with the distance of the workpiece to the coil. Likewise, as the temperature in the wires increases, the wire's electrical resistance would also increase. A higher workpiece resistance would slightly increase the efficiency of induction heating. The current formulation for calibrating the usable power of the induction coil was developed by heating the wires in water, which caused the wires to remain at a similar temperature of the water. Thus the wires only reached approximately one hundred degrees Celsius, much less than the three hundred degrees Celsius the wires experience in the FE model.
2. Determine the probable location of the embedded wires. The importance of the location of wires was highlighted in several of the tests where the elements further away from the wires would take much longer to cure than those elements adjacent to the wires. If it was found that the wires would cluster or arrange themselves in an

irregular pattern during production, these situations would need to be evaluated with the finite element model.

3. Validate the Finite Element simulation with experimental results obtained during production. By placing several thermocouples into the core just after the fibers are wet, the temperature can be recorded for difference places in the composite during curing. These thermocouples would be T-type in order to prevent them from acting as workpieces during the induction heating stage. However, due to the strong electro-magnetic field, even T-type thermocouples will record erroneous data while passing through the induction coil. Thus data can only be gathered through the furnace heating stage.
4. Determine the mechanical properties of the composite rods with the designated parameters.
5. Extend the model to include cooling. The results from this stage could determine where to place the puller, so that the rubber drive belts of the puller do not overheat.

References

[1] Nawy, Edward G. Reinforced Concrete: A Fundamental Approach, Fifth Edition. Prentice Hall: Upper Saddle River, New Jersey. 2003
[2] Meyer, Christian. Design of Concrete Structures. Prentice Hall: Upper Saddle River, New Jersey. 1996.
[3] Mallick, P. K. and S. Newman: Editors. Composite Materials Technology: Process and Properties. Hanser Publishers: New York, New York. 1990.
[4] Daniel, Isaac M. and Ori Ushai. Engineering Mechanics of Composite Materials. Oxford University Press: New York City, New York. 1994.
[5] Boresi, Aurthur P. and Richard J. Schmidt. Advanced Mechanics of Materials: Sixth Edition. John Wiley & Sons, Inc.: New York, New York. 2003.
[6] Ewen, Kristian. (Septermber 2004). Ductility in FRP Rods for Concrete Reinforcement by Interfacial Shearing. University of Ottawa, Ontario, Canada.
[7] Callister, William D. Jr. Materials Science and Engineering: An Introduction, Fifth Edition. John Wiley & Sons, Inc.: New York City, New York, 2000.
[8] Progelhof, R. C. et al. Methods for Predicting the Thermal Conductivity of Composite Systems: A Review, Polymer Engineering And Science. (1976) September, 16, 9, 615 – 625.
[9] Agarwal, B. D. and L. J. Broutman. Analysis and Performance of Fiber Composites: Section Edition. John Wiley & Sons.: New York, New York. 1990.
[10] Tsai, Stephen W. Composites Design: Third Edition. Think Composites: Dayton, Ohio. 1987.
[11] Automation Creations, Inc. "Matweb – The Online Materials Information Resource" <http://www.matweb.com/>. (09 January 2007)
[12] Starr, Trevor F. (Ed). Pultrusion for Engineers. Woodhead Publishing Limited: Cambridge, England. 2000.
[13] Meyer, Raymond W. Handbook of Pultrusion Technology. Chapman and Hall: New York City, New York. 1985.
[14] Murphy, John. Reinforced Plastics Handbook: Second Edition. Elsevier Science Ltd.: Oxford, UK, 1998.
[15] Barbero, E. J. Introduction to Composite Materials Design. Taylor & Francis Group: New York City, New York. 1999.
[16] Moschair, S. M. et al. Pultrusion of Epoxy Matrix Composites: Pulling Force Model and Thermal Stress Analysis, Polymer Composites. (1996) December, 17, 6, 850 - 858.
[17] Liu, X.L. et al. Simulation of heat transfer and cure in pultrusion with a general-purpose finite element package, Composite Science and Technology. (2000) 60, 857 – 864.
[18] Joshi, S.C. et al. Improved cure optimization in pultrusion with pre-heating and die-cooler, Composites Part A. (2003) 34, 1151 – 1159.
[19] Coelho, R.M.L. and V.M.A. Calado. An Optimization Procedure for the Pultrusion Process Based on a Finite Element Formulation, Polymer Composites. (2002) June, 23, 3, 329-341.
[20] Charchad, Y.R. et al. Manufacturing model for pultruded composites, Composites Part A. (1996) 27A, 3, 201-210.
[21] Roux, J.G. et al. Comparison of Measurements and Modeling for Pultrusion of a Fiberglass/Epoxy I-Beam. Journal of Reinforced Plastics and Compounds. (1998) 17, 17, 1557-1579.

[22] Tajima, Yuji. A and Donald G. Crozier. Chemorhelogy of an Epoxy Resin for Pultrusion, Polymer Engineering and Science. (1988) Mid-April, 28, 7, 491-496.
[23] McCrum, N. G., Buckley, C. P., and C. B. Bucknall. Principles of Polymer Engineering: Second Edition. Oxford University Press Inc.: New York, 2002.
[24] Hojjati, Medhi, Johnston, Andrew, and Kenneth C. Cole. (2000). Cure Kinetics of Hexcel W32T8282-42/F155 Graphite/Epoxy Prepreg, Science and Engineering of Composite Materials. 9, 3, 111-122.
[25] Karkanas, P. I. and I. K. Partridge. (2000). Cure Modeling and Monitoring of Epoxy/Amine Resin Systems. I. Cure Kinetics Modeling, Journal of Applied Polymer Science. 77, 1419-1431.
[26] Nunez, L. et al. (1996). Activation Energies and Rate Constants for an Epoxy/Cure Agent Reaction, Journal of Thermal Analysis. 47, 743-750.
[27] Boey, F. Y. C. and Santosh Kumar Rath. (2000). Microwave Radiation Curing of Polymers: Using a Temperature Equivalent Method for Cure Reaction Analysis, Advances in Polymer Technology. 19, 13, 194-202.
[28] Wei, Jianghua and Martin C. Hawley. (1995). Kinetics Modeling and Time-Temperature-Transformation Diagram of Microwave and Thermal Cure of Epoxy Resins, Polymer Engineering and Science. 35, 6, 461-470.
[29] Salla, Josep M. and Xavier Ramis. (1996). Comparative Study of the Cure Kinetics of an Unsaturdated Polyester Resin Using Different Procedures, Polymer Engineering and Science. 36, 6, 835-851.
[30] Hojjati, Mehdi and Suong V. Hoa. (1995). Some Observations in Curing of Thick Thermosetting Laminated Composites, Science and Engineering of Composite Materials. 4, 2, 89-107.
[31] Hojjati, M. and S. V. Hoa. (1994), Curing simulation of thick thermosetting composites, Composite Manufacturing. 5, 3, 159-169.
[32] Opalicki, M., Kenny, J. M., and L. Nicolais. (1996). Cure Kinetics of Neat and Carbon-Fiber Reinforced TGDDM/DDS Epoxy Systems, Jourrnal of Applied Polymer Science. 61, 1025-1037.
[33] Tajima, Y. A. and D. G. Crozier. (1988). Chmorheology of an Epoxy Resin for Pultrusion, Polymer Engineering and Science. 28, 7, 491-495.
[34] Hill, D. J. T., George, G. A., and D. G. Rogers. (2001). A Systematic Study of the Microwave and Thermal Cure Kinetics of the TGDDM/DDS and TGDDM/DDM Epoxy-Amine Resin Systems, Polymers for Advanced Technologies. 12, 169-176.
[35] Fang, X. et al. (2000) A Study of the Kinetics of the Microwave Cure of a Phenylethynyl-Terminated Imide Model Compound and Imide Oligomer (PETI-5), Journal of Polymer Science: Part A: Polymer Chemistry. 38, 2526-2535.
[36] Lee, W. I., Loos, A. C., and G. S. Springer. (1982). Heat of Reaction, Degree of Cure, and Viscosity of Hercules 3501-6 Resin, Journal of Composite Materials. 16, 510-520.
[37] Horie, K., Hiura, H., Sawasa, M., Mita, I., and H. Kambe. (1970). Calorimetric Investigation of Polymerization Reactions. III. Curing Reaction of Epoxides with Amines, Journal of Polymer Science: Part A-1. 8, 1373-1383.
[38] Cole, K. C. (1991). A New Approach to Modeling the Cure Kinetics of Epoxy Amine Thermosetting Resins. 1. Mathematical Development, Macromolecules. 24, 3093-3097
[39] Puschner, H. Heating with Microwaves: Fundamentals, Components and Circuit Technique. Philips Technical Library: Eindhoven, The Netherlands. 1966.

[40] Metaxas, A. C. Foundations of Electroheat: A unified approach. John Wiley & Sons: West Sussex, England. 1996.
[41] Mextas, A.C. and R. J. Meredith. Industrial Microwave Heating. Peter Peregrinus Ltd.: London, United Kingdoms. 1983.
[42] Tanrattankul, Varaporn and Kaew SaeTiaw. Comparison of Microwave and Thermal Cure of Epoxy-Anhydride Resisn: Mechanical Properties and Dynamic Characteristics, Journal of Applied Polymer Science. (2005) 97, 1442-1461.
[43] Matrice Technology Ltd. Microwave Assisted Pultrusion (MAP) Continuous Manufacture of Composite Profiles, Material Technology and Advance Performance Materials. (1999) 14, 4, 183-186.
[44] Rudnev, Valery et al. Handbook of Induction Heating. Marcel Keffer, Inc.: New York, USA. 2003.
[45] Nerg, Janne. (May 2000). Numerical Modelling and Design of Static Induction Heating Coils. Lappeenranta University of Technology, Lappeenranta, Finland.
[46] Chow, Tai L. Introduction to Electromagnetic Theory: A Modern Perspective. Jones and Bartlett Publishers: Sudbury, Massachusetts, 2006.
[47] Davies, E. J. Conduction and induction heating. Peter Peregrinus Ltd.: London, United Kingdoms. 1990.
[48] Zinn, S. and S. L. Semiatin. Elements of Induction Heating. Electric Power Research Institue, Inc.: Palo Alto, California. 1988.
[49] Zinn, Stanley and S. L. Semiatin. Coil design and fabrication: basic design and modifications, Heat Treating. (1988), June, 32 – 36.
[50] Metaxas, A. C. Foundations of Electroheat: A unified approach. John Wiley & Sons: West Sussex, England. 1996.
[51] Rodrigues, J.M.C. and P.A.F. Martins. Finite element modeling of the initial stages of a hot forging cycle, Finite Elements in Analysis and Design. (2002), 38, 295-305.
[52] Grewall, D. A. et al Editor. Plastics and Composites Welding Handbook. Hanser Publishing: Munich, Germany, 2003.
[53] Holman, J. P. Heat Transfer: 8th Edition. McGraw Hill Inc.: New York City, New York, 1997.
[54] Chapman, Alan J. Fundamentals of Heat Transfer. Macmillan Publishing Company: New York City, New York, 1987.
[55] Lienhard, J. H. and J. H. Lienhard. A Heat Transfer Textbook: Third Edition. Phlogiston Press: Cambridge, Massachusetts. 2006.
[56] ABAQUS, Inc. "ABAQUS, Inc." ABAQUS. <http://www.abaqus.com/>. (09 January 2007).
[57] Lutz, Mark and David Ascher. Learning Python: Second Edition. O'Reilly Media, Inc.: Sebastopol, California. 2003.

Appendix A

Epoxy Exothermic Reaction Test

Purpose: Obtain Epoxy's Exotherm and Peak Exothermic Temperature

Overview: The test's procedure was developed by modifying the ASTM standard that is used to obtain the amount of heat generated by the curing of epoxy. The reason for this change was due to the properties of the epoxy; the kickoff temperature is too great for the ASTM test to be conducted successfully at its specified temperature of 23 °C. Instead, the epoxy is cured while it is in a furnace that has a fixed temperature. To remove the heating profile, a second test run is conducted afterwards. By taking the two heating curves and subtracting the second one from the first, the amount of heating by the furnace is removed. Thus, the difference in temperature can be attributed to the exothermic reactions of the epoxy.

In order to further tailor this experiment to generate the results need, the epoxy was combined with a carbon and aramid fibre bundle prior to curing. Tests at different furnace temperatures were taken, these ranging from 100 - 160 °C.

Source: ASTM D 2471-99

Materials:

- 45 ml of epoxy
- Fibre bundle
- Glass tube (20 mm diameter, 50 mm length)
- Mixing Rod
- Three thermocouples
- Computer Terminal
- LabView Computer Program
- Stopwatch
- Aluminum shield
- Aluminum Tape

Procedure:

1. Determine and record the temperature of the room.
2. Set the furnace to the desired temperature and insert a thermocouple into it to allow continuous monitoring.
3. Place in proper proportions the epoxy resin and hardener into a plastic cup and stir it for three minutes; during stirring, the cup is not to be directly held by hand.
4. Record the mass of the bundle and the glass tube. Place the glass tube slightly on the bundle before dipping it into the epoxy mixture for thirty seconds. Slide the glass tube to allow the other portion of the bundle to be wetted with epoxy. This end should also be dipped into the liquid epoxy for thirty seconds.

5. Move the glass tube back into the centre of the bundle. Two thermocouples are then placed into the bundle, one inside the centre of the epoxy mixture and the other near the fringe of the epoxy and glass tube. These thermocouples must be inserted into the bundle sufficiently so that at they pass the glass tube at least by one centimetre.
6. The bundle is affixed to the aluminum shield, using aluminum tape on the glass tube if required.
7. Have Labview start recording values and place the aluminum shield with wetted bundle into the furnace. With a stopwatch, record how long it takes between the activating LabView and closing the door on the furnace after inserting the test specimen.
8. Continue to record the values in LabView. The test is stopped after the noticeable positive difference of temperature between inside epoxy and the furnace has subsided.
9. Remove the specimen and let it cool down. Monitor the internal temperature of the bundle with the thermocouples.
10. Once it reaches room temperature, the second phase of the experiment can commence. Under a different file, start recording the temperature from the three thermocouples.
11. Using the same amount as indicated by the stopwatch, reinsert the cured bundle. The cured bundle remains into the furnace for the same duration as the curing part of the experiment.

Appendix B

Air Properties [54]

Temperature (K)	C_p (kJ/kg K)	ν ($\times 10^6$) (m^2/s)	k (W/m °C)	Pr
350	1.009	20.76	0.03003	0.697
384	1.0124	24.2552	0.032492	0.69156
394	1.0134	25.2832	0.033216	0.68996
400	1.014	25.9	0.03365	0.689

Material Properties [11]

Property	Conductivity (W/m·K)	Specific Heat (J/kg·K)	Density (kg/m^3)
Kevlar	0.04	340	1440
Carbon	0.613	710	1850
Epoxy	0.20	1000	1100
Steel	50.0	500	7800
Carbon composite	0.4065	855	1475
Kevlar composite	0.12	670	1270

Appendix C

Sample calculation

Convection Heat Transfer coefficient @ 220 °C

$$Gr_X = \frac{g\beta|T_W - T_\infty|x^3}{\nu^2}$$
$$= \frac{(9.81)\cdot(1/394)\cdot|22-220|\cdot(0.015)^3}{(25.2832\cdot10^{-6})^2}$$
$$= 26028.41$$
$$Nu^{1/2} = 0.60 + 0.387\left\{\frac{Gr\,\mathrm{Pr}}{\left[1+(0.559/\mathrm{Pr})^{9/16}\right]^{16/9}}\right\}^{1/6}$$
$$= 0.60 + 0.387\left\{\frac{(26028.41)\cdot(0.68996)}{\left[1+(0.559/0.68996)^{9/16}\right]^{16/9}}\right\}^{1/6}$$
$$= 2.2404$$
$$\rightarrow Nu = 5.01947$$

$$h = \frac{Nu\cdot k}{x}$$
$$= \frac{(5.01947)\cdot(0.033216)}{(0.015)}$$

$$\boxed{h = 11.503\ \mathrm{W/^\circ C\cdot m^2}}$$

Obtaining Biot Number

$$Bi = \frac{hR}{k}$$
$$= \frac{(5.01947)\cdot(0.033216)}{(0.015)}$$
$$= 0.21223$$

Using Figure 4.7 & the above Biot number, the Fourier number can be determined.

$$\tau = \frac{Fo \cdot R^2}{\alpha}$$
$$= \frac{Fo \cdot (0.0075)^2}{(3.2233 \cdot 10^{-7})}$$

Temperature	Heating @ 200 °C		Heating @ 220 °C	
	Fourier #	Time (s)	Fourier #	Time (s)
25	0.16	27.9	0.15	26.2
30	0.21	36.6	0.205	37.8
35	0.3	5.4	0.295	51.5
40	0.4	69.8	0.34	59.3
45	0.47	82.0	0.4	69.8
50	0.55	96.0	0.49	85.5
55	0.65	113.4	0.6	104.7
60	0.72	125.6	0.65	113.4
65	0.82	143.1	0.73	127.4
70	0.93	162.3	0.8	139.6
75	1.05	183.2	0.9	157.1
80	1.15	200.7	1.0	174.5
85	1.25	21.1	1.1	192.0
90	1.4	244.3	1.23	214.6
95	1.5	261	1.34	233.8
100	1.6	279.2	1.42	247.8
105	1.75	305.4	1.5	261.8
110	1.85	322.8	1.62	282.7
115	2.0	349.0	1.75	305.4
120	2.2	383.9	1.87	326.3
125	2.4	418.8	2.0	349.0
130	2.6	453.7	2.2	383.9
135	2.8	488.6	2.35	410.1
140	3.0	523.5	2.5	436.3
145	3.3	575.9	2.67	465.9
150	3.6	628.2	2.83	493.9
155	4.0	698.0	3.0	523.5
160	4.3	750.4	3.25	567.2
165	4.55	794.0	3.5	610.8
170	4.85	846.4	3.9	680.6
175	5.5	959.8	4.25	741.7
180	5.9	1029.6	4.5	785.3
185	6.6	1151.8	4.75	828.9
190	8.0	1396.1	5.1	890.0
195	10	1745.1	5.65	986.0

Appendix D

The following is the ABAQUS file that was created by the CAE interface when running a simulation. Note that the Assembly section, which contains the location of nodes, instances, and elements, was omitted below to greatly shorten the length.

```
*Heading
** Job name: Oct16 Model name: Model-1
*Preprint, echo=NO, model=NO, history=NO, contact=NO
**
** PARTS
**
*Part, name="Inner Rod"
*End Part
**
*Part, name="Outer Rod"
*End Part
**
*Part, name="Wire 1"
*End Part
**
*Part, name="Wire 2"
*End Part
**
*Part, name="Wire 3"
*End Part
**
*Part, name="Wire 4"
*End Part
**
*Part, name="Wire 5"
*End Part
**
*Part, name="Wire 6"
*End Part
**
*Part, name="Wire 7"
*End Part
**
*Part, name="Wire 8"
*End Part
**
**
** ASSEMBLY
** ## Note: Removed section to save space ##
```

```
*End Assembly
**
** MATERIALS
**
*Material, name="Carbon Fibre"
*Conductivity
2.,
*Density
1500.,
*Depvar
     1,
*Heat Generation
*Specific Heat
1200.,
*Material, name="Kevlar Fibre"
*Conductivity
 1.5,
*Density
1300.,
*Depvar
     1,
*Heat Generation
*Specific Heat
1100.,
*Material, name=Steel
*Conductivity
50.,
*Density
7800.,
*Specific Heat
500.,
**
** INTERACTION PROPERTIES
**
*Surface Interaction, name=IntProp-1
1.,
*Gap Conductance
800.,   0.
  0., 0.05
*Surface Interaction, name=IntProp-2
1.,
*Gap Conductance
200.,   0.
  0., 0.05
*Surface Interaction, name=_Fibres-Property
1.,
*Gap Conductance
```

```
200.,  0.
 0., 0.05
**
** INTERACTIONS
**
** Interaction: Fibres
*Contact Pair, interaction=_Fibres-Property
_PickedSurf143, _PickedSurf142
** Interaction: Int-3
*Contact Pair, interaction=IntProp-1
_PickedSurf27, _PickedSurf26
** Interaction: Int-4
*Contact Pair, interaction=IntProp-1
_PickedSurf29, _PickedSurf28
** Interaction: Int-5
*Contact Pair, interaction=IntProp-1
_PickedSurf31, _PickedSurf30
** Interaction: Int-6
*Contact Pair, interaction=IntProp-1
_PickedSurf33, _PickedSurf32
** Interaction: Int-7
*Contact Pair, interaction=IntProp-1
_PickedSurf35, _PickedSurf34
** Interaction: Int-8
*Contact Pair, interaction=IntProp-1
_PickedSurf37, _PickedSurf36
** Interaction: Int-9
*Contact Pair, interaction=IntProp-1
_PickedSurf39, _PickedSurf38
** Interaction: Wires
*Contact Pair, interaction=IntProp-1
_PickedSurf25, _PickedSurf24
** ----------------------------------------------------------------
**
** STEP: Induction
**
*Step, name=Induction, inc=500
*Heat Transfer, end=PERIOD, deltmx=30.
0.1, 40.8, 0.000408, 0.5,
**
** LOADS
**
** Name: Induction   Type: Surface heat flux
*Dsflux
_PickedSurf144, SNU, 1.
**
** OUTPUT REQUESTS
```

```
**
*Restart, write, frequency=0
**
** FIELD OUTPUT: F-Output-1
**
*Output, field
*Node Output
NT,
**
** HISTORY OUTPUT: H-Output-1
**
*Output, history
*Energy Output
ALLAE,
*End Step
** ----------------------------------------------------------------
**
** STEP: Furnace
**
*Step, name=Furnace, inc=400
*Heat Transfer, end=PERIOD, deltmx=10.
0.5, 240., 0.0024, 2.,
**
** LOADS
**
** Name: Furnace   Type: Surface heat flux
*Dsflux, op=NEW
_PickedSurf131, SNU, 1.
** Name: Induction   Type: Surface heat flux
*Dsflux, op=NEW
**
** INTERACTIONS
**
** Interaction: Fibres
*Change Friction, interaction=_Fibres-Property
*Friction
0.,
**
** OUTPUT REQUESTS
**
*Restart, write, frequency=0
**
** FIELD OUTPUT: F-Output-1
**
*Output, field
*Node Output
NT,
```

```
**
** HISTORY OUTPUT: H-Output-1
**
*Output, history
*Energy Output
ALLAE,
*End Step
```

The remaining portion of this Appendix is devoted to presenting the Fortran code that was used to in the FEA model. The first subroutine (DFLUX) was used to properly time ABAQUS to the production process used to create the composite rod. For this given example, the production speed is 0.5 metres per minute, with the ABAQUS modeling a 12 centimetre long rod. The second subroutine's (HETVAL) purpose was to relate the amount of heat released to the node's temperature and percentage of cured epoxy. When running a simulation, these subroutines would be enclosed in the same Fortran file, as presented here.

```
  SUBROUTINE DFLUX(FLUX,SOL,KSTEP,KINC,TIME,NOEL,NPT,COORDS,
   1 JLTYP,TEMP,PRESS,SNAME)

    INCLUDE 'ABA_PARAM.INC'

    DIMENSION FLUX(2), TIME(2), COORDS(3)
    CHARACTER*80 SNAME

C Variable
        Alpha = 0.016667
C To change production speed, only modify alpha & step times

C Steps set up for 1.0 m/min, with a 0.12 meter rod


        if (KSTEP == 1) then
                if (coords(3) + time(1) * alpha - 0.12 > 0) then
                        flux(1) = 288000
                        if (coords(3) + time(1) * alpha - 0.33 > 0) then
                                flux(1) = -1
C Cooling could be added here
                        end if
                else
                        flux(1) = 0
                end if


        else if (KSTEP == 2) then
                if (coords(3) + time(1) * alpha - 0.12 > 0) then
                        flux(1) = -0.04068 * (SOL+25) ** 2 - 13.341 * (SOL+25) + 4320.89

                  if (coords(3) + time(1) * alpha - 1.76 > 0) then
```

```
                    flux(1) = -1
                end if

            else
                    flux(1) = -1
            end if

        end if

      RETURN
      END


C       User subroutine HETVAL - Heat Generation
      subroutine hetval(cmname,temp,time,dtime,statev,flux,predef,dpred)

      include 'aba_param.inc'

      character*80 cmname

      real bracket, trate, old

      dimension temp(2),statev(1),predef(1),time(2),flux(2),dpred(1)

      if (temp(1) > 55) then

            old = statev(1)

            if (statev(1) < 0.30) then
                  bracket = -43010 / (8.3144 * (temp(1) + 298.15) )
                  trate = 96010 * EXP(bracket)
                  statev(1) = statev(1) + (trate * dtime/61)
                  flux(1) = 1261125 * trate

            else if (statev(1) < 0.80) then
                  bracket = -42010 / (8.3144 * (temp(1) + 298.15) )
                  trate = 110010 * EXP(bracket)
                  flux(1) = 1261125 * trate
                  statev(1) = statev(1) + (trate * dtime/61)


            else if (statev(1) < 1.00) then
                  bracket = -45010 / (8.3144 * (temp(1) + 298.15) )
                  trate = 92010 * EXP(bracket)
                  statev(1) = statev(1) + (trate * dtime/61)

                  if (statev(1) < 1.0) then
                        flux(1) = 1261125 * trate

                  else
                        flux(1) = 1261125 * (61 * (1 - old))
                        statev(1) = 1.0
                  end if

            else
                  flux(1) = 0
```

```
            end if

else
            flux(1) = 0
end if

return
end
```